TOWARDS AN ENVIRONMENTAL ENERGY RECYCLER AGGREGATOR (EERA) PROTOTYPE BY HARVESTING AMBIENT ENERGY SOURCES FOR LOW-POWERED INTERNET OF THINGS (IOT) DEVICES

Egyetemi doktori (PhD) értekezés

Syeda Adila Afghan

témavezető neve: Dr. Husi Géza

DEBRECENI EGYETEM

Természettudományi és Informatikai Doktori Tanács

Informatikai Tudományok Doktori Iskola

Debrecen, 2020

TOWARDS AN ENVIRONMENTAL ENERGY RECYCLER AGGREGATOR (EERA) PROTOTYPE BY HARVESTING AMBIENT ENERGY SOURCES FOR LOW-POWERED INTERNET OF THINGS (IOT) DEVICES

University doctoral (PhD) Dissertation

Syeda Adila Afghan

Dissertation Supervisor: Dr. Husi Géza

University of Debrecen
Doctoral Council for Natural Sciences and Informatics
Doctoral School of Informatics
Debrecen, 2020

DOCTORAL (PhD) DISSERTATION

Syeda Adila Afghan

Debrecen

2020

University of Debrecen

Faculty of Informatics

Informatics Doctoral School

TOWARDS AN ENVIRONMENTAL ENERGY RECYCLER AND AGGREGATOR (EERA) PROTOTYPE BY HARVESTING AMBIENT ENERGY SOURCES FOR LOW-POWERED INTERNET OF THINGS (IOT) DEVICES

Dissertation submitted in partial fulfillment of the requirements for the doctoral (PhD) degree

In Faculty of Informatics

Written by: Syeda Adila Afghan..... certified ….....

Prepared in the framework of the Informatics doctoral school of the University of Debrecen

(Industrial and Scientific Applications of Informatics)

Dissertation advisor: Dr. Geza Husi

The official opponents of the dissertation:

Dr. ……..
Dr. ……..
Dr. ……..

The evaluation committee:

Chairperson: Dr. ……..
members: Dr. ……..
Dr. ……..
Dr. ……..
Dr. ……..

The date of the dissertation defense: …… 2020

DECLARATION

I, the undersigned (name: Syeda Adila Afghan, date of birth: 07/07/1988), declare under penalty of perjury and certify with my signature that the dissertation I submitted in order to obtain doctoral (PhD) degree is entirely my own work.

Furthermore, I declare the following:

- I examined the code of Debrecen University's Doctoral School of Informatics, and I acknowledge the points laid down in the code as mandatory.

- I handled the technical literature sources used in my dissertation fairly, and I conformed to the provisions and stipulations related to the dissertation.

- I indicated the original source of other authors' unpublished thoughts and data in the references section in a complete and correct way, considering the prevailing copyright protection rules.

- No dissertation which is fully or partly identical to the present dissertation was submitted to any other university or doctoral school for obtaining a PhD degree.

Debrecen, 24/02/2020

Name: Syeda Adila Afghan

Signature:

SUPERVISOR'S DECLARATION

I certify that Syeda Adila Afghan, PhD candidate worked under my supervision from September 2016 to June 2020 as a PhD student of the Doctoral Council of Natural Sciences and Information Technology, Industrial and Scientific Applications of Informatics at Doctoral School of Informatics, Science and Informatics Doctoral Council, University of Debrecen.

The creative activity of the candidate decisively contributed to the preparation of the results in this thesis. I recommend acceptance of the thesis.

Debrecen, 24/02/2020

Name: Dr. Geza Husi

Signature:

Abstract

The global demand for green energy or renewable energy provisions has been increasingly demanding in the last decade and will continue to increase over the coming days, specifically for powering up the Internet of Things (IoT). Hence, the significance and challenges posed for integrating renewable energy in almost all sectors, more importantly for low-powered devices, need to be carefully studied. Considering the small-scale Energy Harvesting (EH) users, who require building their own specific EH system for saving electricity consumption cost on their project. It is essential to have particular expertise and knowledge related to steps involved and how to aggregate and select the specific components for building own EHC. The first and foremost step before implementation of the system on physical hardware is to simulate and model the entire prototype to see the desired result. However, modeling is a necessary tool towards the implementation of the system, and unfortunately, there isn't clear and straightforward user-defined profile available for building an EH based IoT system. Regardless of better insight for energy harvesting based solutions between users, there's still a massive demand among them towards a better knowledge of their own Energy Harvesting System (EHS) for getting maximum efficiency from it, in terms of cost and revenue.

This thesis aims to address the issues mentioned above and to determine a step-by-step approach towards building an EH based IoT module for powering low-powered devices or IoT applications, specifically for small-scale users. In this regard, two energy harvesting sources, Solar and Heat/Thermal energy have been under investigations regarding power generation of specific EH module and to analyse whether these sources could lead to a promising solution and to sustain the powering capacity required by IoT components. Two prototypes for complete EHC setup for both sources have been proposed, and commercially available transducers have been selected for power generation. On the other hand, commercial-off-the-shelf (COTS) power management integrated circuit (PMIC) from Linear Technology; LTC3108 is chosen for a complete power management solution. The transformation of solar and heat energy will be converted into electrical analogy, as this study is entirely based on an electrical perspective. The energy harvesting for both sources is transformed on spice equivalent circuits, where the entire system was built, modeled and simulated with LTspice simulator via solar-to-electrical and thermal-to-electrical analogy. To follow up this correlation, the parameters are extracted

for both commercial products (MC-SP0.8-NF-GCS [Solar], TEC1-12722 [Thermal]) from their manufacturer's datasheet and modeled on the proposed circuitry separately. For solar power generation, the proposed EHC prototype has generated certain levels of power under various solar irradiation and temperature dependent conditions. The range varies between 2.68 mW (minimum generated power) till 108.60 mW (maximum generated power), specifically, under various solar irradiation levels and load configurations. Whereas, for the Thermal EHC prototype, there are two factors under analysis: power generation and performance analysis. In terms of power generation, there are two programmed output voltages (2.3 V, 3.3 V), and accordingly, the power has been generated. Due to the target applications which require lesser temperature gradients such as human body heat harvesting for wearables; therefore, the temperature gradients experimented were 3.5 °C and 4.0 °C. The minimum power generated for TEC1-12722 fused as a Thermal EHC prototype went till 0.688 mW and maximum reached at 1.719 mW. The generated results for both modules are then compared with IoT power constraints and for wearable devices, which typically vary between µW to mW. However, the comparative analysis is carried out between IoT elements such as different types of sensors and microcontroller units (MCU) as well as with already available complete IoT applications. Hence, the measured results produced typical power levels that could be suitable for some of the IoT components and applications. Consequently, this simulation-based analysis towards building an EH based IoT system could be used as a point of reference and provides an insight towards a fundamental step-by-step basis for developing any Solar or Thermal based IoT prototype for specific applications.

Acknowledgments

First and foremost, I want to express my humble and extreme thankfulness to **Almighty Allah** for the opportunity and wisdom **HE** bestowed upon me, the capability and strength, the good health and mindfulness for finishing this research.

I would like to express my sincere gratitude to my supervisor and mentor ***Prof. Dr. Habil Husi Géza*** for his continuous support, excellent guidance, patience, care, and indefatigable efforts for providing me adequate technical expertise and financial support towards my PhD studies and research.

Expressing thankfulness will never be enough for me towards my loving parents and especially most the important person in my life, my father ***Syed Abdul Qayyum Afghan***, who let me pursue my dreams, who raised me like a son, without him this dream will never become a reality.

Thanking to my closest friend ***Ms. Syeda Sadaf Shah***, who was always there for her untiring support, her compassion, her encouragement when things were critical in life. She was always there for me. Also, I would like to thank my incredible companion in Debrecen, my dearest friend ***Ms. Imran Sarihasan,*** without her my PhD life wouldn't be easier, her support and love made everything fall into place.

Also, I would like to thank my husband ***Mr. Bilal Ahmed Shaikh***, for supporting me spiritually, my sisters ***Syeda Saliha Afghan*** and ***Syeda Zuhira Afghan,*** for their moral encouragements and prayers in achieving my goal.

Last but not least, Distinguished members of the dissertation committee headed by ***Dr. Hajdu András*** for their perceptive remarks and reassurance for approving my work and providing exemplary recognition.

Table of Contents

List of Tables

List of Figures

List of Acronyms

AC	Alternating Current
Bi_2Te_3	Bismuth Telluride
COTS	Commercial-off-the-shelf
Cq	Heat capacity
DC	Direct Current
EH	Energy Harvesting
EHS	Energy Harvesting System
EM	Electromagnetic
FF	Fill factor
IoT	Internet of Things
Isc	Short circuit current
IC	Integrated Circuit
Li-Ion	Lithium-Ion
MEC	Micro Energy Cell
MPPT	Maximum Power Point Tracking
MEMS	Microelectromechanical
MCU	Microcontroller units
NRM	Newton-Raphson method
NiCd	Nickel Cadmium
NiMh	Nickel Metal Hydride
PV Cell	Photovoltaic Cell
PENG	Piezoelectric Nanogenerators
PZT	Lead Zirconate Titanate
PVDF	Polyvinylidene Fluoride
PCM	Phase Change Material
PMIC	Power Management Integrated Circuit
RFID	Radiofrequency Identification
R_{TEG}	Electrical Resistance
Rq	Thermal Resistance
RF	Radiofrequency
Se	Seebeck Coefficient
SN	Sensor Node
SHM	Structural Health Monitoring
STFT	Special Trans Function Theory
STC	Standard Testing Conditions
TEG	Thermoelectric Generator
TEM	Thermoelectric Module
UHF	Ultrahigh-Frequency
Voc	Open Circuit Voltage
WSN	Wireless Sensor Network
ZT	Figure-of-Merit

1 Introduction

1.1 Introduction

This world has seen tremendous dimensions when it comes to technological adaptations and innovations. For the last two decades, every now and then has demanded the fastest communication on the go. In the last two decades, the way we interact and communicate has significantly changed with the introduction of sensors. This miraculous technology has impacted drastically in almost every field and technology. This new era of wireless sensors networks (WSN) not only provided valuable services but also demanded various technological advancement at the same time. The wireless sensor networks having the capability of sensing, processing and sending data over a communication channel; are the driving force behind the Internet of Things (IoT). This revolutionary concept as anything, anytime, anywhere, has been addressed by IoT technology which enables any smart object to communicate with each other. It is predicted that by the year 2020, there will be approximately 50 billion devices connected to IoT network, as shown in Figure 1 [1]. It has been reported in 2006 that the number of IoT devices connected via the internet have surpassed human population [2]. IoT market is currently evolving and enhancing at a rapid pace, and according to Verified Market Research, the Global Internet of Things (IoT) Market Size was valued at USD 212.1 Billion in 2018 and is expected to witness a growth of 25.68% from 2019-2026 and reach USD 1,319.08 Billion by 2026 [3].

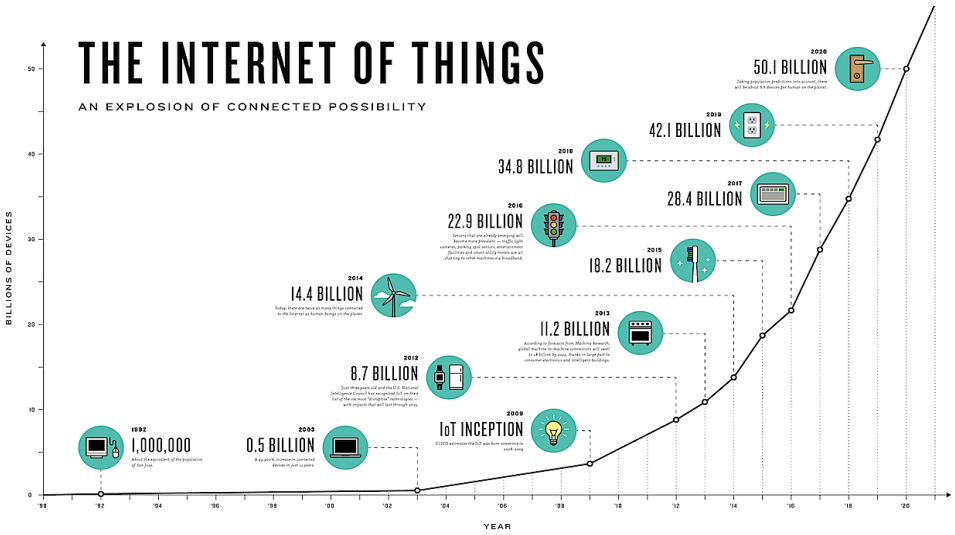

Figure 1.1 The Internet of Things (IoT) connected devices around the globe [1]

However, this limitless, powerful, ubiquitous evolving technology is on the verge of battery power which makes the capacity of this technology limited. IoT devices or sensors need perpetual power, and these sensors are deployed in remote locations where it is highly required to “install and forget” concept for such IoT sensors. The battery pack is an attractive solution for this, but it also comes with a dead-end, as the battery is depleted after a while and needed replacement as an alternative solution for the continuous operation of devices. Even replacement comes with a considerable cost and environmental hazards due to dangerous toxic material exposed by battery degradation [4].

This solution isn’t feasible for long term deployment, whereas billions of connected sensor nodes cannot afford any stoppage, which will severely impact the entire connected system like smart cities etc. It is highly emphasized to come up with an alternative solution, where we can maintain the idea of “install and forget” the device. In this regard, the only solution which could provide uninterrupted green energy is Energy harvesting (EH). The concept states that the surrounding or environmental ambient energy sources available could be transformed to electrical power generation, which can be stored for later use [5]. Therefore, harvesting energy from the environment emerged as a viable option to power IoT sensors or devices.

For designing any EH based IoT device, we need to understand some critical issues. It is mandatory to anticipate the essential criterion as given below:

- To determine the available energy sources and their practicality in terms of scavenging.
- Energy transducers are required for capturing the ambient energy source.
- The energy harvesting circuitry.
- DC-DC converter or specific Power Management Integrated Circuit (PMIC).
- Estimating the required power consumption by the specific IoT device or sensor node and power generation by the transducer.
- The battery storage that matches the transducer when no energy is available.

While working on all above aspects, as well as analyzing and gathering these requirements, the most critical and mandatory step towards designing and implementing any EH based IoT device, is to simulate the whole model beforehand.

This thesis work aims to model and simulate the prototypes for designing an EH based IoT device and giving an insight along with extensive and detailed simulation study founded on various parameters and configurations. This thesis will provide step-by-step guidelines towards

design considerations and targeting on much needed research tools that are currently lacking for simulation studies of energy harvesting sources.

1.2 Problem Statement

The principle prototype for designing any EH based IoT device is still missing due to the stringent nature of all complicated components and heterogeneity. The major hurdle appears when it comes to combining all separate processes as a single system. There is a lack of simulation study or any complex tool where end-users can observe, analyze, and adapt the system based on its prerequisites. For this purpose, the step-by-step guideline is required and thorough understanding of all different phases altogether. However, the critical aspects are given below as a significant motivation for coming up with this study due to such problems:

- Limited battery capacity and battery depletion.
- Highly heterogeneous nature of various components like energy transducers, energy harvesting circuitry, storage devices, etc.
- No user-defined profile or prototype available for designing any EH based IoT product.
- No profile or prototype available combined with Power management IC and Energy source.
- Lack of simulation study on analyzing the performance factors of complete energy harvesting system (EHS) in terms of compatibility, losses, product selection, cause and effect, energy efficiency, maximum power transfer, load sustainability, etc.

1.3 Novelty and Contribution

This thesis will establish an exact structure towards the designing and implementation of any EH based IoT setup. The generic blueprints for two (solar and thermal) energy harvesting based complete systems are proposed separately with extensive analysis and simulation-based studies.

The significant contributions are highlighted as follows:

- IoT design considerations have been appropriately categorized according to the energy harvesting sources, energy transducers, harvesting circuitry, power converters, power consumption, and power generation. The detailed study of all these phases has been simplified and brought up in terms of general guidelines for designing EH based IoT system.

- A systematic literature survey about available energy harvesting sources and energy transducers based on their performance characteristics is done as its mandatory for selecting the product accordingly. Also, a comprehensive review is conducted regarding available battery characteristics in terms of pros/cons.

- The power generation and power consumption analysis for IoT.

- A prototype for Solar energy harvesting has been simulated with a specific commercial-off-the-shelf (COTS) power management IC (PMIC) chip.

- A prototype for Thermal energy harvesting has been simulated with a commercial-off-the-shelf (COTS) power management IC (PMIC) chip.

- Detailed trial and error case studies in graphical representation have been demonstrated in multiple perspectives.

- Simulation-based studies will help to establish the proper implementation of the subject in terms of hardware configuration and performance.

- Understanding of EH transducers, PMICs, storage technologies, and energy sources (Combining all technologies and techniques) in the form of literature, trial and error case studies, and simulation-based analysis.

- Modeling of solar and thermal equivalent circuits after analyzing various models and selecting the best that fits our research profile.

- Determining the systematic way of extracting electrical parameters for both solar and thermal energy transducers from limited available information, i.e., manufacturers datasheet.

1.4 Research Objectives

The main objective of this research is to explore a practical solution to eliminate the need for batteries replacement to power up IoT sensors or components.

1. Finding the minimum output power required for a number of Internet of Things (IoT) devices and applications.

2. Reviewing the energy storing technologies in terms of IoT.

3. Analyzing and reviewing the number of available Power Management ICs and their working profile in terms of compatibility with IoT features and specifically in Energy Harvesting PMICs.

4. Analyzing the design consideration for building Energy Harvesting based self-powered IoT devices.

5. Reviewing the ambient energy sources and associated harvesting techniques.

6. Analyzing the available energy harvesting transducers specifically Solar and Heat/Thermal in terms of harvesting techniques and their generated output power based on various parameters, which affects the performance dependent on multiple situations such as temperature and environmental impacts.

7. To establish a trial and error case study for optimal output power by simulations of commercially available Photovoltaic (PV) module and Thermal module combined with Power Management IC: For analyzing the behavioral response of the system combined with EH based PMIC.

8. Comparative analysis between simulation results and already available experimental results for both prototypes after careful considerations on various environmental conditions and other parameters like cause and effect, product selection, modeling and simulation for producing the optimal output power of harvester. *(Analysed and optimal case study)*

1.5 Dissertation Organisation

In this section, we summarize the content of the remaining chapters of the dissertation, which are described briefly as follows:

Chapter 2 introduces the Internet of Things (IoT) and its influence in upcoming decades, the technological significance provided by this ubiquitous system, and then what exactly limits this pervasive technology, the battery obstacle, and power issues. The response for this concern is being supported by EH technology, its necessity, and its impact as a driving force behind the smart systems around the globe. Almost all available EH sources have been investigated and their associated techniques for harvesting. The general Energy Harvesting System (EHS) has been reviewed and categorized according to several energy harvesting sources.

Chapter 3 discusses the literature review of available energy harvesting sources and their solutions in terms of IoT. This survey is divided into two sections, where the first one is related to overall energy harvesting based IoT applications and selected devices. The other part belongs to the electrical modeling, and relevant methodology towards simulation study is demonstrated. However, the spice modeling and simulation for solar and thermal energy harvesting in terms of electrical perspective is the core piece of this study. The number of spice models and extraction methods have been discussed in detail.

Chapter 4 proposes the research methodology for modeling and simulation of two energy harvesting sources; Solar and Thermal. In this chapter, the step-by-step approach for designing an Energy Harvesting (EH) based system to power up low-powered devices is established. Two prototypes have been proposed for EHS, which are modeled and characterized in various parameters for analyzing the behavior of the system and, most importantly, to generate the output power under different load configurations.

Chapter 5 presents the computational and simulation results for both Solar and Thermal EHC modules along with comparative analysis with number of available energy harvesting modules to verify the accuracy of the acquired results.

Chapter 6 provides the conclusion and summarizes the entire dissertation concerning the contributions and associated publications of entire research objectives framed in that section, and discusses the future directions required to extend this work.

2 Energy Harvesting and Internet of Things (IoT): Background and Evolution

2.1 Introduction

Harvesting energy isn't a new technique as it dates back to the centuries, but the driving force behind this technological advancement came by the advent of the wireless sensor network (WSN). With the introduction of collecting data via sensors had drastically changed the way we perceive the gigantic information network. From industrial sectors until academics, every segment would like to maintain the streamline of continuous data autonomously. The components, mechanics, algorithms, computing, and storing technologies were merged to make a single masterpiece. Sooner this technology evolved and expanded in terms of communication *anytime*, *anywhere* and *every time* and has been recognized as the Fourth Industrial Revolution named as Internet of Things (IoT) [6]. The usage of IoT becomes prominent in various fields of our daily life, like medical implants, wearable devices, smart systems. But there comes the point which proved to become a deadlock after a while for this pervasive and evolving technology, i.e., battery degradation and need for continuous power. It is a massive responsibility for academia and scientists around the globe to ensure the perpetual power of billions of connected devices without any stoppage. This cry demanded to utilize the surrounding ambient energy sources to support power-hungry devices. This chapter will discuss the basis and foundation of energy harvesting and IoT and their related challenges for understanding the necessity and coping powering problems for addressing the solutions towards them.

2.2 Internet of Things (IoT)

A network of everyday objects combined with sensors and connected via the Internet is called the Internet of Things (IoT), as shown in Figure 2.1. In IoT, things are the devices that can be both physical or virtual, which communicate with each other by sensing the data from surroundings, receiving the data, and exchanging information when required [7]. This data can be shared and used to improve the life quality, enhance the industrial processes, and could be utilized in various sectors to augment service levels. IoT is being adopted in almost every industry and is providing services in a wide variety of applications. As estimated by Gartner, the number of IoT devices connected via the internet will reach 20 billion by 2020 [8].

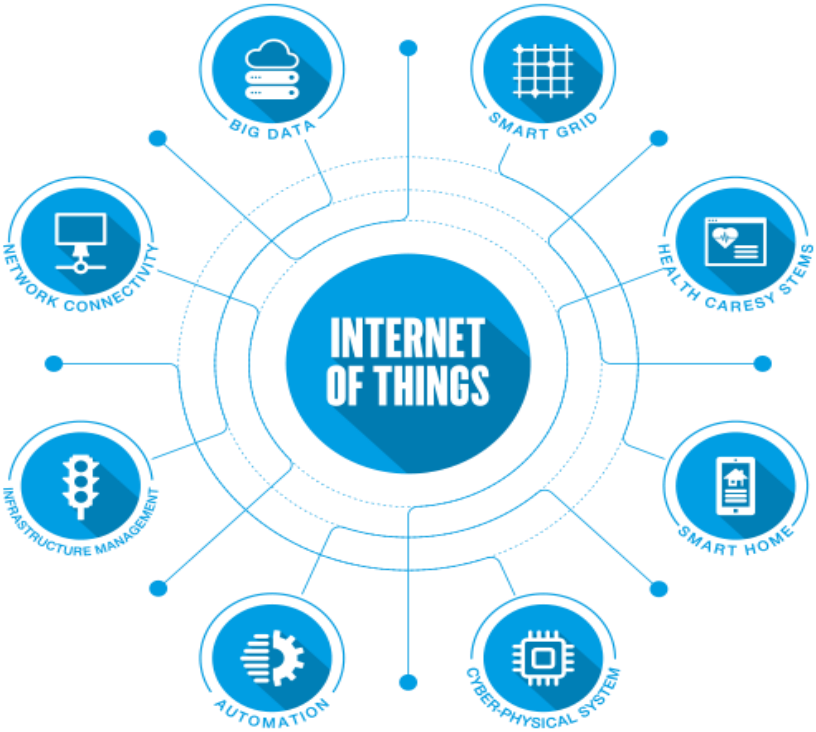

Figure 2.1: Graphical representation of the Internet of Things (IoT) [7]

2.2.1 Types of Internet of Things (IoT)

There are four different application types of IoT recognized by Third generation partnership project (3gpp) [9]. These are categorized as:

- Type 1: The applications under this type consist of health monitoring, assisted living, wearables, tracking, and bicycle tracking. They could be supported by energy harvestings as their battery life is of 5 years, having lower latency of about 30 seconds and medium coverage. Wearable devices like smartwatches require longevity for several days, whereas, Set-and-fort devices like home security requires several years of longevity. Therefore, battery replacement is inconvenient. On the other hand, some devices are battery-less and self-powered such as smart cards and RFID tags [4].
- Type 2: The family consists of applications like industrial asset tracking, agricultural livestock, microgeneration, and real-time monitoring. In this category, the battery requirement is 5 to 10 years, medium coverage, and lower latency (less than 1 second).
- Type 3: This type works on both indoor and outdoor coverage; indoor includes smart meter, smart building, smart parking, home automation, and industrial machinery

control. For outdoor coverage; smart cities, agricultural stationary asset monitoring, waste management, and environmental data aggregation. These applications require a battery life of around 10 to 15 years, prolonged coverage, and 10 to 60 seconds of latency.

- Type 4: The applications under this category are main powered due to their stationary deployment, which includes home appliances, smart city light systems, and vending machines. They have low mobility support, consists of both indoor and outdoor coverage, and latency is less than 30 seconds.

2.2.2 Powering the Internet of Things (IoT)

To power up this advanced technology, we need to provide constant power support to these devices, as mostly type 1,2 and 3 are battery-powered and requires life span of around 5 to 15 years. Type 1 device can be recharged quickly, but other types require replacement and maintenance, which is again a critical challenge. To survive this battery obstacle, we need alternative energy solutions, and the most promising one is energy harvesting as an alternative to batteries [10].

2.3 Limited Fossil Fuels: Why Energy Harvesting

This world has limited fossil fuels, and they are declining with every passing moment as this alarming situation is already predicted by the researchers every now and then [11] [12]. In this regard, it has been emphasized to go green and find out alternative energy solutions. This is not happening soon, but still, precautions are required to be proactive, act before it’s too late. Another situation that makes it more critical is battery depletion; after a few years of usage, the battery needed to be replaced, which is again a challenging task to achieve. Because mostly the IoT sensors are deployed in an isolated place where it is almost impossible to reach and maintain after a few years. The actual need is to go battery and maintenance-free. Therefore, energy harvesting is the rescuer in it and only hope to cope up with this problem.

2.4 Energy Harvesting: A savior

Energy harvesting, also known as power scavenging, is a process to convert ambient energy sources from surroundings into electrical energy, which can be stored and used in powering autonomous devices [13]. Mostly it is quite popular due to its enormous contributions in solar technology and electro-dynamo, however thanks to digital trends and mechanics, it can be used in various forms and innovative ways, specifically for IoT.

This technology is also supporting the challenges acclaimed by global warming and climate change due to its nature of reusability, i.e., converting wasted energy. The energy could be captured from different sources and in numerous ways, which involves various mechanisms to brought up electrical power in a usable form.

2.5 Energy Harvesting System

For building any energy harvesting system, we require some of the major components to develop a renewable system that can perpetually power electronic devices. To build a system, a general prototype has been established, which can be seen in Figure 2.2 [14]. The basic building blocks of any energy harvesting system (EHS) has been mentioned along with major components in it.

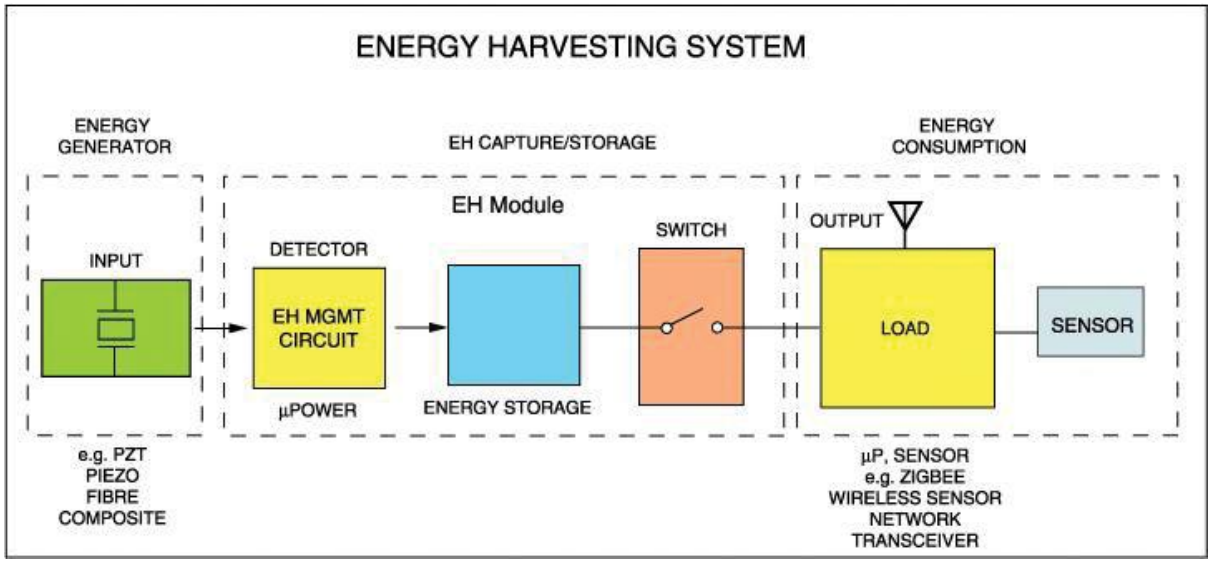

Figure 2.2: General Block diagram of Energy Harvesting System [14]

Inside any EHS there are several subsystems working hand in hand, which includes the (a) ambient energy harvesting source captured by energy transducer or energy generator element, (b) an electronic circuitry containing power management system such as AC-DC, DC-DC converters and PMICs, (c) an energy storage like rechargeable batteries, (d) and the target application which is consuming the required power, i.e., IoT applications, sensor nodes, wearable devices, etc.

2.6 Energy Harvesting Sources and their associated technologies

The environment is surrounded by a considerable amount of energies within us, which we are even unable to see from the human eye. These energy sources comes-up under two categories which are; ambient energy sources and external energy sources [15]. The ambient energy sources are easily accessible from our surroundings and don't require any external system to extract the energy, consisting of solar, thermal, vibrational and radiofrequency, etc. However, external sources include human power or mechanical sources [16].

2.6.1 Light Energy Harvesting

Solar energy harvesting is considered as one of the most ubiquitous renewable energy sources which are abundantly available and free. The reported average solar energy being received at the earth's surface is approximately 10^{18} kWh/year, with the surface power density of around 1353 kW/m^2 [17]. However, the energy harvested from solar ranges from 100 mW/cm^2 to 100 W/cm^2 [18].

This type of energy comes under two forms; artificial indoor lights as well as sunlight, which is plentifully available around the globe and can be transformed via photovoltaic techniques [19]. It can be achieved by a solar energy harvesting transducer known as Photovoltaic cell (PV). These cells are manufactured by a semiconductor material, and with the effect of photovoltaic, the incident light on the cell is converted into electrical energy. A potential difference is generated when free electrons produced at PN junction under the sunlight are moving towards the N-type and P-type semiconductor, as shown in Figure 2.3 [20].

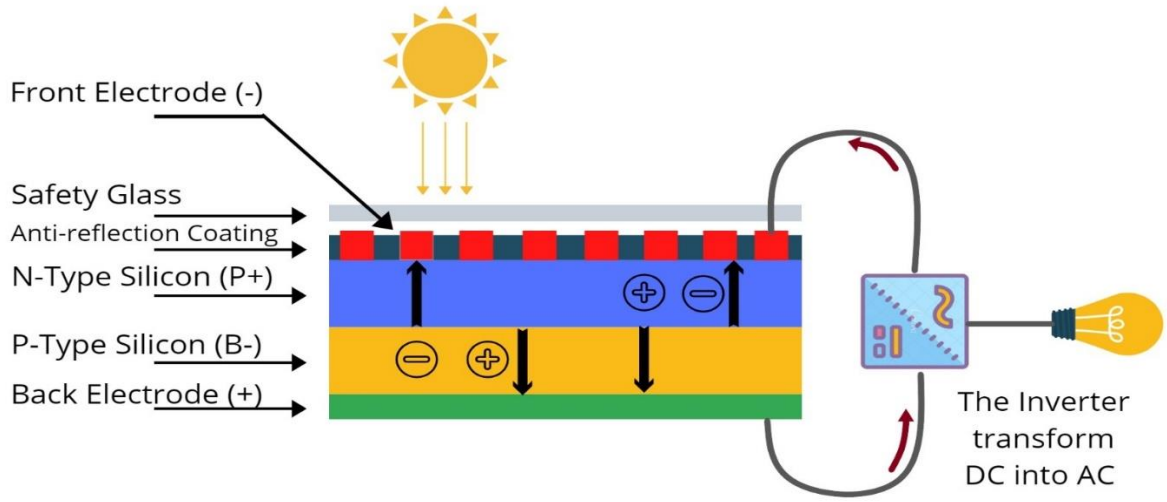

Figure 2.3: Solar cells element structure [20]

For defining the solar cell's performance and comparing it with other cells, the most commonly used parameters applied is the conversion efficiency of a solar cell. The conversion efficiency is defined as the ratio of converted output energy from the cell to the input energy from the sun [21]. Apart from this, the performance is also measured based on the intensity of the incident light, spectrum, and the temperature on the cell. In this regard, the conditions for measurement must be controlled and standardized. The measurement standards for terrestrial solar cells are given as AM (Air Mass) 1.5 conditions and Temperature of 25°C.

The equation for calculation of efficiency is defined as [22]:

$$\eta(\%) = \frac{P_{max}}{P_{in}} = \frac{V_{oc} \times I_{sc} \times FF}{P_{in}} a \times 100 \tag{2.1}$$

Where *Voc* belongs to open-circuit voltage for solar cell, *Isc* is short circuit current, and *FF* is the fill factor. Open circuit voltage is the maximal voltage produced by the solar cell when there is no current and short circuit is the condition, then the voltage across the solar cell is zero.

Open-circuit voltage and short-circuit current are the maximum voltage and current from the solar cell, and on these two points, the power of a cell is zero.

By using the equation of fill factor, we can determine the maximum amount of power from a solar cell, by utilizing the short-circuit (Isc) current and open-circuit voltage (Voc).

The equation for FF is defined as [21]:

$$FF = \frac{P_{max}}{V_{oc} \times I_{sc}} = \frac{V_{max} \times I_{max}}{V_{oc} \times I_{sc}} \tag{2.2}$$

The efficiency of a PV cell highly depends on the material and the type which we are using, as PV cells are classified under three categories; silicon, semiconductor compounds, and novel materials [23]. Apart from that, the EH techniques are also required to extract as much power as possible, like maximum power point tracking (MPPT) algorithms, which plays a pivotal role in the maximum power of the PV cell [24]. Even though energy scavenging from solar energy is a scalable method, which is usually limited by the intensity of light and availability due to which additional storage units are required to support the continuous supply of the harvested energy.

2.6.2 Electromagnetic Energy Harvesting

Radiofrequency (RF) is a wide frequency band of electromagnetic waves that range from 300 GHz to 3 Khz. These Electromagnetic (EM) waves are available in huge amount within our surrounding and could be collected from sources like TV (41- 250 Mhz, 470 – 950 Mhz); MF (AM Radio, 526.5 – 1705 Khz); FM (87.5 – 108 Mhz); GSM (850/1900 or 900/1800 Mhz); WiFi (2.45/5.0 GHz), 3G, 4G, CDMA and ISM (Industrial scientific medical, 2400 Mhz [25], [26]. In terms of harvesting the RF signal, the actual components behaving as transducers for collecting RF are antenna and a rectifier unit, as demonstrated in Figure 2.4. Therefore, A radiofrequency-based energy harvesting system is used to transform electromagnetic energy into a usable continuous voltage (DC) to power low-powered electronic devices and WSN [27]. The most crucial factor that makes this ambient source favorable is that it is independent of environmental conditions like weather, temperature, and climate.

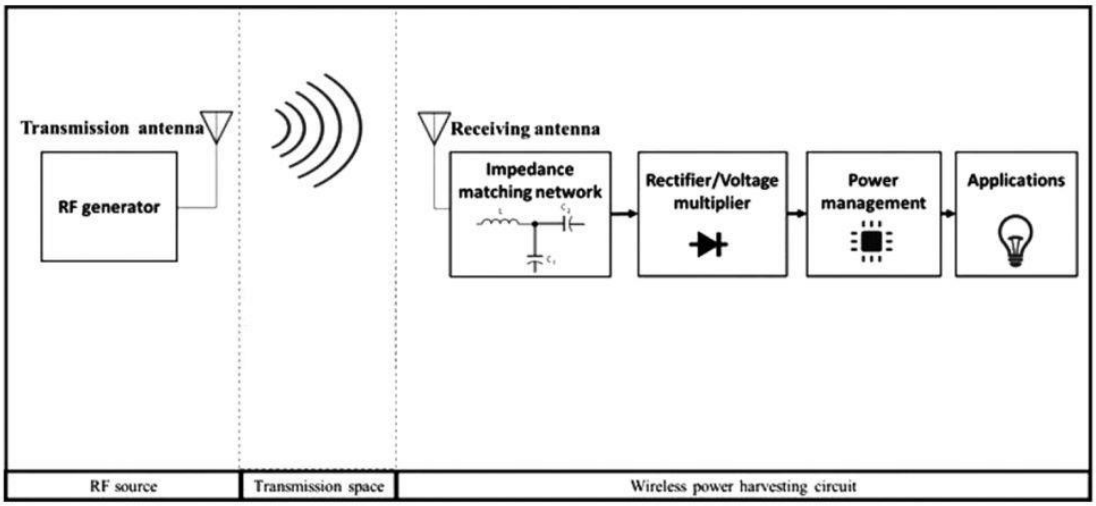

Figure 2.4: Radio Frequency based Energy Harvesting setup [27]

When it comes to power transmission, RF harvested power ranges from 1 µW to 189 µW with the help of dedicated RF transmitters at the frequency of 900 MHz within a very short distance of around 5 m to 4.1 Km [26]. However, the amount of extracted power highly depends on the source of power and the range. Thanks to the development of new wireless technologies, which made it possible to have numerous RF transmitters on hand and now it became a challenge for the engineers that how they will collect the ambient energy source to power small electrical devices like backscatter radio sensor network [28]. The power collected by the receiving antenna can be calculated by the Friss formula for a transmitter and receiver.

$$P_R = \frac{P_T G_T G_R \lambda^2}{(4\pi R)^2} \tag{2.3}$$

Where P_R refers to the receiving power, Transmitted power is denoted by P_T,G_T is representing the transmitting antenna, and receiving antenna gain is demonstrated by G_R, λ represents the wavelength of transmitting wave, whereas the distance of the separation between receiving and transmitting antenna is given by *R*.

The free space path loss is given by,

$$P_L = \frac{(4\pi R)^2}{G_T G_R \lambda^2} = \frac{(4\pi f R)^2}{G_T G_R C^2} \tag{2.4}$$

$$P_L(dB) = 32.44 + 20\ \log_{10}(f) + 20\ \log_{10}(R) - G_T - G_R$$

Where P_L is the free space path loss, f is the frequency of transmitting wave [29].
The relation between received power and the distance is given by [30] and can be seen in Figure 2.5, where he attributed the novel technologies their impacts, conversion efficiencies required, and size of the antenna. All these parameters significantly impact the output power of the receiving antenna.

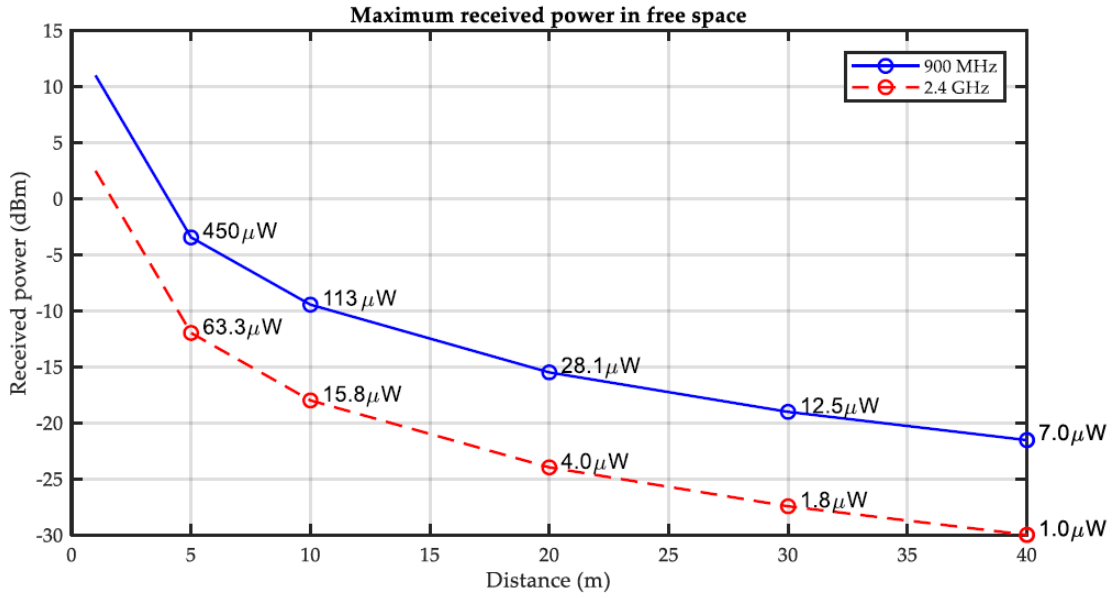

Figure 2.5: The relation calculated between Received power (dBm) and Distance (m) [30]

The RF-based IoT system has a sustainable future due to various advancements in wireless communication protocols, which are focusing mainly on maximizing the efficiency and design of RF transmitters and could support wide applications.

2.6.3 Thermal Energy Harvesting

Thermal energy could be obtained from the available heat in the environment as well as generated heat during any process, mostly known as waste heat. Thermal energy could be harvested either from thermoelectric or pyroelectric effect. Categorizing thermoelectric effects as Peltier, Seebeck, and Thomson, these could support to generate power when there is availability of heat [31]. In order to extract thermal energy, it is required to have a thermal gradient which is depending upon the temperature difference between the environment and heat source, as well as the conversion efficiency of the transducer. Thermal energy harvesting is referred to as the process of transforming thermal gradients into electrical energy. In broad terms the thermoelectric power is produced from two physical effects; The Seebeck effect and Peltier effect. The generation of power due to thermal gradients is accredited to the Seebeck effect [32], whereas, in the reverse condition the current is applied to the thermoelectric module (TEM) which results in heat absorption at one junction and heat release at the other is known as Peltier effect [33]. The working phenomenon for both effects is being demonstrated in Figure 2.6. Considering the dynamics of the thermoelectric device, it is made up of two primary junctions, which are known as P-Type (high concentration of positive charge) and N-type (high concentration of negative charge) elements. The tightly packed thermoelectric couples are connected electrically in series and thermally in parallel as shown in the Figure 2.7.

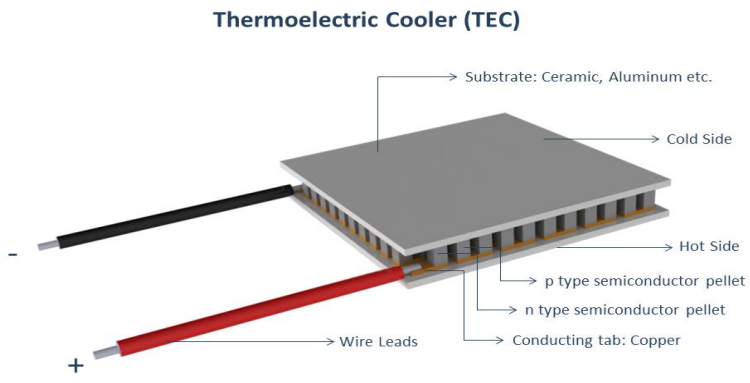

Figure 2.6: Configuration of Thermoelectric Cooler (TEC)

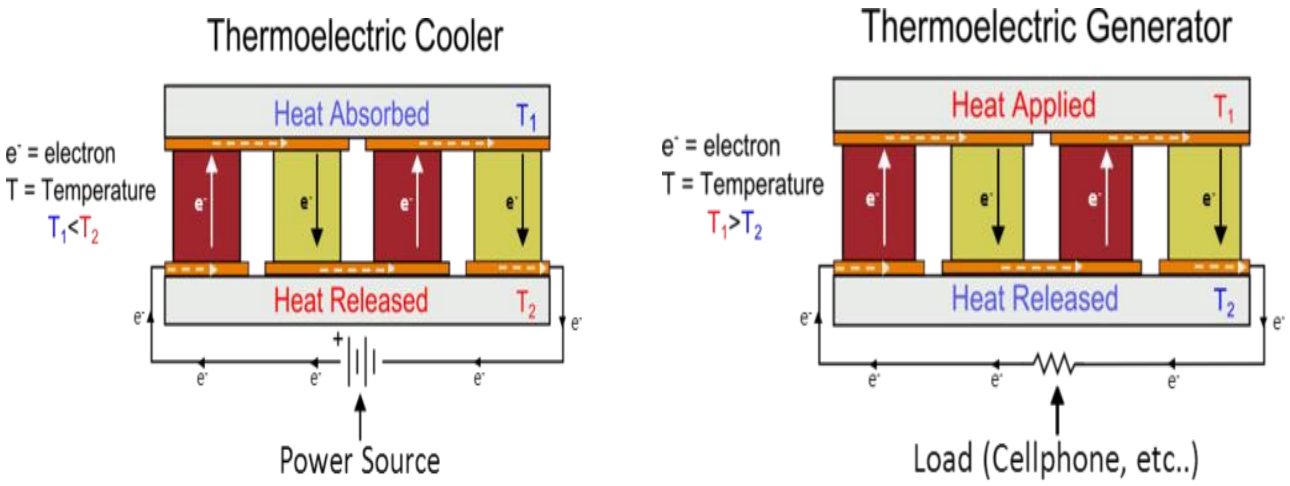

(a) (b)

Figure 2.7: Representation of (a) Peltier Effect (Cooler) and (b) Seebeck Effect (Generator) [34]

The important parameters which make them ideal for their usage in green and renewable technology like WSN and IoT applications are due to their compact size, robust, reliable as they don't have moving parts.

For analysis of the performance of TEG, various research has been done on improving the efficiency of TEMs as their conversion efficiency is as low as 12 %.

The Seebeck equation is defined as:

$$V = \alpha(T_h - T_c) \tag{2.5}$$

Where *V* is the thermoelectric voltage, *α* is denoted as the Seebeck coefficient, and *(Th - Tc)* is the thermal gradient or temperature difference across the junctions.

In order to analyze the efficiency of thermoelectric generators, a parameter called Figure-of-merit (ZT) is tested, which is based on thermoelectric material. It is basically a function of various transport coefficients denoted in the following equation:

$$ZT = \frac{\sigma\alpha^2 T}{k_c + k_l} \tag{2.6}$$

Where electrical conductivity is denoted by *σ*, the Seebeck coefficient is represented by *α, T* denotes the mean operating temperature, and *K* represents the thermal conductivity. The electronic and lattice contributions are indicated by *c* and *l* on k.

One important aspect to consider here is that the higher Figure-of-merit corresponds to the higher efficiency of the TEG [35]. However, various contributions have been inducted by researchers to enhance the Figure-of-merit for many industrial and energy related applications. Among all, the most important parameters in the thermoelectric device is its material. The commonly used material in TEG is Bi_2Te_3 (Bismuth telluride) since 1954 due to its low thermal conductivity and higher electrical conductivity, which gives about 0.7 – 0.8 ZT at room temperature [36]. Apart from Bi_2Te_3, other thermoelectric materials have been introduced which includes, SiGe [37], $CoSb_3$ [38], PbTe [39], Mg_2Si [40] and $BiSbTe_3$ [41].

Thermoelectric harvesters could be a viable option due to their safety, durability, and high stability, but there is one trait that limits this technology is its lower conversion efficiency as the disadvantage of thermoelectric energy harvesting.

2.6.4 Mechanical Energy Harvesting

The mechanical energy is available in various forms in our surroundings, such as vibrations, human motion, mechanical rotating, wind blowing, vehicle driving, and ocean surfing. This type of energy could be transformed into electrical power generation for low-powered devices like IoT sensors. In broad terms, these forms of energy are categorized as intermittent, steady-state, and mechanical vibrations. In order to scavenge these types of sources, there are different transducer techniques to capture energy.

2.6.4.1 Piezoelectric Energy Harvesting

The mechanical energy, such as strain/stress, could be harvested by using the effect of piezoelectricity into electrical energy. This type of energy could be generated from various sources like body motion, vibrations, airflow, and acoustic noise. In general terms, piezoelectricity is the process of converting mechanical energy into electrical employing the inherent polarization of crystals. The crystal structure is deformed when the stress or strain is applied to the piezoelectric material, which results in the electrical charge movement [42]. Its working principle is shown in Figure 2.8, which on the opposite surfaces of the dielectric, positive and negative charges are produced due to an external force applied.

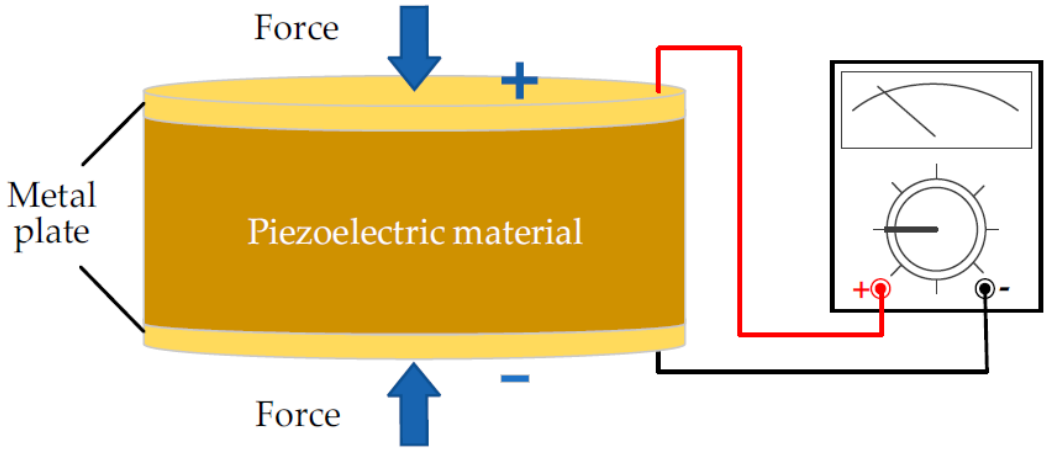

Figure 2.8: Working principle of harvesting Piezoelectricity [42]

The material used inside a piezoelectric module are piezoelectric ceramics and polymers [43].

The polarization charge density is measured by the following equation:

$$\rho = dX \tag{2.7}$$

Where ρ represents the polarization charge density, the piezoelectric coefficient is denoted by d and, X is the stress applied.

This charge density produces electrical field and potential, which is given as:

$$E = \frac{\rho}{\varepsilon} \tag{2.8}$$

Where the divergence of the electric field is given by E, ρ is the charge density, ε represents the permittivity.

By designing any piezoelectric based device, which includes a piezoelectric material, an electronic circuitry, and electrodes, the electric current could be generated by the piezoelectric principle and could be used as an electrical energy source.

The conversion efficiency of piezoceramic material is much higher, which makes it a leading technology in industrial as well as research domains with few possible limitations. On the other hand, piezopolymers are extensively used for sensors, specifically biomedical sensors due to their properties like deformation, and being lightweight makes it appealing, but their conversion efficiency is lower as compared to piezoceramics [44].

To achieve higher efficiency of the piezoelectric device, nanomaterials came under observation after the introduction of piezoelectric nanogenerators (PENG) [45]. This technology than later became a great deal of attention, and the latest developments and investigations came into existence. From the structure of PENG, such as vertically grown PENG [46], laterally assigned PENG [47], stretching type PENG [48] etc., till the analysis of various semiconductor materials like CdS [49], GaN [50], InN [45].

Despite all these efforts, piezoelectric materials will eventually degrade by the time, and this flaw will lead towards lower conversion efficiency. However, these challenges require tremendous research to further cope up with problems as still, it's a long way to go before supporting as a commercial product for EH products.

2.7 Comparison of Energy Harvesting techniques and their associated technologies along with harvested power

The complete list of energy harvesting sources, along with the number of parameters and transducers, is compiled for more accessible analysis and understanding. The essential factor in interpreting is the power generation of all the above-mentioned energy harvesting sources and their conversion efficiency. These are the complete energy harvesting sources, as highlighted in Table 2.1 [51].

Table 2.1: Comparison of Energy harvesting sources along with their power generation efficiency

Energy Source	Conditions	Conversion efficiency	Harvested Power	Transducers
Solar	Indoor	3% - 7%	621 µW	Photovoltaic
	Outdoor	6% - 35%	1350 mW	
Radiofrequency	GSM	5% - 15%	1 mW	R.F generator
	WiFi	5% - 25%	10 nW – 0.1 µW	
Vibration	Mechanical motion	20% - 40%	200 µW – 40 mW	Piezoelectric generator
Thermal	Human	0.8% - 4%	0.5 mW – 5 mW	Thermoelectric generator
	Industry	1% - 7%	3 mW – 50 mW	

2.8 Hybridization of Energy Harvesting

As discussed in previous sections along with comparison and their harvesting power from different sources, still there's a huge requirement to fulfill the power-hungry device. The single harvesting source strategy is not enough to provide ample power requirements. Not only the required power is a hurdle, but also the availability of specific power source depending on various conditions is changeable. In this regard, another strategy that is being focused on harvesting enough energy at all times is to integrate more than one sources altogether in a single circuit. Recently various hybrid prototypes have been investigated to analyze the compatibility and working mechanism of different sources. As every source requires different rectification techniques, therefore heterogeneity is always there, and we need to design such circuitry in a way that can handle multiple rectifications and could generate regulated voltage for a particular application [52]. Some of the demonstrated multi-source prototypes are given as solar and mechanical harvesting, solar and thermal harvesting, mechanical, and thermal harvesting. As a rule of thumb, solar and thermal generate direct current (DC), whereas, piezoelectric generates alternating current (AC). The prototypes are demonstrated in Figure 2.9.

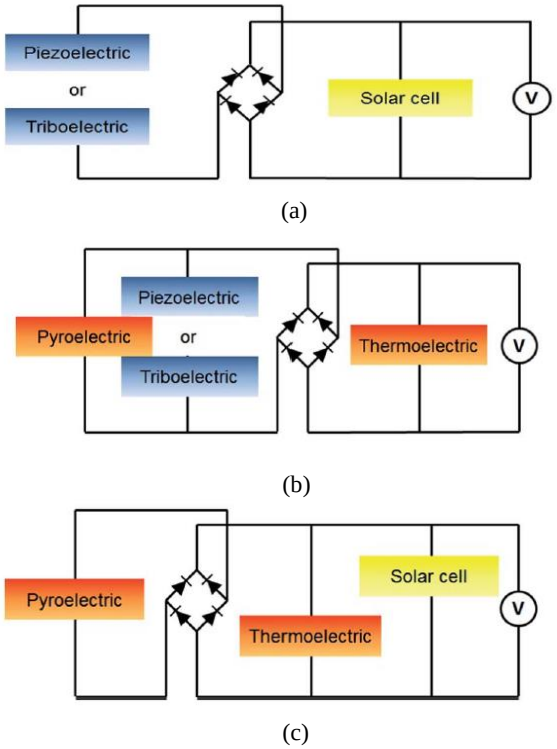

Figure 2.9: Electric circuit designs for hybrid energy harvesters. (a) Mechanical energy + solar energy, (b) mechanical energy + thermal energy, and (c) thermal energy + solar energy [53]

2.9 Power Management in Energy Harvesting System

Any collected energy source from the environment cannot be in an operational form to directly connect it to power up the electronic system. For instance, considering body temperature ambient source, TEG generates very low DC voltage, whereas RF and piezo outputs produce AC voltage and require rectification process. Therefore, it is mandatory to have a power converter to transform the generated power into operational power, which behaves as an interface between generated energy and output load. There are four different categories for power converters that include AC – AC, AC – DC, DC – AC, and DC – DC [54]. Managing power is a critical challenge to be addressed when it comes to IoT and EH based systems. How efficiently the sporadic power is being transformed and maximizing efficiency without overlooking the harvesting principles is a critical aspect. In this regard, researchers have been coming up with the latest developments in power management modules like System on Chip [55], Power management techniques [55], and Power management IC [56]. Regarding our research questions, our work will be based on DC – DC converters and will be described accordingly.

There are two variations in DC – DC converters, defined as Linear regulator and Switch Mode Power Supply (SMPS), where linear regulators work for transforming higher input voltage to lower output voltage, and SMPS operates either as step-up or step-down regulator. The significant differences between both categories are elaborated in Table 2.2 [57] in terms of efficiency, complexity, and other parameters.

Table 2.2: Comparison between Linear Regulator and Switching Regulator

	Linear Regulator	**SMPS**
Function	Only operates as step-down, where the input voltage is higher than the output voltage	Operates in both modes; step-up and step-down
Efficiency	Lower in efficiency, depends on input and output voltage difference	Higher in efficiency, except at lower load configuration
Complexity/BOM	Lower in complexity, requires only bypass capacitor	Higher, requires diode, inductor and filter capacitors
Cost	Low	High, due to external components
Ripple/Noise	Low	High, due to switching of control signals

2.10 Power Management Integrated Circuit (PMIC) For Energy Harvester

It is required to interface the harvested energy from the ambient energy source and the output load through a power converter. As the harvested energy can't sustain or unable to generate the proper amount of power directly towards the load. However, power converters are needed to transform the generated power into the required power level. The power management integrated circuit (PMIC) is used to provide the management on transducer and energy collection channels, the storage element consisting of a battery, supercapacitor, etc., and the processing unit which is connected for output load. There are several vendors available producing commercial-off-the-shelf (COTS) PMICs and varies in terms of specifications and attributes. The basic functionality for any PMIC includes; capturing the minuscule energy from the transducer, transforming the harvested power towards the required load setup through DC-DC converter, and managing the energy generation and energy consumption balance as the critical factor.

Some of the energy harvesting based PMICs specifically designed for solar and thermal energy harvesting applications are mentioned below [58].

Maxim's MAX17710; a PMIC from Maxim Integrated, which is designed for charging and protection of micro-energy cell (MEC)s. It supports a variety of energy harvesting transducers such as solar, thermal, and RF-based sources. Manages the transformation of load and conversion techniques accordingly by providing the regulated voltage at the output. It can harvest the energy from low energy sources into the usable output from 1 µW to 200 µW. This system provides battery protection by two thresholds for undervoltage and overvoltage circumstances, specifically for small batteries. The start-up input voltage for boost converter can be as low as 750 mV, and after stabilizing the initiation process, it could harvest the energy as low as 250 mV. Apart from this, the ultra-low-quiescent current low-dropout LDO linear regulator could be formatted for three different output settings, which are 3.3 V, 2.3 V, and 1.8 V [59].

Texas Instrument's BQ25504; manufactured by Texas Instrument (TI) PMIC designed for transforming microwatts into milliwatts efficiently from number of ambient energy sources. This IC consists of a boost converter that could be initialized from a voltage as low as 330 mV and will sustain the operation even from an input voltage as low as 80 mV. As it is specially designed for high impedance sources like solar and thermal, therefore it contains the maximum power point algorithm (MPP or MPPT) for extraction of maximum power from the source and

matching the source impedance with load impedance. Furthermore, this IC is designed for supporting maximum and minimum operating voltages of storage units programmed for undervoltage and overvoltage protection to protect the storage from overcharging and discharging [60].

SPV1050 from STMicroelectronics; a PMIC designed for harvesting energy from solar cells and thermoelectric generators. This IC can operate from as low as 180 mV for cold start activation. It also contains the maximum power point tracking (MPPT) algorithm for extracting maximal output power levels. It allows charging for any type of battery, such as thin films, NiCd, Lithium-Ion, and supercapacitor while monitoring the over-discharge of the battery. The system is having the capability of both buck-boost and boost configuration. The MPPT is user programmable by introducing the resistor input divider and permits the maximum power under various temperature and irradiance levels [61].

LTC3105 from Linear Technology; a high efficiency step-up DC-DC converter that is capable of operating from an input voltage as low as 200 mV. This IC includes a maximum power point controller (MPPC) that can enable the operation from low input voltage. MPPC is programmable by user by precise formulation provided in the datasheet. Most importantly, the output voltage can be adjusted between 1.8 V and 5 V [62].

LTC3108 from Linear Technology; a PMIC consisting of a DC-DC converter for low input energy sources. It is capable of harvesting energy from an input voltage as low as 20 mV. Like other PMICs, this doesn't contain the MPPT algorithm having lower inefficiency. The best part in this system is that it provides four different output voltage settings for specific applications which are 2.35 V, 3.3 V, 4.1 V, and 5 V. It also contains the storage capacitor for providing power to the application when there's no availability of energy source [63].

Table 2.3: Comparison of various Power Management ICs (PMIC)

PMIC	**Cold start activation voltage**	**MPPT**	**LDO**
MAX17710	750mV	No	1.8V, 2.3V, 3.3V
BQ25504	330mV	Programmable	No
SPV1050	180mV	Hardware set	1.8V, 3.3V
LTC3105	200mV	Programmable	2.2V
LTC3108	20mV	No	2.2V

2.11 Battery/Storage device considerations

It is challenging to utilize the harvested energy source from solar, thermal, and mechanical, directly to any target application for powering electronic devices, due to unstable and uncontrollable features of ambient energy source. In this regard, we need to store this harvested energy in a storage element such as capacitors or batteries, which are used to control and stabilize the power output for specific applications.

The selection of storage devices depends on the requirement of the application, as there are various factors for deciding the option like charge/discharge rates, power ratings, and capacity. However, considering the necessary properties for storage device, we will be covering two categories of storage elements: Primary or secondary batteries and Supercapacitors.

2.11.1 Batteries

The selection is involved based on various properties and performance factors for fulfilling stringent requirements of stable output power; some of them are the size, weight, cost, lifetime, and charging cycles. Not only this, but also application perspective is considered while selecting batteries such as operating conditions or environment where it will be deployed also impacts the performance of the system such as climatic conditions (tropical vs. arctic areas) [64].

There are two types of batteries, which are primary and secondary. ***Primary batteries*** are only for single use, also known as non-rechargeable. These batteries have a wide range of advantages such as low cost, almost ten years lifetime, various sizes, and shapes for a variety of applications. These batteries include Alkaline, Hg (oxidized mercury), Zinc-air battery, Lithium primary battery. Their major disadvantage is replacement once their lifecycle is ended, these batteries are wasted.

Secondary batteries are also known as rechargeable. Mostly, these batteries can be found in high power-consuming equipment like mobile phones, laptops, mp3 players and watches, etc. There are various types of rechargeable batteries, which include, Lithium-ion battery, Lithium polymer, lead-acid, Nickel-cadmium (NiCd), Nickel-metal hydride (NiMh). Their common usage is due to their performance, low maintenance, and being economical. Despite all these factors, they have certain limitations like their charging/discharging rate is still limited by cycling capacity [65].

Some of the battery parameters of battery types are highlighted in Table 2.4 [66], [67], for considering various properties like voltage ratings, temperature range, capacity and energy density, etc.

Table 2.4: Basic properties of various battery types

Type	Rated Voltage (V)	Capacity (Ah)	Temperature range(°C)	Cycling capacity (-)	Specific Energy (Wh/kg)
Lead Acid	2	1.3	-20- 50	500 – 1000	30 – 50
NiCd	1.2	1.1	- 40 - 70	10,000 – 20,000	45 – 80
NiMh	1.2	2.5	- 20 - 40	1000 – 20,000	60 – 120
Li-Ion	3.6	0.74	-30 - 40	1000 – 100,000	75 – 200
MnO_2Li	3	0.03 – 5	- 20 - 60	500 – 1000	30 – 50
$LiSOCl_2$	3.6	0.025 – 40	- 40 - 85	-	350

2.11.2 Supercapacitors

Supercapacitors, also known as ultracapacitors or double-layer electrolytic capacitor. As compared to batteries, they have a higher number of charging/discharging rates as compared to lithium-ion and lower voltage limits. However, according to the functionality aspect, supercapacitors lie somewhere in between rechargeable batteries and electrolytic capacitors. Classifying supercapacitors based on the type of electrolyte and electrodes used are given as: Double-layer capacitors (Their energy storage method is electrostatic), Pseudo-capacitors (storage method is electrochemical), and Hybrid-capacitors (having both features of double-layer and pseudo-capacitors).

There are certain advantages of supercapacitors over rechargeable batteries:

- Charge/discharge cycles are more abundant and longer life (10 to 20 years).
- Having a higher charging rate and could be charged within seconds [68].
- Easy interfacing, easy installation and flexible mountings.
- They have a wide range of operating temperatures varying from - 45°C to + 55°C [69].

Nevertheless, this technology has certain limitations such as the self-discharge rate, which is significantly higher than lithium-ion batteries, which is approximately 10 – 20 % of its charge

per day. On the other hand, there is a gradual voltage loss in which the output voltage is decreasing linearly with their charge [70].

Supercapacitor types are compared in Table 2.5 [69], based on various characteristics.

Table 2.5: Basic properties of various Supercapacitor types

Type	Rated Voltage (V)	Temperature range(°C)	Life cycle (-)	Specific Energy (Wh/kg)
Maxwell PC10	2.50	- 40 - 70	500,000	1.4
Maxwell BCA P0350	2.50	- 40 - 70	500,000	5.1
Green-cap EDLC	2.70	- 40 - 60	>100,000	1.47
EDLC SC	2.70	- 40 - 65	1,000,000	3 – 5
Pseudo SC	2.3 – 2.8	- 40 - 65	100,000	10
Hybrid SC	2.3 – 2.8	- 40 - 65	500,000	180

While designing any energy harvesting based system, the selection of energy storage should be catapulted based upon the source of energy, load profile, system design criteria, discharge rates, energy density, and other performance characteristics, to match the battery characteristics and input/output profile of the EH system. However, the selection of batteries will overall impact the performance of energy harvesting system.

2.12 Power consumption and Power generation: IoT and EH

As described in previous sections, the energy scavenging from the environment should be at least in milliwatts. The energy harvesting power ranges from µW to mW, as described in Table 2.1, more specifically, an overview of various energy sources concerning their generated intermittent power demonstrated in Figure 2.10 [71].

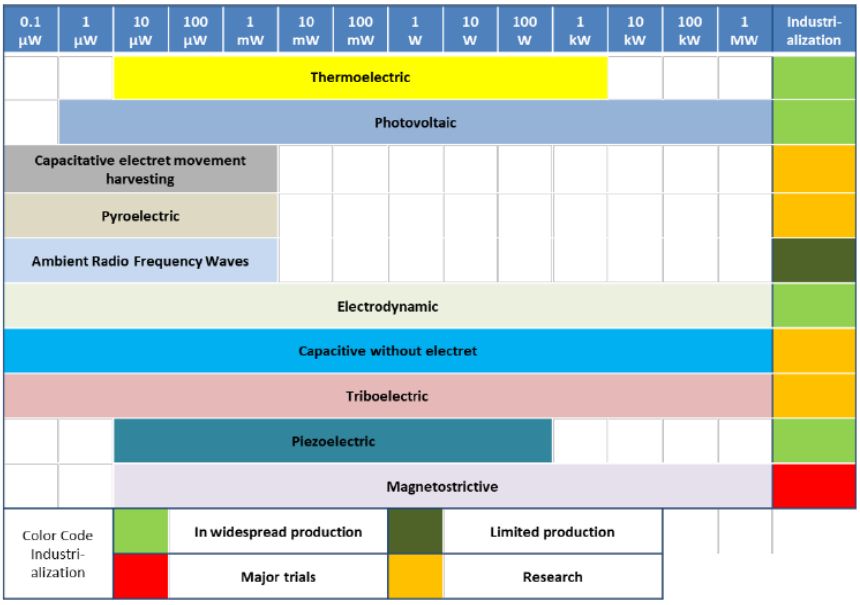

Figure 2.10: State of EH technologies and their generated intermittent power [71]

Considering the power consumption of IoT devices and sensors, which usually ranges between 0.1 µW and 1 W. As shown in Figure 2.11 [72], where harvested power is compared with generated power along with IoT devices and their associated powering requirement.

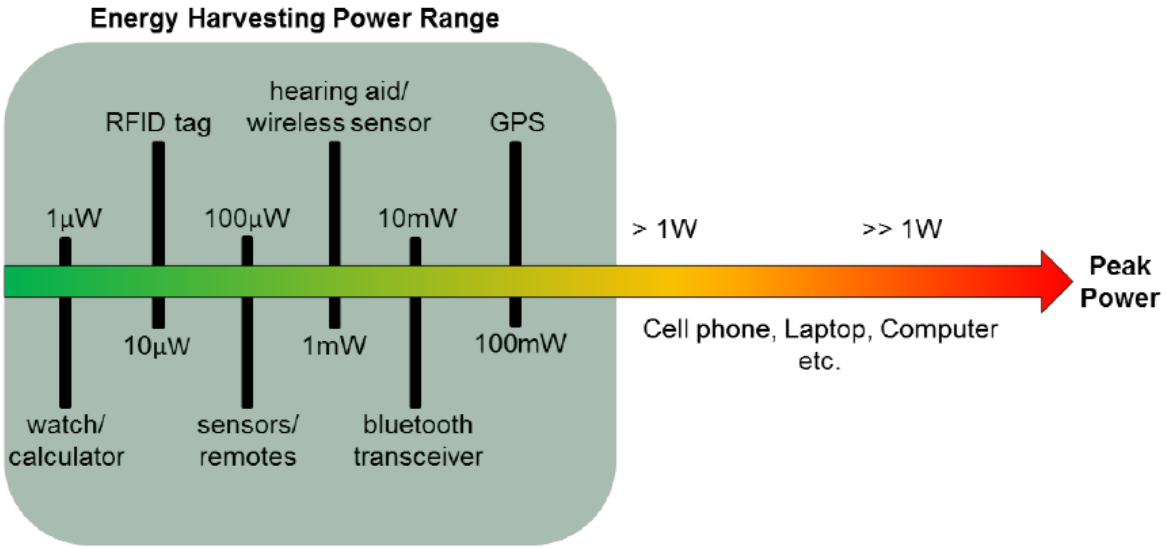

Figure 2.11: Power consumption overview of devices incl. Energy harvesting power range [72].

Therefore, designing any EH based system, we need to analyze the target application requirement in terms of power consumption, energy storage technology, energy transducers, and harvesting techniques. These critical factors are essential to consider before designing the EHS.

3 Literature Review

3.1 Introduction

This literature survey is categorized into two sections; the first one is related to overall energy harvesting based IoT applications and their associated devices. The other section belongs to the electrical modeling, and relevant methodology towards simulation study is demonstrated. However, the spice modeling and simulation for solar and thermal energy harvesting in terms of electrical perspective is the core piece of this study.

3.2 General Review

3.2.1 Solar Energy

This source is highly investigated due to its rich and abundant availability. It has the highest powering density amongst all available renewable energy sources. Researchers have contributed to bring up various solutions related to WSN and their associated applications. Let's have a look at some of the proposed prototypes to power up WSN. For *Monitoring Vibration On Bridges Through Solar Powered WSN* prototype was reported by Lee et al. [73] and Chung et al. [74]. The experiment was operating at high power dissipation, and the monitoring system was functioning continuously; as a result, the sensor node only sustained for a few hours. However, large solar panels and external battery backups are required for longer operating duration. A system proposed by Raghunathan et al, a *Solar Energy Based Wireless Heliometer Sensor Node,* as shown in Figure 3.1 [75].

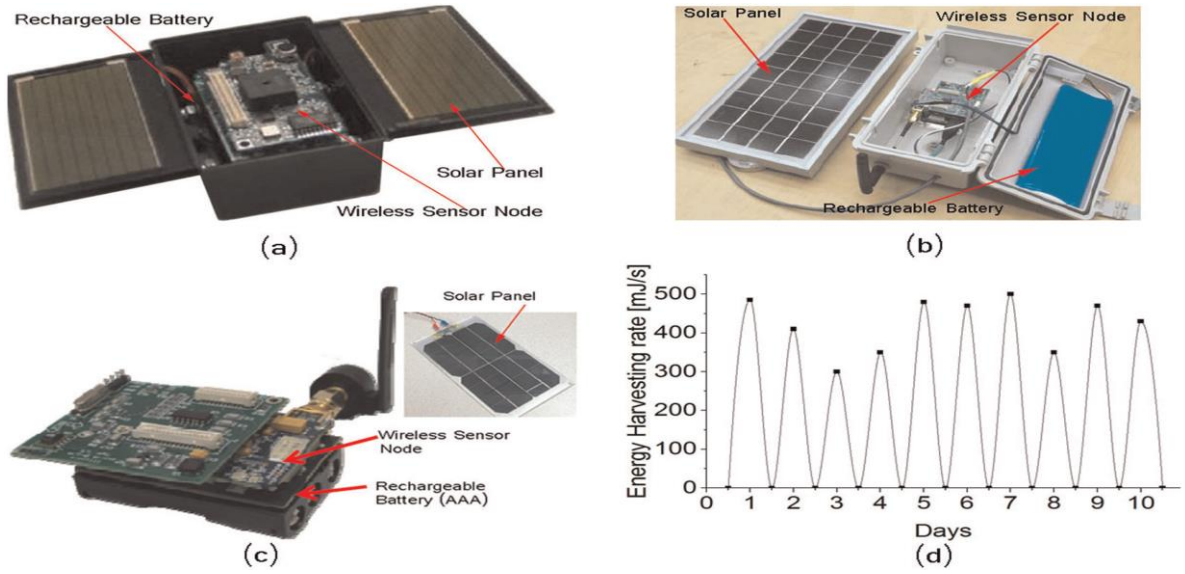

Figure 3.1: (a–c) Solar energy harvesting for SHM applications and (d) harvested solar energy distribution over 10 days [75]

The experimented results revealed that this harvester could produce maximum output power till 260 mW at 12:30 pm and 3:00 pm 200 mW, whereas, the battery was able to charge from solar panel every day sufficiently.

A *Single Source Solar Energy Harvesting Based Hydrowatch* [66], which utilizes the *TelosB* [76] platform, an algorithm for impedance matching, i.e., Maximum power point tracking (MPPT), and two Nickel metallic hybrid (NiMH) batteries as shown in Figure 3.2. Due to the algorithm, it was possible to obtain higher efficiency by generating the maximum output power of 276 mW at a voltage rating of 3.11 V. The battery consists of trickle charge circuitry and does not require any software control.

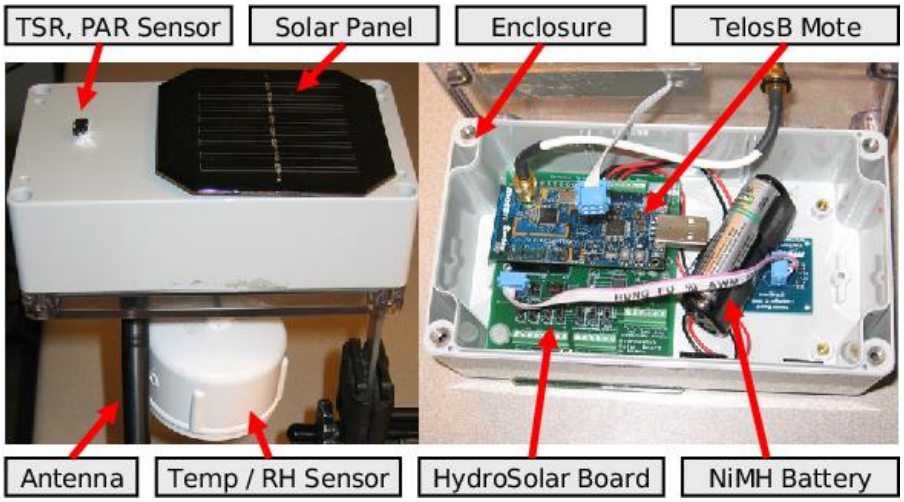

Figure 3.2: HydroWatch weather node [66]

Another reported solution for *Solar Energy Harvesting Based Sensor Node Heliomote* [77], can be seen in Figure 3.3. It consists of two NiMH batteries and is built on *Mica2* [78] platform, but the MPPT algorithm is not used for efficiency. It generates 198 mW of solar power output at a voltage rating of 3.3 V. This system comes up with a module to protect the rechargeable batteries for overcharge and undercharge scenario. It is necessary in terms of efficiency of heliomote, if it is overcharged, then it may lead to inefficiency of heliomote around 80-84%.

Figure 3.3: Heliomote: an energy harvesting sensor node, which provides environmental energy tracking capabilities [77]

A prototype experimented for bridges and transport infrastructure by Nazir et al. [79], based on *Solar Energy Harvesting Autonomous Wireless Sensors For Structural Health Monitoring (SHM)*. The system was able to generate more than 1300 mW of solar power at the output. For SHM system, another solution proposed by Ravinagrajan et al. [80], which *is Solar Energy Harvesting Based Dynamic Voltage And Frequency (DVFS) Method.* The power generation and power consumption are being adjusted by the availability of surrounding energy and the required power from the SHM system.

3.2.2 Mechanical Energy

Mechanical energy harvesting is categorized as Piezoelectric material vibrations and electromagnetic generator vibrations. The energy generated by piezoelectric is due to vibrations of piezoelectric patches or mechanical rotations, whereas, the electromagnetic energy is caused by the relative movement of the coil and magnet.

3.2.2.1 Piezoelectric Energy Harvesting Solutions

One of the earliest prototypes were suggested by Renaud et al. [81], for harvesting vibrational energy, in which *Microelectromechanical (MEMS) System-Based Lead Zirconate Titanate (PZT) Cantilever Design* was proposed. In this setup, the critical limitation is due to the inadequate frequency range by the cantilever based PEH system, where these devices operate based on the resonant frequency. An improved version of this system was reported by Liu et al. [82], in which they utilize *An Array of PZT Cantilevers* consisting of various mechanical dimensions and different resonant frequencies for improving the bandwidth of the device. *A*

MEMS-Based Autonomous SHM System was proposed by Pasquale et al. [83], in which a nickel electroplating approach was used in the system to improve the vibration frequency bandwidth till 400 Hz. Solutions were also proposed in various practical applications for wearables such as *Energy Harvesting Based Shoes* by Kymissis et al. [84] from MIT Media laboratory by utilizing PZT and polyvinylidene fluoride (PVDF) as demonstrated in Figure 3.4.

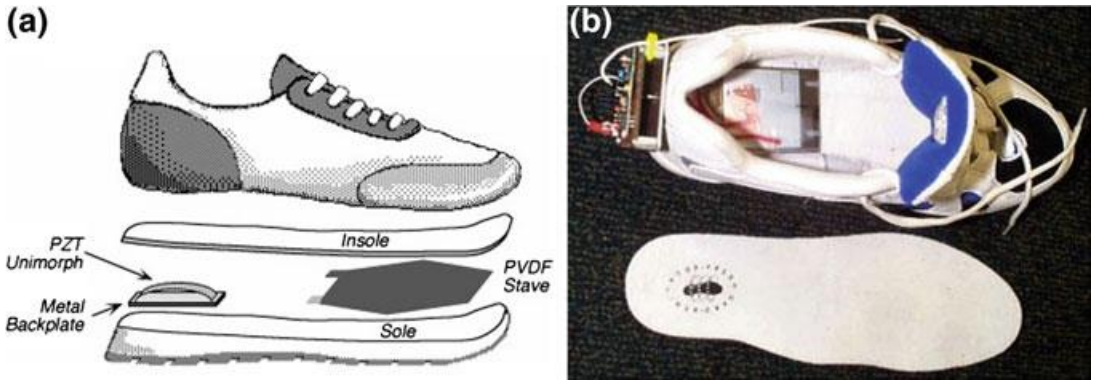

Figure 3.4: (a) Schematic diagram of the shoe-based energy harvesting device. (b) Photograph of the fabricated prototype [84]

This system was able to generate enough power to at least power up radiofrequency identification (RFID) tag. For supporting human wearable applications, ZnO nanowire-based energy harvester was investigated [85]. Lee et al. [86] designed *A Flexible Nanowire Based Piezoelectric Nanogenerator* as shown in Figure 3.5, and was able to produce an output voltage of 50 mV and output current till 200 nA. This energy was generated based on the fluttering motion of wind energy. Another system reported by Lin et al. [87], for *Transparent Flexible Nanogenerators* which were able to generate an output voltage of 8 V and output current of 0.5 μA, having the power density of 5.3 μW/cm^3. The system was detecting vehicle weight and monitoring vehicle through self-powered sensor.

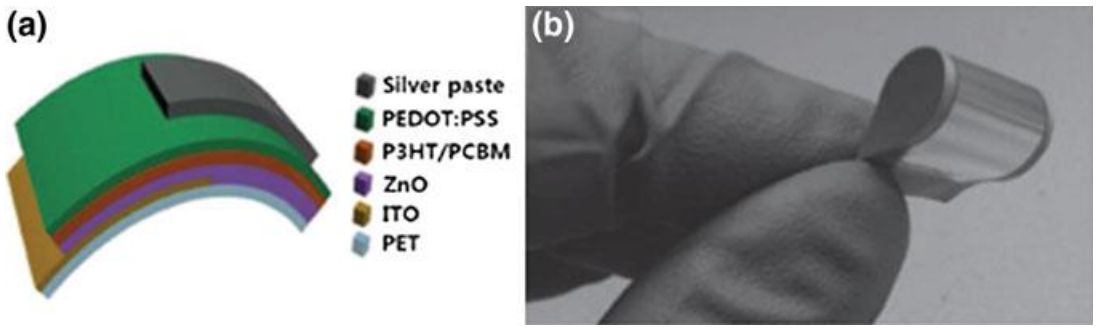

Figure 3.5: (a) Schematic diagram of the ZnO film based piezoelectric nanogenerator on a PET substrate. (b) Photograph of the super flexible piezoelectric nanogenerator [86]

3.2.2.2 Electromagnetic Energy Harvesting Solutions

The working principle of electromagnetic induction follows this type of energy harvesting, and the maximum harvested output voltage is reported until 0.1 V [88]. Various prototypes have been developed to analyse the power generation that could support IoT based applications. A prototype demonstrated by Cepnik and Wallrabe [89] in Which *A Flat Electromagnetic Energy Harvester* is used consisting of microfabricated serpentine springs for generating in-plane movement as shown in Figure 3.6. This system could generate an average power of approximately 12 µW with an acceleration rate of 1 ms^{-1}.

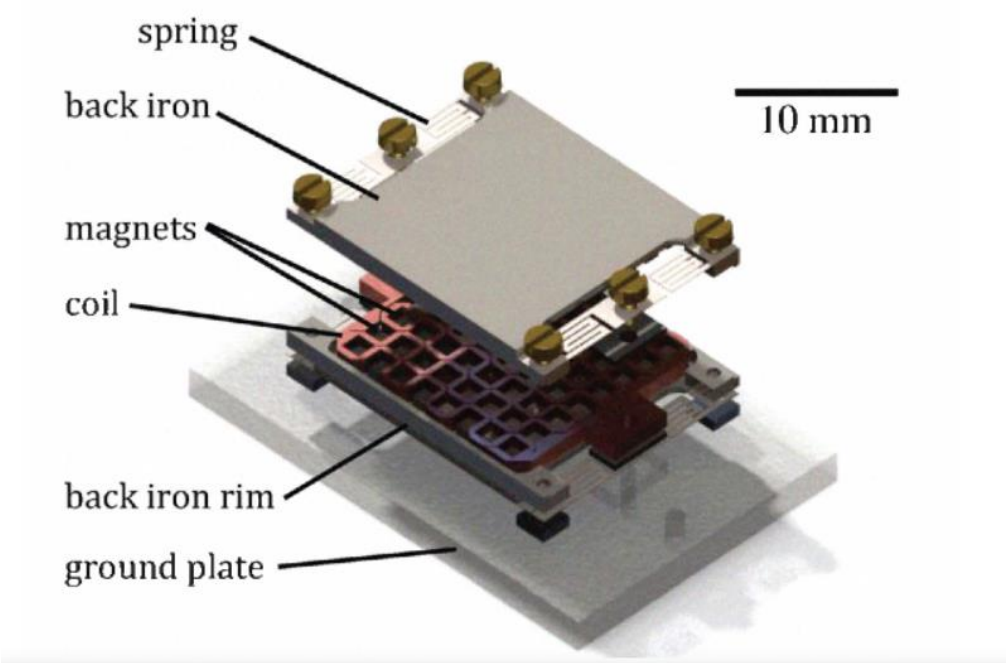

Figure 3.6: a flat energy harvester using serpentine springs for in-plane movement [89]

Another significant contribution by Donelan et al. [90] has proposed a complete *Biomechanical Energy Harvester Based on Electromagnetic Induction* System. This device is prepared explicitly for powering up prosthetic limbs and to charge other low-powered medical devices as represented in Figure 3.7. The primary benefit of using electromagnetic based energy harvesters over piezoelectric energy harvesters is due to lower device impedance, which makes them appropriate for large scale energy production but for small scale system, the decrement in size makes the coil and magnet design a critical challenge to address.

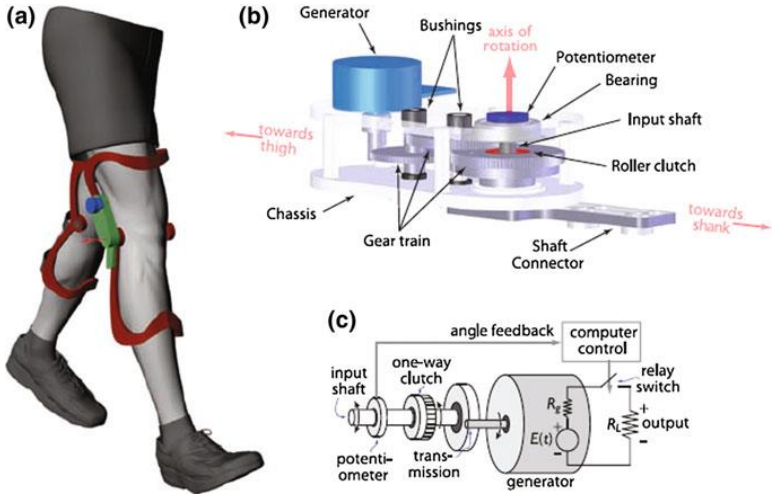

Figure 3.7: Biomechanical energy harvester (a) Device consisting of an aluminum chassis [green] and generator [blue] mounted on an orthopedic knee brace [red] (b) The chassis includes of gear train as generator (c) Schematic of a computer-controlled feedback system [90]

3.2.3 Thermal Energy Harvesting Solutions

This type of energy is considered as a viable option for powering WSN from surrounding heat or wasted heat from industrial sectors. Its major advantage over other ambient sources is due to its sustainable and reliable conversion of heat energy into electric energy without any moving parts. The solutions have been presented to target numerous applications to power sensor nodes through thermoelectric generators (TEG). One of the systems demonstrated by Samson et al. [91] where the *Prototype was Installed on an Aircraft Fuselage, consisting of a TEG with a Heat Storage, A Wireless Sensor Unit and a Voltage converter* as shown in Figure 3.8. The temperature difference for TEG was sustained by the phase change material (PCM) water contained inside heat storage. This system was capable of power up wireless sensor unit along with powering consumption of 189 µW at the voltage rating of 3.3 V.

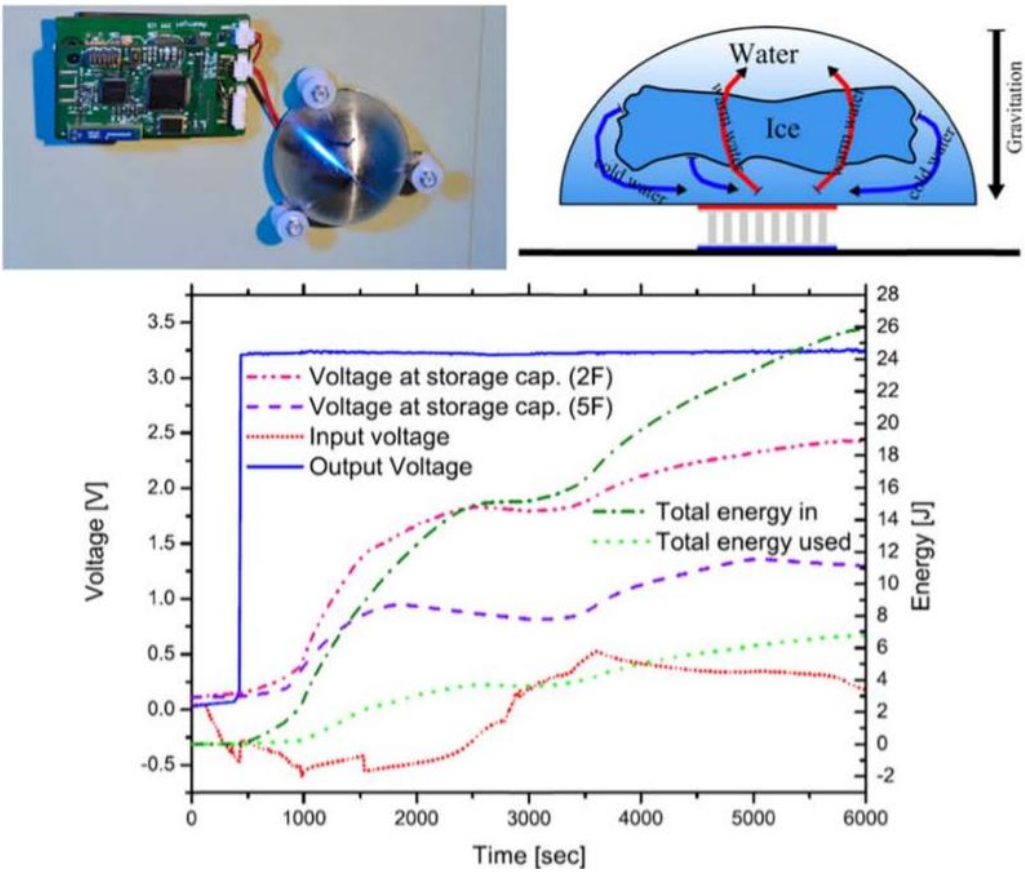

Figure 3.8: Wireless sensor system powered by aircraft specific thermoelectric energy harvesting [91]

The demand for flexible TEGs has been increased for supporting a variety of applications. As traditional TEGs are in stiff dimensions, which usually limit their use. In this regard, Kim et al. [92] proposed a *Flexible Thermoelectric Generator System to Power Wireless Sensor Node,* which is attached to a heat pipe, as demonstrated in Figure 3.9. The temperature difference is set to 20 °C and 70 °C from the heat pipe, and the surrounding air can harvest the maximum power of around 2.2 mW cm^{-2}. This power is boosted by Power management integrated circuit (PMIC) till 4.2 V and 3.3 V., The integrated TEG with WSN, can transfer and collect data from surroundings.

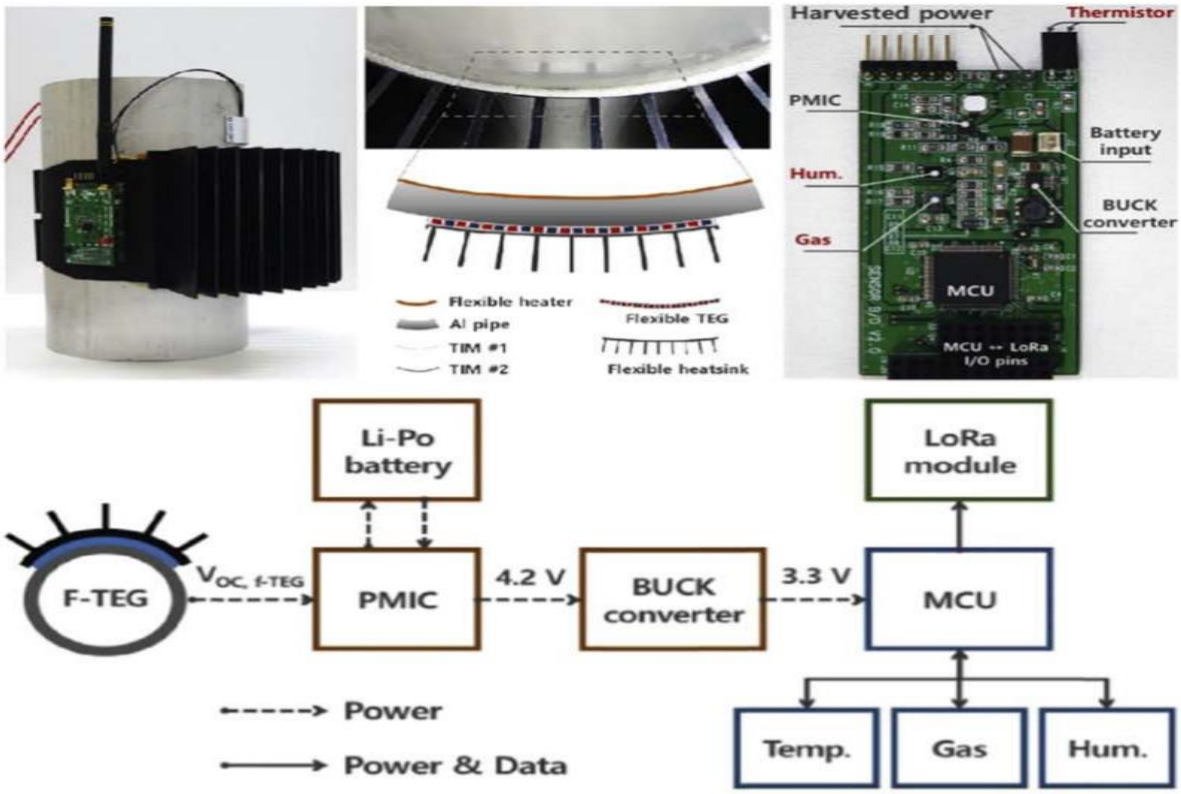

Figure 3.9: System of wireless sensor nodes powered by a flexible thermoelectric generator [92]

Another prototype for the flexible thermoelectric generator was demonstrated by Lezzi et al. [93] in which *Wireless Sensor Nodes are Integrated with Thermoelectric Generator*, as shown in Figure 3.10. In an experimental setup, the devices are attached vertically on a heat pipe, where harvested energy is boosted with a commercial DC-DC (LTC3108) PMIC. The generated power is being stored in a supercapacitor to operate the WSN for transmitting data on the temperature.

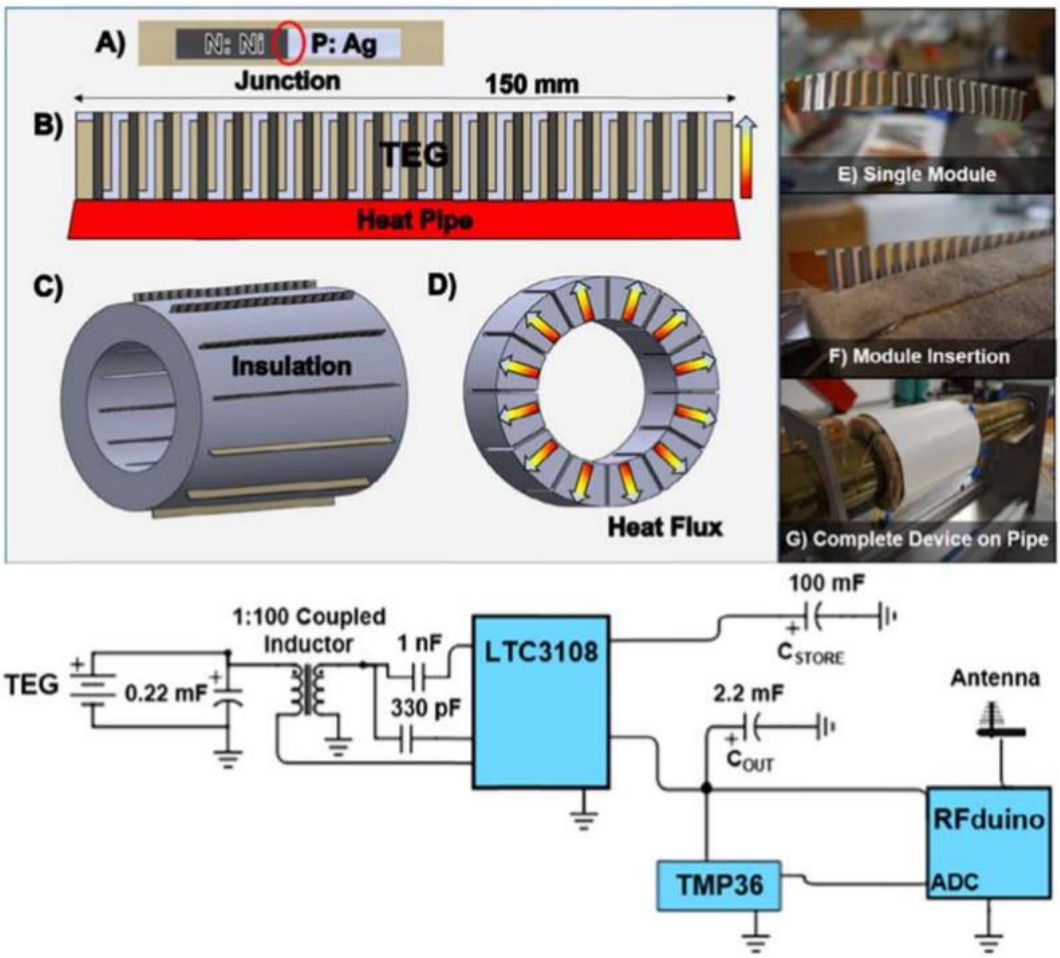

Figure 3.10: Thermoelectric generator for powering wireless sensor [93]

Apart from this, the usage of such remarkable technology has got considerable attention for medical and health care applications, specifically targeting human body heat using as a heat source to support this criterion. Thielen et al. [94] have demonstrated a *Flexible TEG on Wrist,* which is integrated with DC-DC converter as in Figure 3.11. The system utilizes two variations of TEG; which are (a) µTEG which consist of lower thermal resistance and higher output, and (b) mTEG having higher thermal resistance and lower electrical resistance.

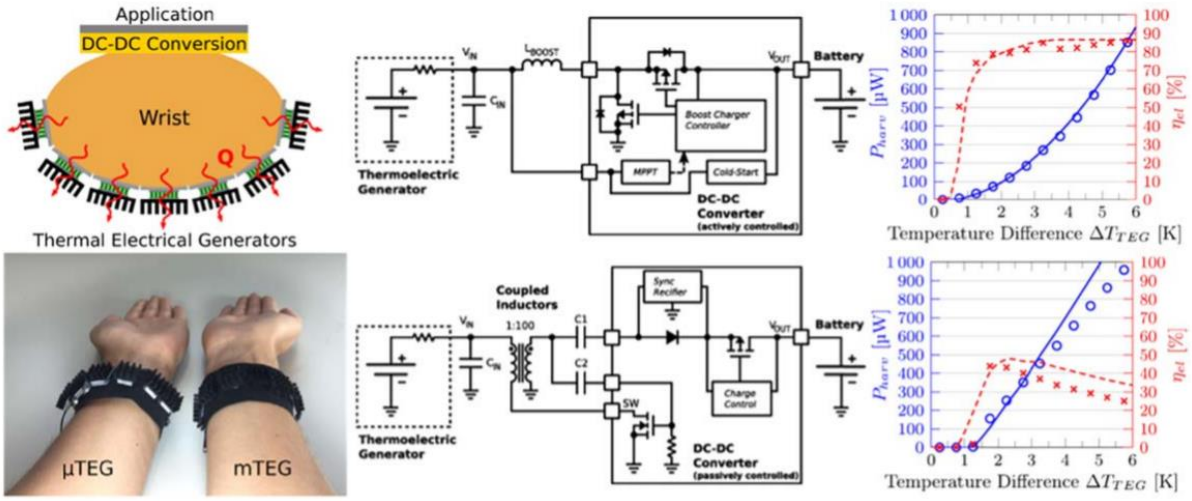

Figure 3.11: A body heat-powered wearable thermoelectric system and its conversion performance [94]

Both modules represented maximum conversion efficiency of around 24 %, and maximum output power ranges from 13 to 14 μW/cm^2.

3.2.4 Radiofrequency Energy Harvesting Solutions

The radiant energy in the form of radiofrequency (RF) is released from cellular towers, televisions, network routers, smartphones, and microwave. The RF energy harvesting systems can transform the electromagnetic energy into direct current (DC) for powering the low-powered IoT devices and WSNs. Due to one substantial benefit, which makes it preferable over solar, thermal, and other ambient sources is its indoor availability [95]. Various prototypes have been brought up to support a variety of applications, including smart homes, environmental monitoring, and health monitoring [15]. A system designed by Kim et al. [96], for *Powering an Embedded Microcontroller-Enabled Sensor Application via Ultrahigh-Frequency (UHF)* digital TV signal (512-566 MHz). They also added the dual-band (915MHz/2.45GHz) as an energy harvester. The prototype is demonstrated in Figure 3.12.

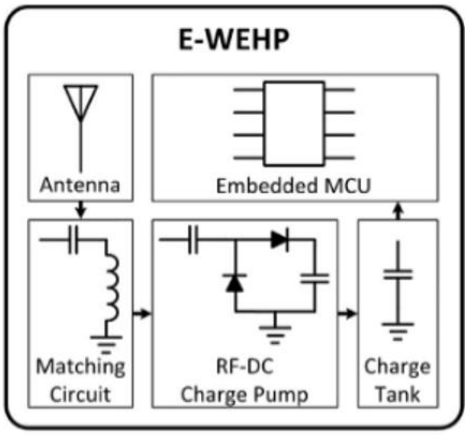

Figure 3.12: Powering an Embedded Microcontroller-Enabled Sensor Application via Ultrahigh-Frequency [96]

Another prototype reported for harvesting radiofrequency and transferring it wirelessly has been under highlight. In this regard, a system named *PowerCast* [97] has been designed who could charge electronic devices wirelessly from a certain distance, as shown in Figure 3.13. This setup includes an embedded solution that provides around 50 mA of current at a voltage rating of 5 V and works on a 915 MHz ISM band for transferring energy in the air. However, still, this solution is being limited by the objects in surroundings such as walls and trees. This system can provide around 16.115 mW of power at a distance of 0.6 m having a suitable antenna. Nevertheless, the power will start to degrade as soon as the distance will be increased (26 µW at a 4 m distance) [98].

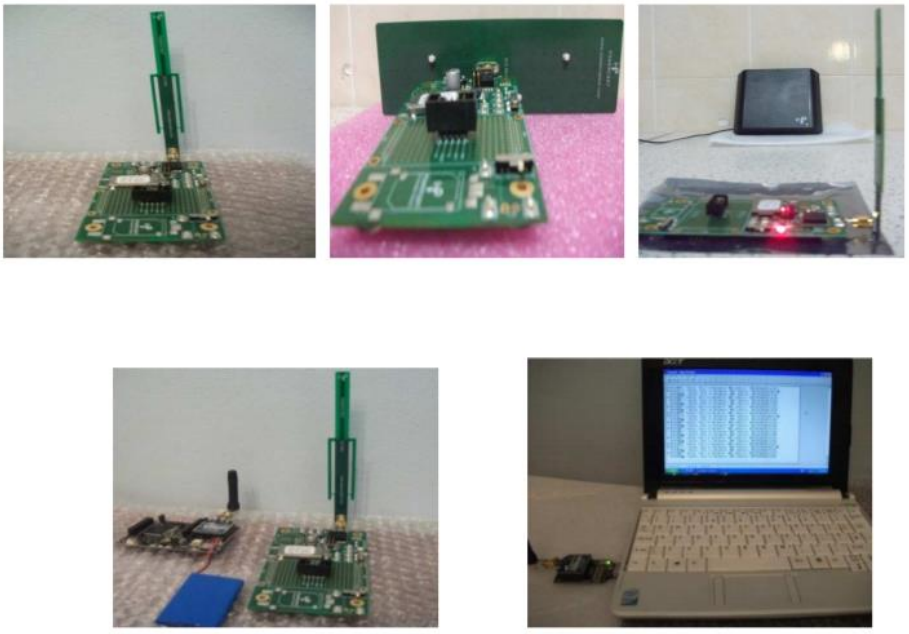

Figure 3.13: PowerCast Hardware setup [97]

The systems have been proposed in terms of extending lifespan and a broad range of applications utilizing RF for WSN-based Internet of Things (IoT). *A Self-Sustainable RF-EH Algorithm for IoT* proposed by Nyugen et al. [99] as shown in Figure 3.14. This device is adapting the energy harvesting period according to the stochastic features of incoming RF energy at sensor nodes (SN) and upcoming traffic load from IoT applications.

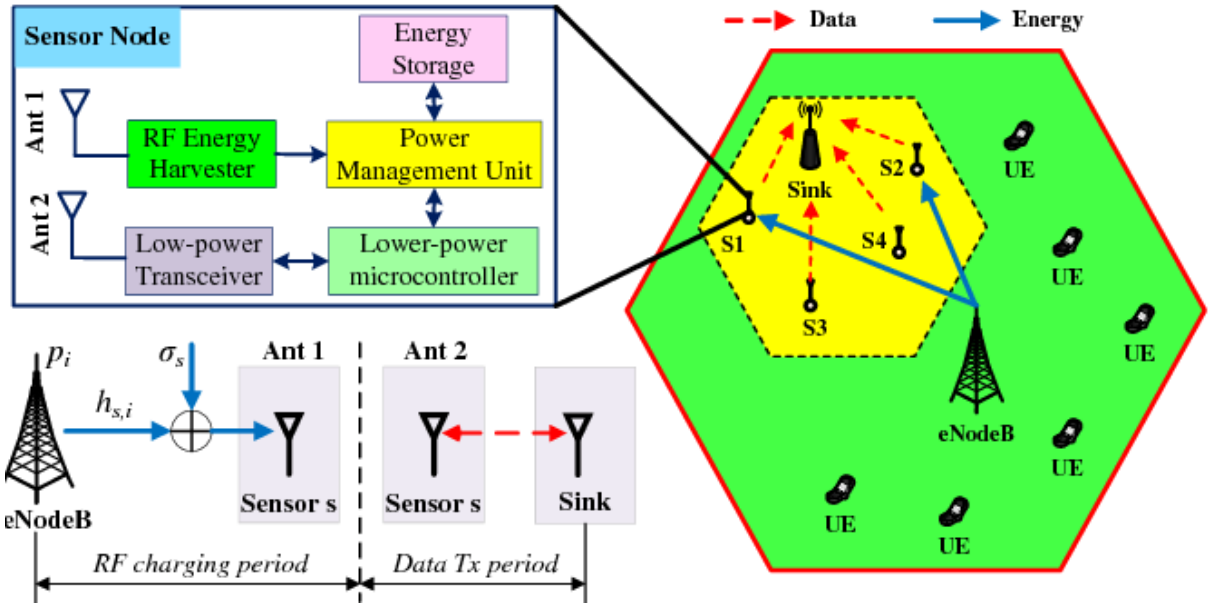

Figure 3.14: A model of RF-based energy harvesting for sensor nodes [99]

3.3 Specific Review

3.3.1 Solar Energy, Photovoltaic System and Need for Modelling

A Photovoltaic (PV) system converts the sunlight energy into electrical energy. The essential component of a PV system is a PV cell. According to the excessive need for powering sensor nodes from solar, have been continuously investigated. For any electronic application to harvest energy and then sustain the required load at the output requires power converters, a system must be studied to understand energy harvesting circuitry before implementing it to the real system. But before all these steps, one must understand and analyze the behavior and response of a PV system, and in this regard, the PV system must be modeled over a circuit simulator. As PV devices consisting of several parameters, owns a nonlinear I – V characteristics, which must be modified or adjusted by numerous experiments on simulators [100]. For such a dynamic study of a PV system that includes analysis of converters, maximum

power point (MPP) algorithms, and more specifically for modeling the whole system, we need mathematical models to represent the PV system in circuit simulators [101].

The latter section will describe the different ways and mathematical models to simulate the PV system as an equivalent circuit model.

3.3.2 I – V characteristics of Solar Cell

To measure the I – V characteristics of a solar cell, an equivalent solar circuit is required. The equivalent solar circuit is the amalgamation of a current source, which is a light generated current and the diode. This characteristic curve helps to identify various solar cell parameters such as Short circuit current (Isc), Open circuit voltage (Voc), fill factor (FF), and efficiency. Figure 3.15 represents the I – V characteristics of the solar equivalent circuit [102].

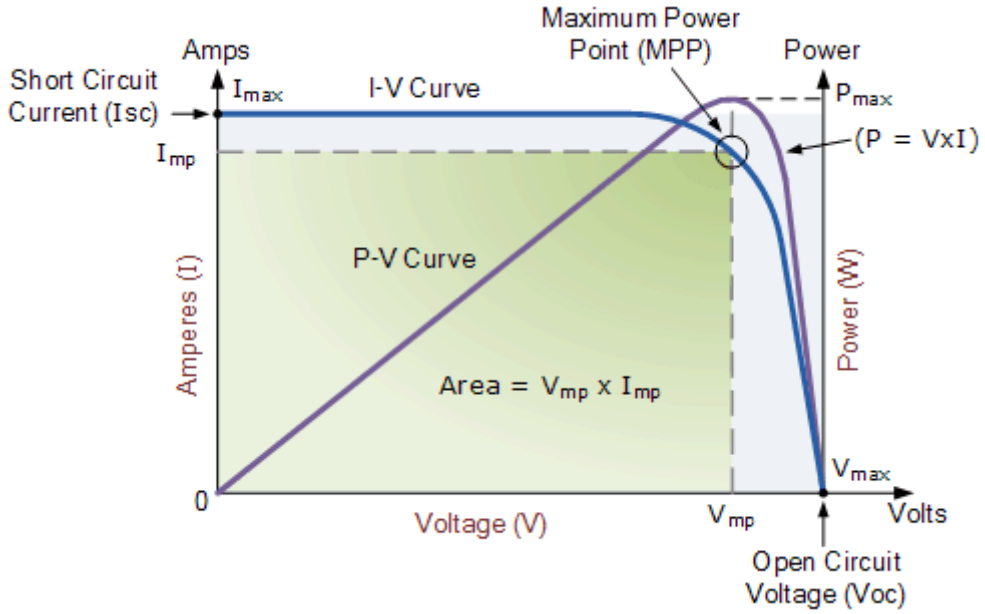

Figure 3.15: I – V curve of a typical solar cell [102]

Here Isc denotes the short circuit, as it's the current through the solar cell when the voltage across the solar cell is zero, or it is the maximum current when voltage is zero. Voc is for open-circuit voltage when it is representing the maximum voltage when current across the solar cell is zero, or it's the maximum voltage when current is zero. For calculating the maximum power Pmax of a solar cell, it is determined as the product of maximum current and maximum voltage.

3.3.3 Modeling of Photovoltaic devices

The equivalent solar circuit represents the modeling of a PV system; they define the complete I – V characteristics as a continuous function for a set of operating conditions of a cell, module, or an array. There are four solar equivalent circuit models, and three of them are used to present a single diode model as an ideal solar cell, and the remaining demonstrates the double diode model as the practical solar cell, as shown in Figure 3.16.

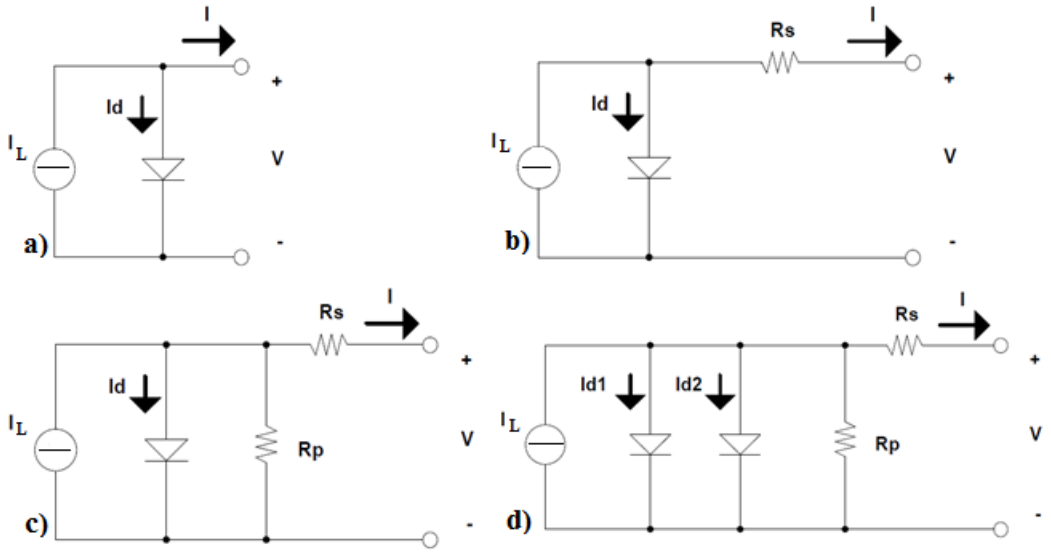

Figure 3.16: Equivalent circuit of a PV cell (a) Ideal, (b) with series resistance Rs, (c) with series and parallel resistance, Rs and Rsh, (d) with two diodes [103]

3.3.3.1 Ideal Solar Cell (1M3P)

Considering the diode in terms of features that are similar to the exponential I – V characteristics of a solar cell, that's why the equivalent circuit model is represented with diode [104]. The ideal solar cell consists of a current source in parallel with a single diode, as shown in Figure 3.17. In an equivalent circuit, there are a set of parameters that are to be defined and calculated to analyze the PV response. In this model, it has three unknown parameters to be considered.

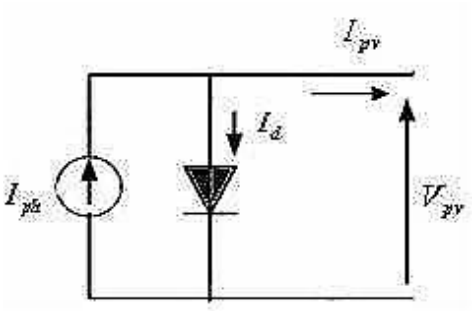

Figure 3.17: Equivalent model of single diode ideal solar cell (1M3P) [104]

The basic characteristics equation for output current of an ideal PV cell can be deduced from Kirchhoff's law [105]:

$$I_{pv} = I_{ph} - I_d \tag{3.1}$$

$$I_{pv} = I_{ph} - I_s \left[\exp\left(\frac{q.V}{m.k.T}\right) - 1\right] \tag{3.2}$$

Where, I_{ph} denotes the photocurrent (A), I_s is the reverse saturation current (A), I represents the output current of PV cell (A), V is for output voltage (V), electron charge is denoted by q (1.602 e^{-19} C), k represents Boltzmann constant (1.380 e^{-23} J/K), Temperature of PN junction by T (Kelvin) and a denotes quality factor.

The effect of irradiance and PN junction temperature conditions are represented as; the short circuit current I_{sc} is denoting the higher value of the generated current by the PV cell, and the open-circuit voltage V_{oc} represents the higher value of voltage at the output terminals [101].

This situation will be carried out as:

$$I_{sc} = I_{pv} = I_{ph}$$

For open circuit voltage $V_{pv} = 0$;

$$V_{pv} = V_{oc} = \frac{mkT}{q} \ln\left(1 + \frac{I_{sc}}{I_S}\right) \tag{3.3}$$

For short circuit current $I_{pv} = 0$;

The equation for output power is:

$$P = V_{pv}\left[I_{sc} - I_s\left(e^{\frac{qVpv}{mkT}} - 1\right)\right] \tag{3.4}$$

3.3.3.2 Solar Cell with Series Resistance (1M4P)

To predict more accurate behavior, a series of resistance can be added to the PV model. The equivalent circuit model related to 1M4P is represented in Figure 3.18. This model consists of four unknown parameters, which includes; m, I_{ph}, $I_{s,}$ and R_s. It is also called a single mechanism, Four parameters [104].

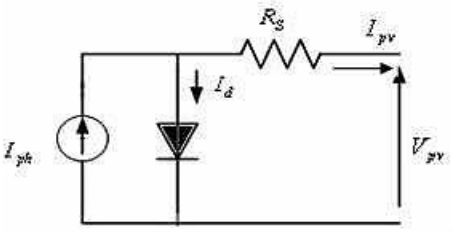

Figure 3.18: Equivalent model of single diode solar cell with series resistance (1M4P) [104]

For 1M4P, the diode current will be given as:

$$I_d = I_s\left(e^{\frac{q(Vpv + Rs\ Ipv)}{mkT}} - 1\right) \tag{3.5}$$

In this manner, the I – V characteristics equation along with single diode and series resistance will be given as:

$$I_{pv} = I_{ph} - I_s\left(e^{\frac{q(Vpv + Rs\ Ipv)}{mkT}} - 1\right) \tag{3.6}$$

Considering the irradiation and temperature of PN junction, adding the series resistance in the model infers the usage of recurrent equations for identifying the output current in the function of the terminal voltage. For this purpose, the iterative technique was tried for positive currents [106].

3.3.3.3 Solar cell with Series and Shunt Resistance (1M5P)

This photovoltaic model consist of a current source represents the light flux, a single diode connected in parallel with two resistors, one in series and shunt in parallel, which are modeling the losses. This model is also known as Single diode, five parameters (1M5P); configuration can be seen in Figure 3.19. This system comprises of five unknown parameters; m, I_{ph}, I_s, R_s, and R_{sh} [107].

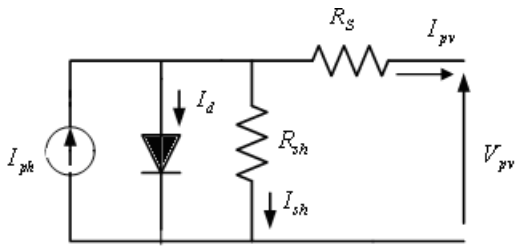

Figure 3.19: Equivalent model of single diode solar cell with series and shunt resistances (1M5P) [107]

For 1M4P, I – V characteristics equation will be deduced by Kirchhoff's law as:

$$I_{pv} = I_{ph} - I_d - I_{sh} \tag{3.7}$$

The diode current will be given as:

$$I_d = I_s\left(e^{\frac{q(Vpv+Rs\ Ipv)}{mkT}} - 1\right) \tag{3.8}$$

For shunt current I_{sh}, $I_{sh} = \frac{V+Rs\ Ipv}{R_{sh}}$

The output equation for single diode in terms of PV cell output current and terminal voltage is given by following equation:

$$I_{pv} = I_{ph} - I_s\left(e^{\frac{q(Vpv+Rs\ Ipv)}{mkT}} - 1\right) - \frac{V_{pv} + R_s I_{pv}}{R_{sh}} \tag{3.9}$$

3.3.3.4 Double Diode Solar Equivalent Circuit Model

This model consists of two diodes as a PV cell equivalent, which can be seen in Figure 3.20. This model contains five parameters in such a way that the first two parameters denote the saturation current I_{S1}, I_{S2} for both diodes D_1, D_2 respectively. Ideality factors for both diodes as m_1, m_2 as the third and fourth parameter, whereas the fifth parameter is represented as photovoltaic current I_{ph}. The resistor R_s is connected in series, and Shunt resistor R_{sh} connected in parallel. The voltage as a function across the device is denoted in terms of the ideality factor. The value for the ideality factor reaches around one when the recombination is dominated by the bulk regions and surfaces in the device at a higher voltage. For lower voltages, the ideality factor comes around two, when the recombination in the junctions dominates. This criterion of recombination is modeled by adding another diode D_2 in parallel with the first diode D_1 , and assigning the value for ideality factor m_2 equals two [108].

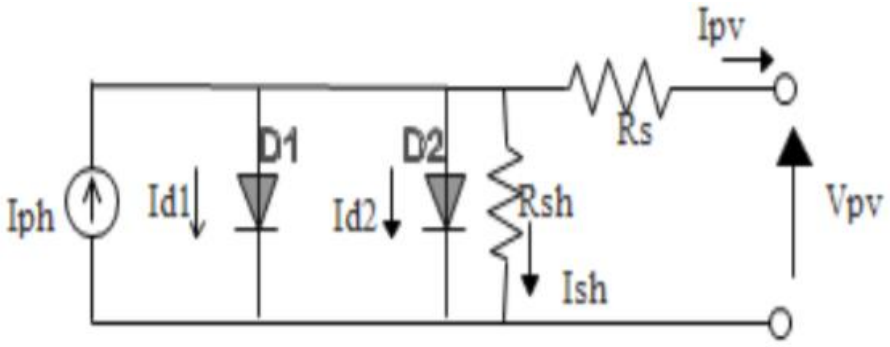

Figure 3.20: Solar equivalent circuit of Two diode model with series and shunt resistance [108]

The characteristics equation will be inferred by using Kirchhoff's law:

$$I_{pv} = I_{ph} - I_{d1} - I_{d2} - I_{sh} \dots\dots\dots \quad (3.10)$$

For First Diode D_1, the current will be:

$$I_{d1} = I_{s1}\left\{e^{\frac{q(Vpv+Rs\ Ipv)}{m1kT}} - 1\right\} \dots\dots$$

For Second Diode D_2, the current will be:

$$I_{d2} = I_{s2}\left\{e^{\frac{q(Vpv+Rs\ Ipv)}{m2kT}} - 1\right\} \dots\dots$$

For Shunt current R_{sh} is given as:

$$I_{sh} = \frac{Vpv + Rs\ Ipv}{Rsh} \dots\dots$$

For Two diode Model D_1, D_2 with series resistance R_s and shunt resistance R_{sh}, the output current Ipv is given as:

$$I_{pv} = I_{ph} - I_{s1}\left\{e^{\frac{q(Vpv\ +\ Rs\ Ipv)}{a1kT}} - 1\right\} - I_{s2}\left\{e^{\frac{q(Vpv+Rs\ Ipv)}{a2kT}} - 1\right\} - \frac{Vpv + Rs\ Ipv}{Rsh} \quad (3.11)$$

In Two diode model setup, now it contains two unknown ideality factors, which ultimately increases the number of equations, and hence calculations become more complex. However, on lower temperature and irradiance, the double diode model provides accurate characteristics curve as compared to the single diode model.

Therefore, considering above mentioned factors, in terms of feasibility and faster results, the single diode model is preferable and having less computational error as compared to double diode model and is suitable for power planning system purpose [109].

3.3.4 Solar Cell Parameter Extraction Methods

The extraction of parameters for any solar cell plays an essential role in the simulation and modeling of a PV system. The accuracy of the system ultimately depends on the mathematical module and parameter extraction method used. There are numerous techniques available to model the PV system, and they are categorized as *analytical, iterative,* and *evolutionary,* as shown in Figure 3.21.

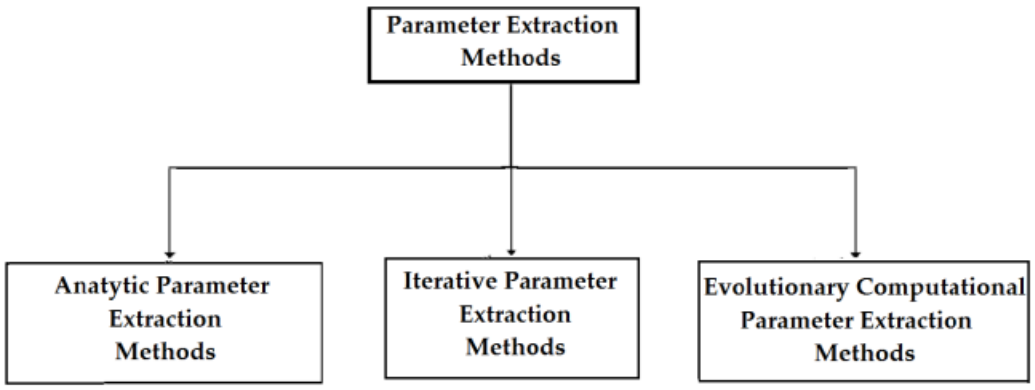

Figure 3.21: Classification of parameter extraction methods of the PV panel [110]

3.3.4.1 Analytic Parameter Extraction Methods

These types of methods are used more frequently for estimating the parameters with mathematical equations. The factor which is considerable in the calculation is that they provide results accurate, faster, and yet simpler. These equations are solved in a single iteration and do not require much computational time.

For calculating four parameters, a simple analytical method by M. de Blas et al. [111] was proposed. This method does not include the magnitude of Shunt resistor (Rsh) in PV cell parameter extraction. The researchers have introduced several methods with the usage of Lambert W-function in the extraction of parameters. An analytical method proposed by J. Cubas et al. [112], for turning the series resistor (Rs) equation into an explicit expression with the use of Lambert W-function. This method was implemented to analyze the I – V characteristics of two solar panels (Monocrystalline and Polycrystalline) at various temperatures and irradiance levels. Zhang et al. [113] projected the method with the use of Lambert W-function and a simple fitting technique to calculate all required parameters. This method was experimented on numerous solar devices that includes, Silicon based solar cells and solar modules, tandem organic solar cells, standalone organic cells, multi-junction solar cells, and dye-sensitized solar cells.

Another technique, named as a Pattern Search (PS) optimization procedure which is presented by M. R. AlRashidi et al. [114]. This method does not require derivates and makes it easier to handle the objective functions which were not always continuous or differentiable. A technique named Special Trans Function Theory (STFT) proposed by A. Jain et al. [115] for calculating the solar cell parameters. In this technique, the complete I – V characteristics were utilized without making any assumptions; hence results were generated accordingly. In comparison with Lambert W-function, STFT produced more accurate results in lesser calculation time.

The situation which occurs in analytical technique is that these methods operate efficiently under standard testing conditions (STC). But for solar models performing over a wide range of temperature conditions that are changing continuously, these models become unsuitable for them due to the implicit nature of mathematical modeling of the PV system [116].

3.3.4.2 Iterative Parameter Extraction Method

Throughout the years, various iterative methods were proposed by researchers. A. Mohapatra et al. [117] came up with the trust-region-delog method by comparing it with Villalva's iterative algorithm. In terms of parameter extraction, all five parameters were calculated by trust-region-delog method, whereas Villalva's method extracted only two parameters (Rs, Rp). Another popular method that works as a basis towards further modeling algorithm is the Newton-Raphson method (NRM), which is considered as the best-root finding method. One thing which needs to take care of while working with this method is the selection of initial conditions, as the entire accuracy of modeling and convergence depends on the best variety of initial parameters [118]. The method based on Lambert W-function using the NRM algorithm was proposed by F. Ghani et al. [119] to calculate the series and shunt resistance numerically where the current is expressed as a function of voltage explicitly. R. Khezzar et al. [120] have shown the comparison of three different techniques for parameter extraction, which are the slope method based on geometric calculation, the explicit method which is founded on analytical expression, and the iterative method built on the numerical resolution.

The problems are also reported for methods based on NRM, where it is required to calculate all five unknown parameters. In the NRM technique, another methodology called the Jacobian matrix is also needed to calculate. This matrix comprises of twenty-five elements of single and double derivate terms, which makes NRM a complicated version, quite lengthy and prone to errors [116]. This algorithm also reported the singularity problem, which is division by zero, could occur if the initial conditions are not selected appropriately. Apart from this, the

boundary conditions aren't considered for the parameters (Rs, Rsh, and a). Hence, intensive approximation is needed to solve the five-parameter extraction, and calculated parameters by NRM algorithm are found to be incorrect [116], [120].

3.3.5 Evolutionary Computational Parameter Extraction Method

The problems related to both iterative and analytical techniques can be resolved by the evolutionary methods, which utilizes Artificial intelligence (AI) to extract parameters of the solar cell, have been investigated recently. In this method, global optimization techniques are used, in which they practice iterative growth (such as the development of population). The parallel processing is handled by a guided random search for the selection of this particular population according to the desired result. These processes are stimulated by the evolution mechanism such as Genetic algorithm (GAs) [121], Simulated annealing (SA) [122], Cuckoo search [123], Particle swarm optimization (PSO) [124], Artificial bee colony (ABC) [125], etc. are used to get required solar cell parameters. Based on GA, the method proposed by M. Zagroba et al. [121] was applied to extract electrical parameters of the solar module numerically. Another approach related to GA, but combined with Nelder-Mead (NM) as a hybrid genetic algorithm proposed by J. K. Maherchandani et al. [126] in which GA generates the required data for population and NM is applied to enhance the accuracy of the generated information for the selected population.

In terms of swarm intelligence for the extraction of solar cell parameters, this technique utilizes the field test data, which is generated from the PV sensor array. The sampled data were selected arbitrarily and was used as a training setup for PSO [124]. The method based on ABC algorithm for the extraction of solar parameters was presented by M. Ketkar and A. M. Chopde [125]. In this technique, it comprises of three elements; employed forager, unemployed forager, and sources of food. The paper has presented various other methods to enhance the performance of the ABC algorithm for solving parameter optimization issues.

3.3.6 Solar Cell Modelling

The last decade has witnessed numerous modeling studies for analyzing the behavior of the solar module by applying several procedures and experimenting with associated parameters with the help of different simulation software. A solar module proposed by Banu and Istrate [127] for analyzing the I – V and P – V characteristics curve with the help of a curve fitting tool and empirical data was proposed, as shown in Figure 3.22. This paper highlighted a

limitation for generating required I – V and P – V curve is that, if there's experimental setup provided for analysis, then the data could be generated; otherwise it's difficult to gather the essential data.

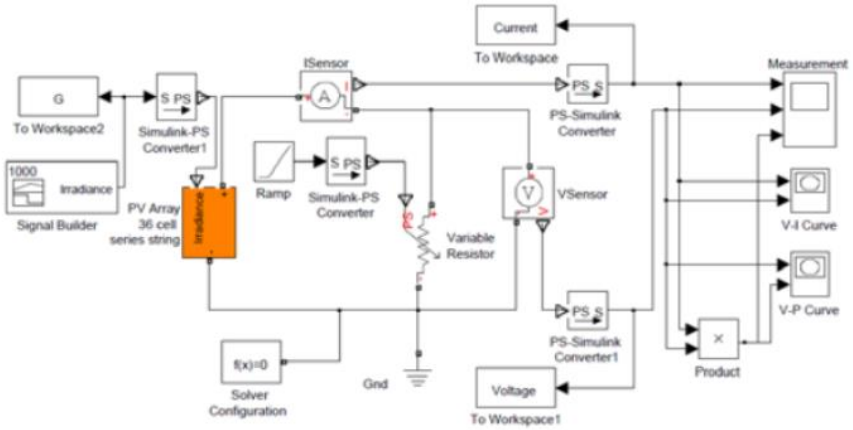

Figure 3.22: Simulink Model for PV Arrays by Banu and Istrate [127]

Another modeling system reported by Adamo et al. [128] for the IP10P solar PV model developed on already available evaluation software toolkit from MATLAB and LabVIEW has presented the calculation of required PV parameters and modeling the system under summer outdoor conditions. Number of PV models was simulated on MATLAB/Simulink application to analyze the operational and behavioral features of PV modules. The simulated data were compared with experimental results to see the difference in mathematical models [129]. The solar PV mathematical modeling in MATLAB was presented by Yatimi and Aroudam [130]. The model was simulated in the actual climatic situation of Tétouan-Northern Morocco. However, the detailed description of the simulation model used wasn't revealed by the authors as can be seen in Figure 3.23.

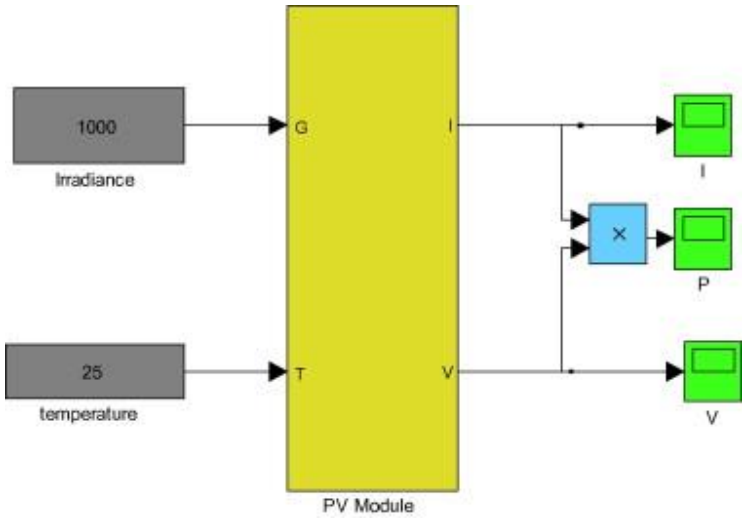

Figure 3.23: Complete PV model simulation by Yatimi and Aroudam [130]

The simulation module was presented by Mohammedi et al. [131] for modeling the number of solar models to extract their required parameters efficiently. The simulated data was used as a benchmark to compare it with the experimental data of the solar models. They also presented the performance of the simulated model to be utilized for the water pumping system. The prototype reported by Javier et al. [112] demonstrated the modeling of two commercial PV panels (Monocrystalline, Multicrystalline) under various temperature and irradiation levels by using LTspice simulator (Linear Technology Corporation, Milpitas, CA, USA), a Simulation Program with Integrated Circuit Emphasis (SPICE) software to analyze the performance and behavior of the system as shown in Figure 3.24. The authors implemented analytical formulation with the use of Lambert-W function to extract the panel parameters and have compared them with other extraction techniques.

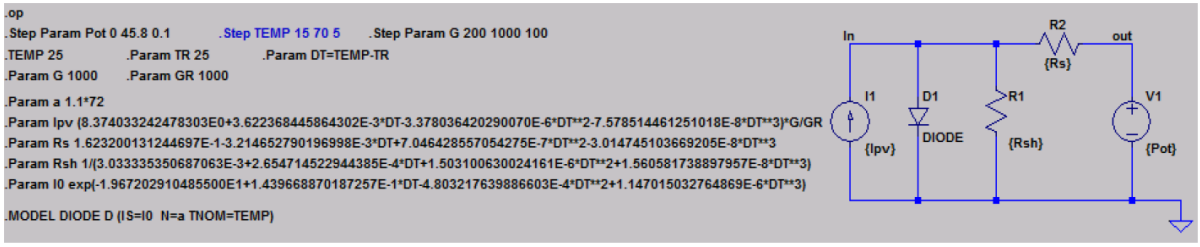

Figure 3.24: Javier et al. LTspice model for monocrystalline and multicrystalline [112]

The simulation study for the KC200GT PV module is reported by Pendem and Mikkili [132] in MATLAB/Simulink system where they have discussed the impact of partial shading in P – V characteristics curves. But unfortunately, the detailed description for the PV module in phase wise development is not mentioned. Therefore, it's challenging to reproduce the PV simulation model. The PV model module modeling in MATLAB is demonstrated in Figure 3.25.

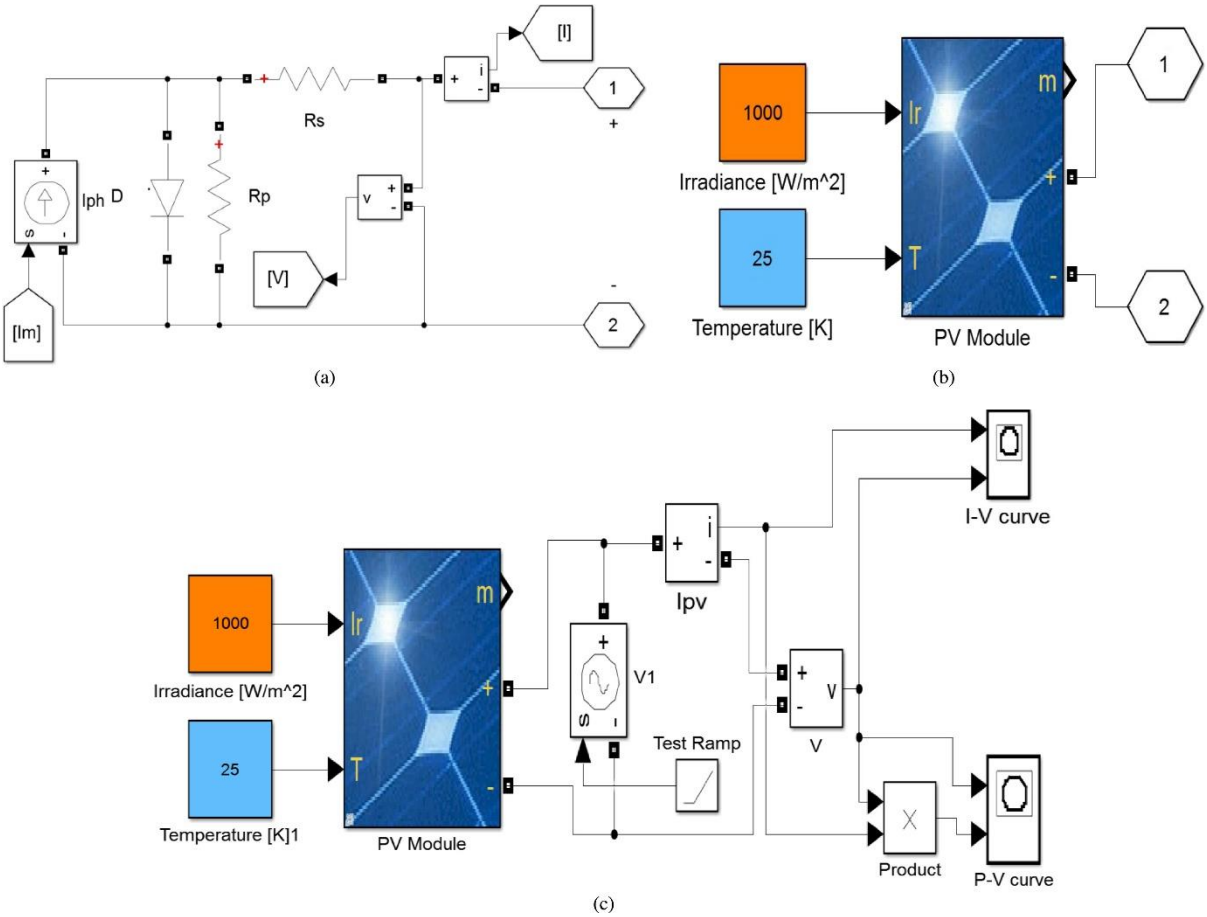

Figure 3.25: PV module modeling in MATLAB/Simulink. (a) Equivalent circuit of PV Module, (b) Subsystem model of PV module and (c) PV module simulation for output power, voltage, current and I–V and P–V characteristics [132]

Analyzing the above-mentioned PV models for solar energy harvesting, it can be concluded that there is a huge need and scope for modeling and simulation analysis studies for PV systems.

3.3.7 Thermal Energy, Thermoelectric Generator (TEG), and Need for Modelling

Thermoelectric energy harvesting received a lot of attention in recent years for analyzing their efficiency for converting thermal energy into electrical one [133]. However, various researchers are striving hard for the development of complete autonomous systems for powering WSN nodes. To obtain this system, numerous steps are required before building energy harvesting based application, out of them the most critical and mandatory one is modeling process. As there is a lack of dedicated tools handling complex modeling and simulation mechanism of thermoelectric devices in electrical and thermal domains. It raised the attention towards the development of mathematical models to facilitate the design and analysis process of thermoelectric coolers [134] and thermoelectric generators [135].

For designing any thermal-based energy harvesting application, the main concern is related to the maximum power transfer to the load. Therefore, its significant to perform simulation-based experiments under various cases and scenarios for the extraction of maximum power from the harvester.

3.3.8 Thermoelectric Generator Equivalent Circuit for Modelling

As our research work is grounded on an electrical perspective only, therefore, the power generation from TEG is focused based on circuit simulation criteria. In terms of electrical outlook, a TEG can be modeled as a constant voltage source in series connected with an internal resistance and a load resistance, as shown in Figure 3.26.

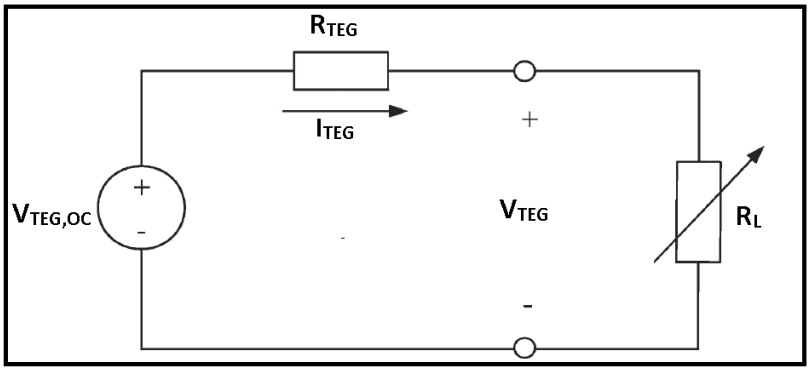

Figure 3.26: TEG electrical Model [136]

The temperature difference across TEG to the corresponding output voltage can be defined according to the formula given as [34]:

$$V_{TEG,OC} = S_e . dT \tag{3.12}$$

$$dT = T_{HOT} - T_{COLD} \tag{3.13}$$

Where, $V_{TEG,\,OC}$ represents the open-circuit voltage of TEG, S_e denotes the Seebeck coefficient of TEG expressed in mV/°K, the Temperature difference across TEG cold and the hot side is denoted by dT (where T_{HOT} is the temperature on the hot side and T_{COLD} for cold side temperature).

The power delivered to the load is calculated according to the equation given as:

$$P_{LOAD} = I^2{}_{TEG} R_L \tag{3.14}$$

$$P_{LOAD}\frac{V^2{}_{TEG,OC}}{\frac{R^2{}_{TEG}}{R_L}+2R_{TEG}+R_L} \tag{3.15}$$

Where P_{LOAD} denotes the power delivered to the load by TEG, I_{TEG} represents the output current of TEG, R_{TEG} is the internal resistance of TEG, the voltage drop across the load is given by V_{TEG}, and R_L is for external resistance.

However, the TEG current is given by:

$$I_{TEG}=\frac{V_{TEG,OC}}{R_{TEG}+R_L} \tag{3.16}$$

When the internal resistance of TEG matches the external resistance of the load, at that moment maximum power transfer from TEG to load occurs, given by equations below:

$$R_{TEG}=R_L \tag{3.17}$$

$$P_{TEG}=\frac{V^2{}_{TEG,OC}}{2R_{TEG}} \tag{3.18}$$

$$P_{TEG}=\frac{Se^2\Delta T^2}{2R_{TEG}} \tag{3.19}$$

At maximum transfer moment, the output voltage will be halved of the open circuit measurement of TEG [137].

$$V_{LOAD,MP}=\frac{1}{2}V_{TEG,OC} \tag{3.20}$$

Where $V_{LOAD,\ MP}$ represents the voltage across the load at maximum power transfer, or it is equivalent to half of the TEG open-circuit voltage.

3.3.9 I – V and P – V Characteristics of TEG

The electrical equivalent circuit for TEG described above corresponds to the Figures 3.27 and 3.28, as characterization of TEG could be graphically plotted and analyzed in terms of I – V and P – V curves for various temperature gradients. As the voltage supplied to the load

decreases with the current, and when the load and internal resistance match, the power supplied to the load reaches its maximum range.

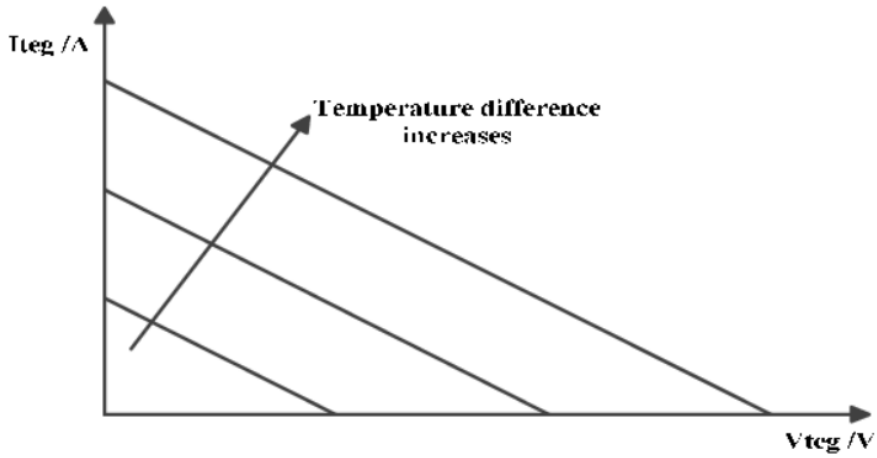

Figure 3.27: Output I – V characteristics of the TEG module

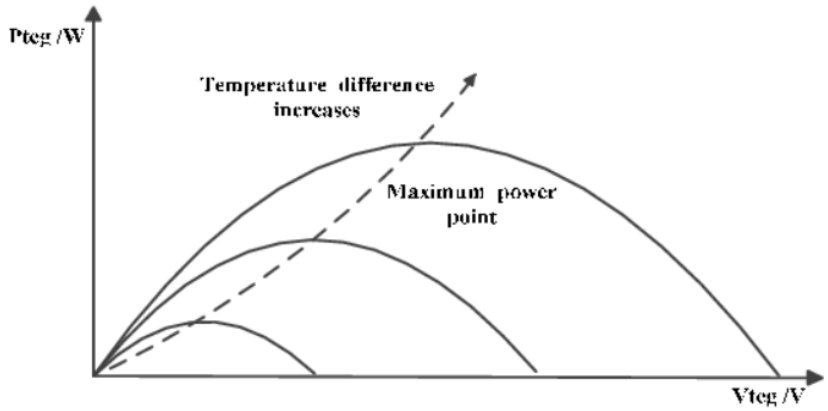

Figure 3.28: Output P – V characteristics of the TEG module

3.3.10 Parameter Extraction for TEC/TEG

Due to numerous vendors preparing TEGs in the market consisting of various parameters and having different specifications. Therefore, there isn't any standard method available for the extraction of parameters. As the manufacturer's datasheet does not reveal much about the characteristics of TEGs in terms of associated parameters. Mostly these missing parameters in datasheet make it harder for researchers and engineers to acquire required data when it comes to simulating the module in SPICE simulators and accurately mimic the performance from the datasheet. Regarding our research's aspect, which is purely electrical, the parameters of interest are Seebeck coefficient (Se) and TEG internal resistance (R_{TEG}).

3.3.10.1 Parameter Extraction through Thermocouple Scaling

One of the methods for calculating TEG parameters is through thermocouple scaling. Some of the researchers have extracted parameters through this methodology [138], [139], where engineers are required to have specific thermocouple scaling knowledge for obtaining the parameters of the module.

In this method, for calculating Se, we require number of thermocouples to be multiplied with the Se coefficient. For R_{TEG}, the device properties and assembly data, like resistivity per unit length, the total length of thermocouples, cross-section area of thermocouples, and filling factor are needed for calculating the internal resistance [139]. However, most of the time, this data is not available revealed by various manufacturers in their datasheet, which makes it way more difficult to extract these parameters through this methodology. So, we cannot always apply it to different TEG modules.

3.3.10.2 Parameter Extraction through Datasheet and Device Geometry

One of the researchers, Moumouni et al. [140], proposed the step-by-step technique to extract the required parameters of the TEG module, in which the data could be calculated by analyzing two sources; manufacturer's datasheet and information regarding device's geometrics. This data could support for estimating the parameters for thermal capacities and resistance values of selected TEG. The author has calculated eleven parameters of the TEG model (2411G-7L31-15CX1) [141] in a way as it is categorized in terms of electrical and thermal parameters, as shown in Table 3.1.

Table 3.1: Electrical and Thermal parameters of TEG 2411G-7L31-15CX1

TEM Datasheet		**Device Properties (Ceramic Plates)**		**Device Geometrics (TEM Module)**	
1	Electrical resistance	5	Aluminum thermal resistance	7	Mass of ceramic plates
2	Seebeck coefficient	6	Aluminum thermal capacity	8	Molar heat capacity of ceramic plates
3	Thermal resistance			9	Mass of Bismuth Telluride (Bi_2Te_3)
4	Thermal insulation			10	Molar heat capacity of Bi_2Te_3
				11	Overall heat capacity of TEM

The parameters calculated from datasheet belong to the 1st column of Table 3.1, where it contains four parameters, the second column representing the parameters extracted based on

the device's properties, whereas the third column showing the parameters relating to the device geometrics.

3.3.10.3 Parameter Extraction through Manufacturer's Datasheet Only

The method proposed by Kubov et al., for extracting parameters from limited data i.e., manufacturer's datasheet only, where authors presented the methodology on how we can calculate the required data regarding Seebeck coefficient, Internal resistance, and Thermal resistance with limited information through 7-step approach [142]. In this paper, the data utilized to calculate the Se and R_{TEG} are the maximum input voltage denoted by V_{opt}, maximum dissipated power at 0°C temperature difference $Q_{cold,}$ and the hot side temperature represented by T_h. At first, it is required to get the values for $V_{opt,}$ $Q_{cold,}$ and T_h from the performance curves of heat power dissipation (Q_c) vs operating voltage (V) demonstrated in the datasheet, which can be seen in Figure 3.29.

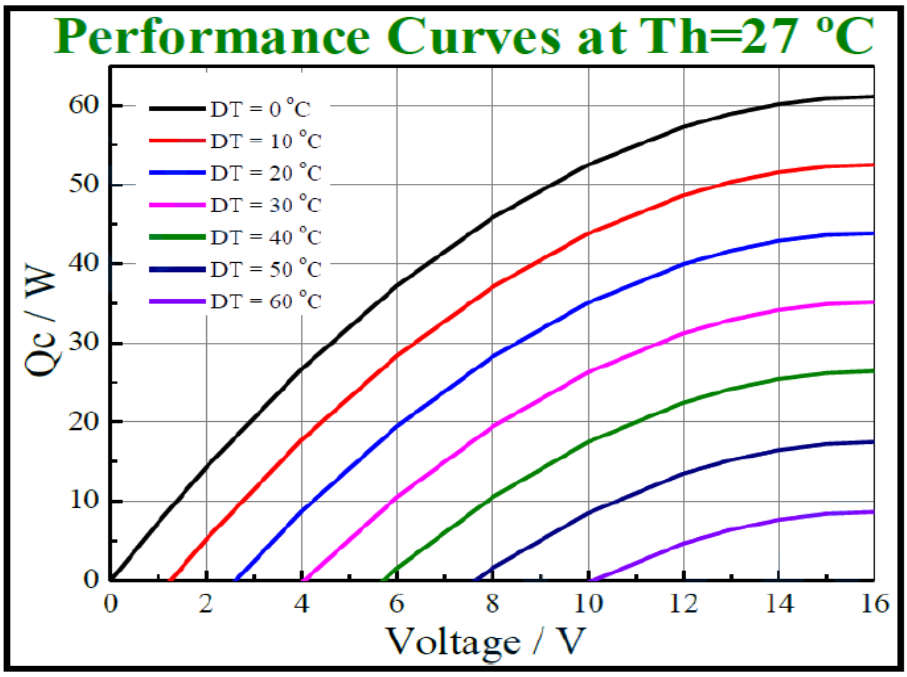

Figure 3.29: Performance curves for TEC1-12706 [143]

The related calculation is done in such a way that, firstly, the maximum output voltage has been analyzed from the graph, afterward, the Seebeck coefficient could be calculated by applying the formula. In the third step, we need to analyze the maximum performance at zero temperature difference, i.e., Q_{cold}; this could be used to determine the electrical resistance. Whereas, for thermal resistance, the Quality factor (ratio of thermal to electrical resistance) is

required to calculate the value. In this way, through a simple seven-step approach, these parameters could be extracted.

By analyzing the above three mentioned parameters extraction techniques, the most straightforward and simplistic procedure, which is best suitable for this research profile, is the third method for the extraction of parameters. Still, this method could not be generalized for all TEG modules, but usually, most of the TECs are used as TEGs [144], and such performance curves are available in the manufacturer's datasheet. Therefore, this technique could be applicable in many cases.

3.3.11 Spice Modelling of TEG

In this section, the numbers of TEC/TEG spice models will be discussed and their approach towards modeling in terms of parameters used and the type of equivalent circuits in their proposed work for modeling thermal to electrical analogy.

The spice model proposed by Chen et al. [145] for TEG in transient analysis via an electro-thermal structure. The authors modeled the heat transfer rate for analyzing the impact of thermo-electric coupled multi-field of TEG. However, the typical values were selected for hot and cold sides (Th and Tc), which cannot mimic the dynamic characteristics of the system. Another spice model highlighted by Chavez et al. [146] for modeling the Peltier cooler by three port spice models by considering the electrical parameters for heat transfer, as shown in Figure 3.30.

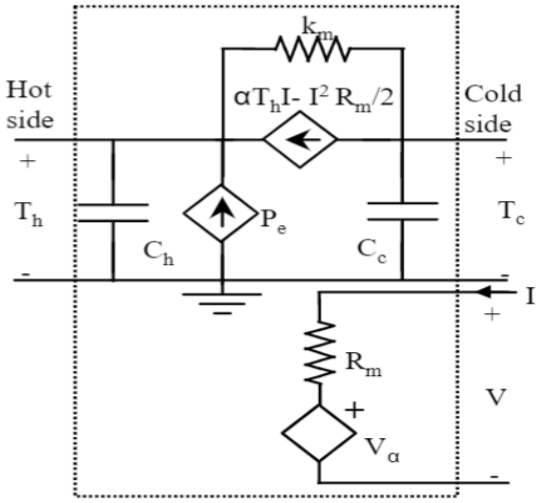

Figure 3.30: Chavez et al Spice Model [146]

Another study was reported for analyzing the modeling of TEC and TEG in terms of electrical equivalent circuit by Simon and Sam Ben-Yaakov, as shown in Figure 3.31. This study

revealed that the modeling of both modules is almost same, in such a way that the same electrical model could be used for simulating the different behaviors, only by providing the direction of current in reverse [147]. But their model couldn't produce the accurate simulation result, as thermal resistance and thermal capacitance of the TEG module wasn't considered in the equivalent circuit.

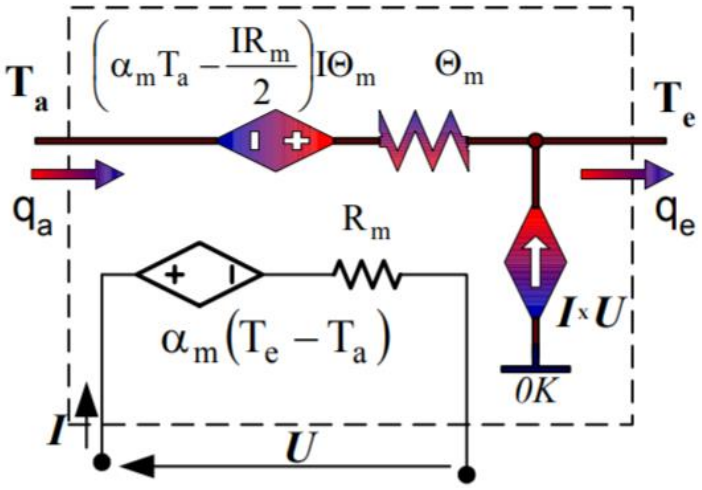

Figure 3.31: Simon and Sam Ben-Yaakov Spice model [147]

An improved version for micro TEG was proposed by Mirocha and Dziurdzia [148] for spice simulation in which the Peltier model's dependence of internal resistance varying with temperature differences was also applied on the model as demonstrated in Figure 3.32. Hence the model proved to be accurate when it was considered under the small temperature range.

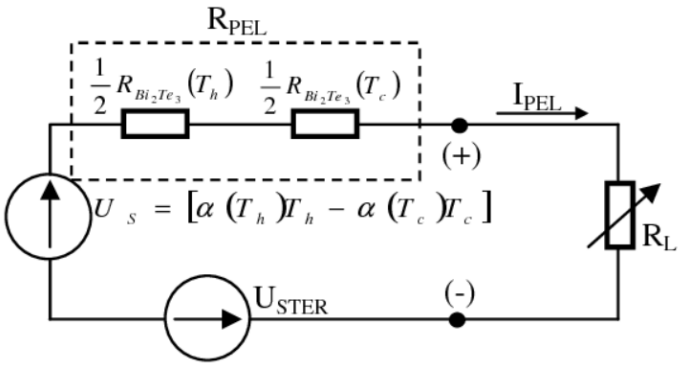

Figure 3.32: Mirocha and Dziurdzia Spice model [148]

An LTSpice based energy harvesting circuit was proposed by Mihail [149], for analyzing the variations in different thermal parameters such as thermal conductance, Seebeck coefficient, and internal resistance. In this model, the heat transfer was from hot to the cold side and related

to DC- DC converter LTC3105 to enhance the output voltage of TEG according to the required output power level of the system.

Yacouba Moumouni and R. Jacob Baker [150] proposed the LTSpice model for TEG in which they included the intrinsic internal parameters of varying temperatures. To raise the accuracy of the model, the impact of the parasitic component and their temperature dependence were also taken into consideration. The model was used to analyze the characteristics and performance of commercial TEM. The model has utilized the reverse polarity to operate the TEC as a TEG. Though the simulation data was compared with experimental data, which showed the error rate around 5.47%, which was due to internal parasitic components and heterogeneous physical blocks as mentioned by authors. The LTspice model can be seen in Figure 3.33.

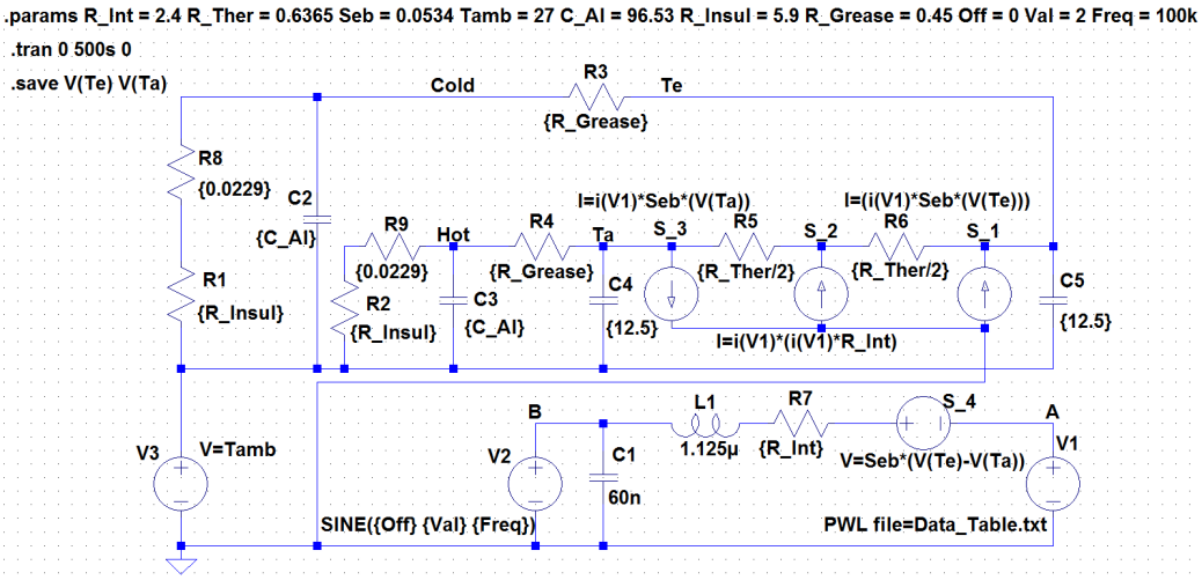

Figure 3.33: LTspice model of a TEM with the internal parasitic LC values [150]

The interconvertible spice model proposed by Kubov et al. [142] in LTSpice for both Peltier and Seebeck effect, which converts electricity into heat and heat into electricity, as shown in Figure 3.34. It contains a small set of variables, which are Seebeck coefficient Se, Electrical resistance Rteg, Thermal resistance Rq and Heat capacity Cq. The first two parameters belong to the electrical aspect, and the remaining two defines thermal aspects. This model is providing a straightforward approach and contains symmetric structure of the electrical scheme; it also provides transparency in the SPICE model, which could be transferred and adapted in an extended version.

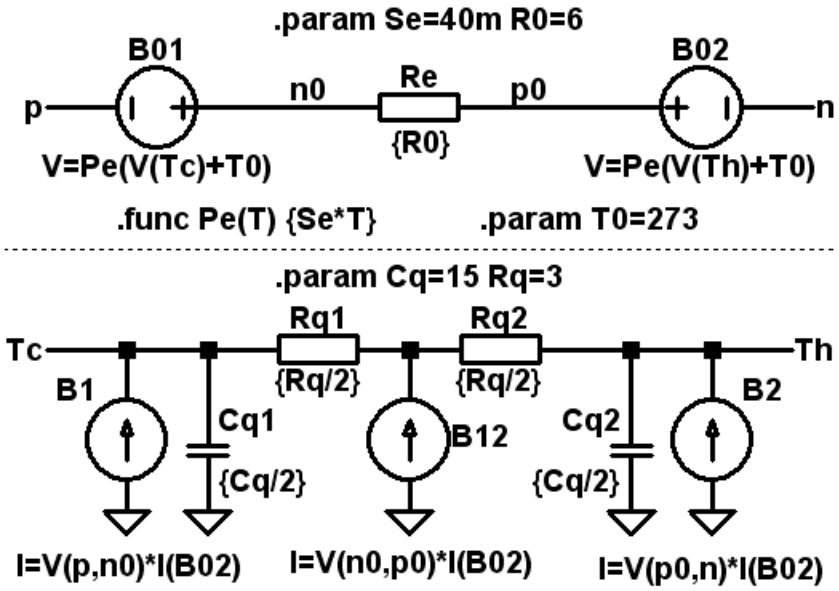

Figure 3.34: Kubov's LTspice-model of Peltier–Seebeck element [142]

Therefore, by analyzing all the above-mentioned models for simulation and modeling and according to the required research profile, the Kubov's model has been selected due to its simplicity and straightforward approach in parameter extraction.

4 Proposed Research Methodology

4.1 Introduction

The modeling and simulation study has been carried out for two energy harvesting sources; Solar and Thermal. This study aims to establish a systematic step-by-step approach for designing an Energy Harvesting (EH) based system to power up low-powered devices. Mostly, dedicated tools are absent for simulating and modeling the energy harvesting system, and it's providing the hurdle for end users who would like to build their target applications and requires proper guidance in a short period. Through this simulation study, two prototypes for harvesting energy systems are modeled and characterized in various parameters to analyze the behavior of the system and, most importantly, to generate the output power under different load configurations.

Before implementation of the system on physical hardware, it's highly required to build a prototype and analyze the various responses within the system, precisely the compatibility issues, power generation and power consumption, load requirement, and sustainability.

The generated power will be compared with already designed solar and thermal energy harvesting models in terms of power generation, and the output will be compared to the IoT power requirement of a specific application at the end.

The visual representation of the entire workflow is demonstrated in the next section for proper understanding of the building approach of any energy harvesting based application.

4.2 Proposed Methodology for Achieving Research Objectives

Considering the energy harvesting current users, there isn't any standard and clear user-defined profile available for building an EH based IoT system. The users ranging from industrial sectors to private sectors would like to save their project-related costs for electricity consumption. Regardless of better insight of energy harvesting based solutions between users, there's still a massive demand among them towards a better knowledge of their energy harvesting system for getting maximum efficiency from it, in terms of expenditure and returns. Apart from this, both solar and thermal energy sources are highly complicated as they are dependent on environmental conditions, and their selection of the transducers will directly impact the output. These stringent setups are making modeling a necessary tool towards building and optimization of the EH system.

The comprehensive approach has been carried out for modeling and simulating the chosen energy harvesting sources. Each segment contains extensive literature and solution-based criteria in it, which will be described in detail in upcoming sections.

For a general understanding of the procedure, Figure 4.1 is demonstrated here, as it starts from the selection of energy harvesting sources as the basis towards the energy power generation for circuitry. Chapter 3 has discussed available energy harvesting sources in detail about their associated transducers and related application. Hence, according to the research profile, two sources have been taken under consideration; Solar and Thermal.

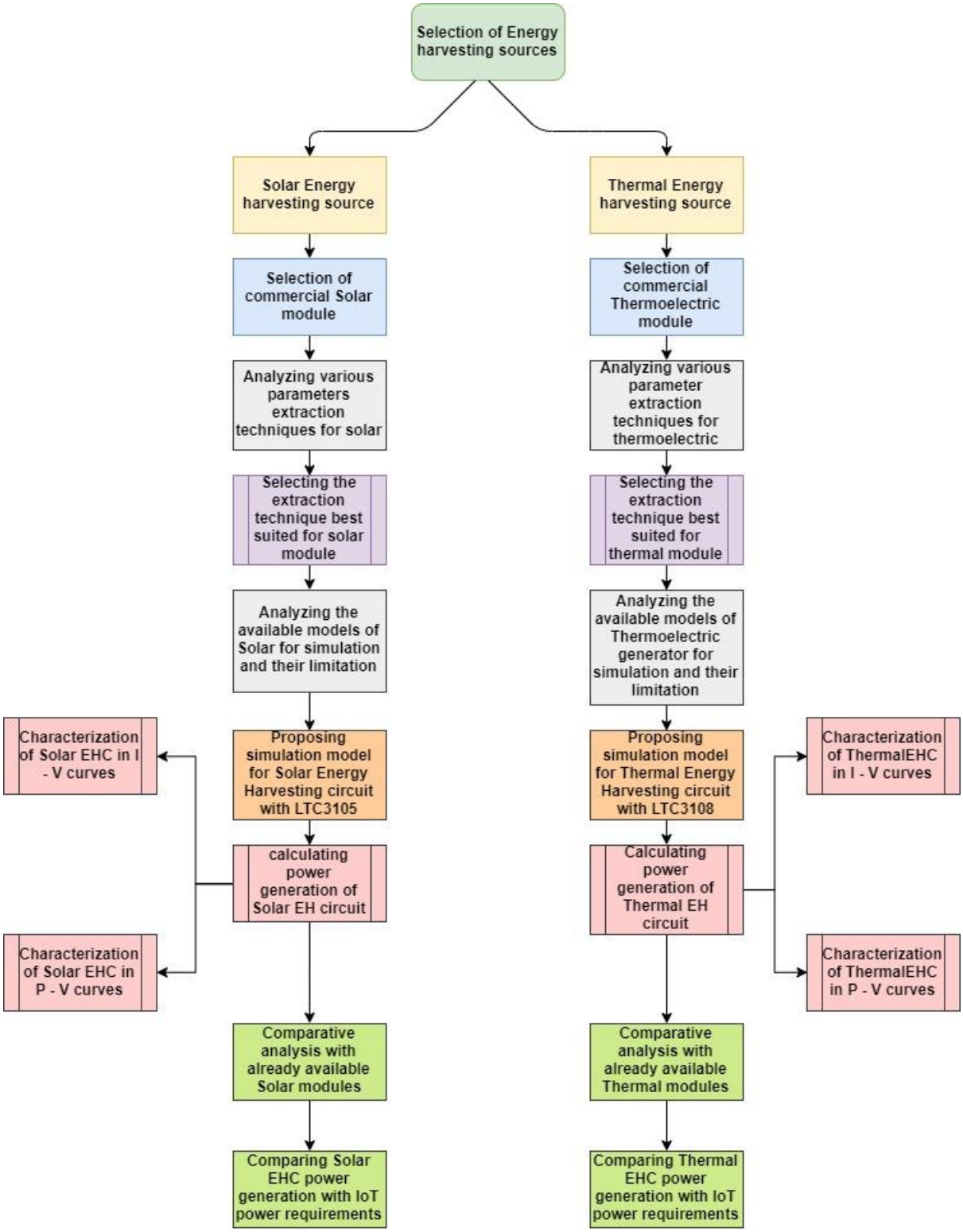

Figure 4.1: Systematic procedure towards building a Solar and Thermal based Energy Harvesting circuitry for low-powered devices.

4.3 Solar Energy Harvesting Module

For building an Energy harvesting based simulation setup, the first and the principal characteristic is to harvest the solar energy. One aspect to understand here is that it's a purely electrical circuit simulation analysis. Therefore, the selected commercial device will be modeled and simulated on the simulator under several scenarios to analyze the behavior of the entire setup and output power generation. The modeling of solar modules is traditionally achieved through experimental structures and numerical fittings, which is, however, not practical and affordable for small scale users to analyze the characteristics and efficiency of the panel due to limited information available in manufacturer's datasheet.

4.3.1 Selection of Solar Module for Modelling

For harvesting solar energy, it is required to have a transducer to transform solar energy into electrical energy. Here, the selection of the module and related techniques are implemented after a thorough investigation of the solar energy. In this regard, a commercial solar model MC-SP0.8-NF-GCS from Multicomp [151] has been selected to analyze the behavior of the module over the number of parameters for characterizing the Energy harvesting system's requirement. This module is specifically designed for energy harvesting based applications specifically in wearable devices. This product claims to have a higher efficiency rate, easy installation, withstanding high wind pressure, and snow load. This module is chosen due to its features supporting IoT and power generation requirements, matching this research profile so far. Figure 4.2 demonstrating the dimensions in millimeters and physical appearance of the solar module.

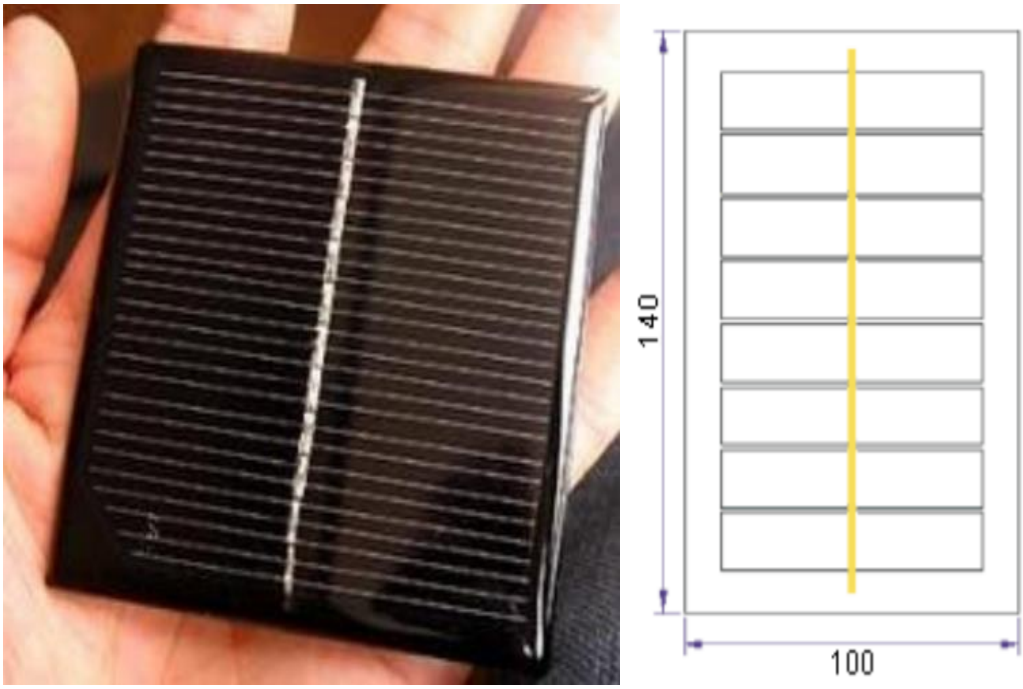

Figure 4.2: Muticomp's Solar model MC-SP0.8-NF-GCS along with dimensions

4.3.2 Mathematical Modelling of Solar Equivalent Circuit

To simulate the actual commercial solar model on the simulator, it is required to transform the characteristics of the chosen model in terms of electrical specifications over the simulator. For this purpose, the equivalent circuit is a tool which could help to mimic the definite circuitry for analysis and designing purpose. In terms of the solar model, the equivalent solar circuit is required for modeling the system.

Various solar equivalent circuit models have been discussed in Chapter 3, section 3.4.4, with basic understanding and their associated derived equations. However, according to research parameters, the recommended model which has been chosen for simulation purpose is **Single Diode Five parameters (1M5P)** [107] consisting of Series resistor *(Rs)* and Shunt Resistor *(Rsh)* as shown in Figure 4.3.

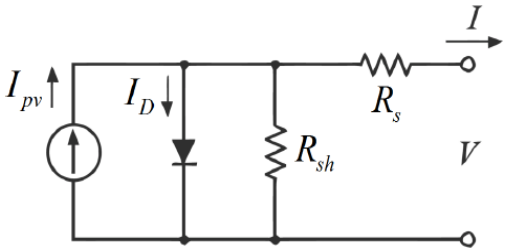

Figure 4.3: Single Diode Five parameters (1M5P) Solar equivalent circuit [107]

As this circuit has already been described, the characteristic equation for calculating the unknown parameters will be given as:

$$I = I_{PV} - I_O - I_{sh} \tag{4.1}$$

To fully define the relationship between the output current of the photovoltaic cell and the terminal voltage for the single diode model is given by the following equation:

$$I = I_{pv} - I_o\left[exp\left(\frac{V + IR_s}{aV_T}\right) - 1\right] - \frac{V + IR_s}{R_{sh}} \tag{4.2}$$

Along with Thermal Voltage; $V_T = n\frac{KT}{q}$ [V]

Where *Ipv* denotes the current generated by the incidence of light, *Io* denotes the saturation current of a diode; *Rs* represents the series resistance, For leakage current *Rsh* is denoted as Shunt resistor, *a* is the ideality factor, *Vt* is the thermal voltage, *q* as an electron charge, the Boltzmann constant *K*; the n as number of cells in series and *T* as the temperature.

4.3.2.1 Lambert W-Function; Transforming Implicit Expression into Explicit

For determining the values of Rs and Rsh resistors depicting the losses inside the solar module, it is mandatory to calculate the voltage and current of the solar module. This calculation ends up in creating the implicit expression. The problem arises when it comes to solving implicit expressions, as they consume a lot of time and are unstable at the same time. In this regard, we need to solve this expression into the one which could be solved quickly. Therefore, this expression can be converted to an explicit by applying the Lambert W-function strategy in such a way that voltage could be resolved as the function of the current and vice versa [152] [153].

The equation follows the four-boundary condition expressed in detailed derivation by [112].

The implicit expression for Rs is derived as:

$$\frac{aV_TV_{mp}(2I_{mp} - I_{sc})}{\left(V_{mp} - I_{sc} + V_{oc}(I_{mp} - I_{sc})\right)(V_{mp} - I_{mp}R_s) - aV_T(V_{mp}I_{sc} - V_{oc}I_{mp})} = \exp\left(\frac{V_{mp} + I_{mp}R_s - V_{oc}}{aV_T}\right) \tag{4.3}$$

Equation for shunt resistor Rsh:

$$R_{sh} = \frac{(V_{mp} - I_{mp}R_s)(V_{mp} - R_s(I_{sc} - I_{mp}) - aV_T)}{(V_{mp} - I_{mp}R_s)(I_{sc} - I_{mp}) - aV_T I_{mp}} \tag{4.4}$$

Equation for saturation current $I_{0:}$

$$I_0 = \frac{(R_{sh} + R_s)I_{sc} - V_{oc}}{R_{sh}\exp\left(\frac{V_{oc}}{aV_T}\right)} \tag{4.5}$$

Equation for photocurrent I_{pv}:

$$I_{pv} = \frac{R_{sh} + R_s}{R_{sh}} I_{sc} \tag{4.6}$$

As equation is in implicit form, which will now be transformed into explicit by applying Lambert W-function [153].

Lambert W-function W(Z) is denoted as:

$$z = W(z)e^{W(z)} \tag{4.7}$$

Here z represents any complex number.

For solving the exponential equation, following equivalence will be used for applying the Lambert W-function:

$$X = Ye^{Y} \Leftrightarrow Y = W(X) \tag{4.8}$$

Now Equation for Rs will be written as after applying the equivalence:

$$-\frac{V_{mp}(2I_{mp} - I_{sc})}{V_{mp}I_{sc} + V_{oc}(I_{mp} - I_{sc})}\exp\left(-\frac{2V_{mp} - V_{oc}}{aV_T} + \frac{(V_{mp}I_{sc} - V_{oc}I_{mp})}{\left(V_{mp}I_{sc} + V_{oc}(I_{mp} - I_{sc})\right)}\right) =$$
$$\left(\frac{I_{mp}R_s - V_{mp}}{aV_T} + \frac{(V_{mp}I_{sc} - V_{oc}I_{mp})}{\left(V_{mp}I_{sc} + V_{oc}(I_{mp} - I_{sc})\right)}\right)\exp\left(\frac{I_{mp}R_s - V_{mp}}{aV_T} + \frac{(V_{mp}I_{mp} - V_{oc}I_{mp})}{\left(V_{mp}I_{sc} + V_{oc}(I_{mp} - I_{sc})\right)}\right) \tag{4.9}$$

$$\frac{I_{mp}R_s - V_{mp}}{aV_T} + \frac{\left(V_{mp}I_{sc} - V_{oc}I_{mp}\right)}{\left(V_{mp}I_{sc} + V_{oc}\left(I_{mp} - I_{sc}\right)\right)} =$$

$$W_{-1}\left(-\frac{V_{mp}\left(2I_{mp} - I_{sc}\right)}{\left(V_{mp}I_{sc} + V_{oc}\left(I_{mp} - I_{sc}\right)\right)}\exp\left(-\frac{2V_{mp} - V_{oc}}{aV_T} + \frac{\left(V_{mp}I_{sc} - V_{oc}I_{mp}\right)}{\left(V_{mp}I_{sc} + V_{oc}\left(I_{mp}I_{sc}\right)\right)}\right)\right) \quad (4.10)$$

Here W_{-1} denotes the negative branch of Lambert W-function, and for solar cells or panels, this part is lower than (-1). Therefore, the explicit expression will be derived for Rs as:

$$R_s = A\left(W_{-1}(B\exp(C)) - (D + C)\right) \quad (4.11)$$

Where;

$$A = \frac{aV_T}{I_{mp}}$$

$$B = -\frac{V_{mp}(2I_{mp}I_{sc})}{(V_{mp}I_{sc} + V_{oc}(I_{mp} - I_{sc}))} \quad (4.12)$$

$$C = -\frac{2V_{mp} - V_{oc}}{aV_T} + \frac{(V_{mp}I_{sc} - V_{oc}I_{mp})}{(V_{mp}I_{sc} + V_{oc}(I_{mp} - I_{sc}))}$$

$$D = \frac{V_{mp} - V_{oc}}{aV_T}$$

Now we got a fully decoupled set of explicit equations for all required parameters of the equivalent circuit. As Lambert W-function assisted in clearing the implicit Rs and transforming it into explicit. This tool is utilized explicitly for solving exponential equations such as I – V curves for solar modules [154].

4.3.3 Parameter Extraction of Commercial Solar Module

There are three classifications regarding parameter extraction for solar module categorized as *analytical*, *iterative,* and *evolutionary,* as mentioned in the detailed description in Chapter 3.

For accurate modeling, it is important to have almost precise parameters for modeling, as it will ultimately impact efficiency and real-time simulation output of the module. Out of three, two parameter extraction categories were considered in calculation and then compared the open circuit testing data with the actual manufacturer's datasheet to analyze the accuracy is calculated and experimental data from the datasheet. The steps involved in the selection and analysis of parameters are highlighted in Figure 4.4, which will be easier to understand the steps involved in the critical calculation of data.

The selected categories for parameter extraction were analytical and iterative. From each group, the best possible method is selected.

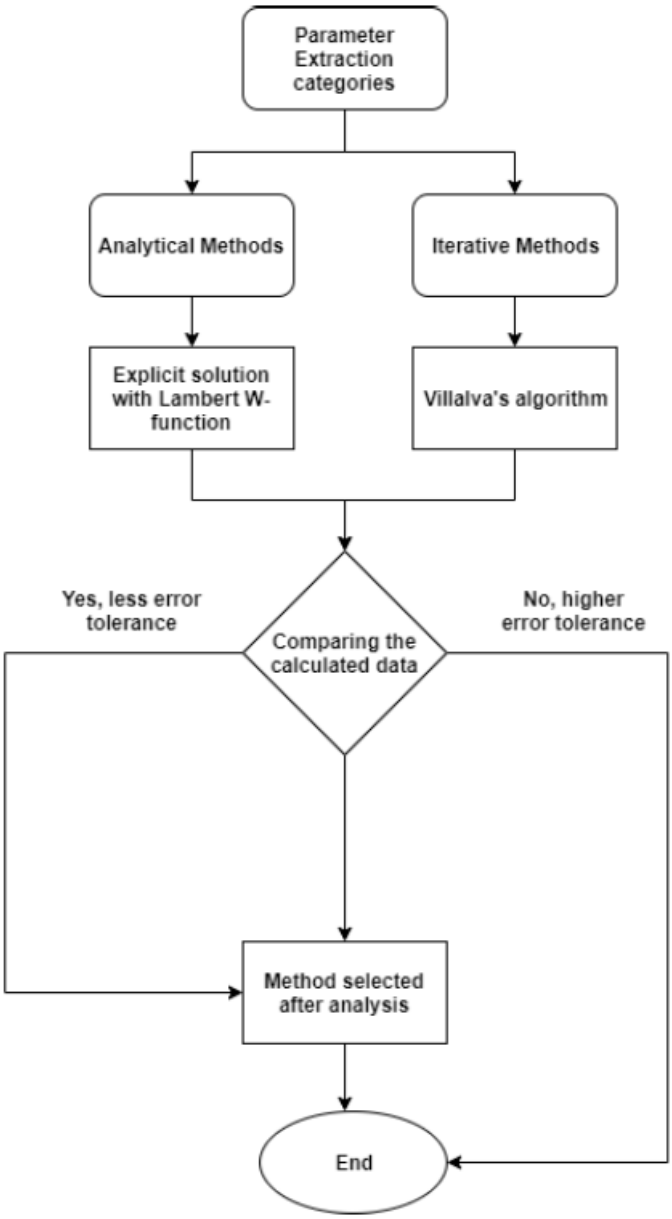

Figure 4.4: Step-by-step analysis and calculation towards the selection of parameter extraction technique

For extraction of parameters, the analytical procedure has been applied, as this is easier to be used by small scale users and represents a solution to this problem, due to their simplicity and minimum data requirement (included in the datasheet) for modeling solar behavior.

Selecting the ideality factor is the first step towards parameter extraction for unknown parameters. The reason for introducing the ideality factor is due to the limited data available from the manufacturer's datasheet containing only three characteristic points for the I – V

curve, these data points are not enough to calculate the five parameters of the equivalent circuit. Therefore, various authors proposed to introduce the ideality factor (a) for reducing the number of parameters to four [155]. The general value has been suggested in a bracket [1, 1.5] for almost all types of cells [156].

After obtaining all the desired equations, the five unknown parameters needed to be identified and then calculated. The unknown parameters are; I_L, I_0, R_s, R_{sh}. As the selected solar module is of polycrystalline type, hence the proposed ideality factor suggested by [157] is given as a = 1.3, this value is independent of irradiation and temperature levels.

The following procedure is applied to calculate the parameters from the manufacturer's datasheet:

- Approximating the ideality factor, "a" as 1.3 (Polycrystalline Cell)
- Calculating the Series Resistance Rs with Equation 5
- Calculating the Shunt Resistance Rsh with Equation 7
- Calculating the Saturation Current Io with Equation 8
- Calculating the Photodiode Current Ipv with Equation 9

After the selection of the module, the next step belongs to the extraction of parameters, which itself is a challenging task. The literature survey and analysis have been carried out to select the best possible and straightforward method to apply on the model. Hence out of all those techniques, three were selected; Iterative algorithm, Lambert W function, and without Rp. The calculations were carried out separately to find out the five parameters for the selected module on MATLAB software.

The electrical characteristics are needed towards the extraction process of five parameters from the manufacturer's datasheet. Mostly, the manufacturers don't reveal much information in terms of electrical power generation and different levels of solar irradiation and temperature levels. However, these five parameters are required to be extracted from limited available information through a number of derived equations for the solar equivalent model.

The electrical characteristics of the selected model from the manufacturer's datasheet are represented in Table 4.1; this data will be inserted into the derived equations to calculate the equivalent circuit parameters. These parameters are considered at (STC) Standard Test Conditions as 1000 W/m^2 incident usual radiance, Cell temperature at 25 °C and Air Mass AM1.5g.

Table 4.1: Electrical Specifications of MC-SP0.8-NF-GCS from Multicomp

Characteristics	Specifications
Maximum Power Pmax	0.8 W
Maximum Power Voltage (Vmp)	3.85 V
Maximum Power Current (Imp)	0.21 A
Open Circuit Voltage (Voc)	4.80 V
Short Circuit Current (Isc)	0.23 A
Temperature Coefficient of Isc (alpha)	0.06%/K
Temperature Coefficients of Voc (beta)	-0.36%/K
Temperature Coefficients of Pm	-0.45%/K

The extracted data will be inserted in the above-derived equations on the MATLAB platform, as shown in Figure 4.5.

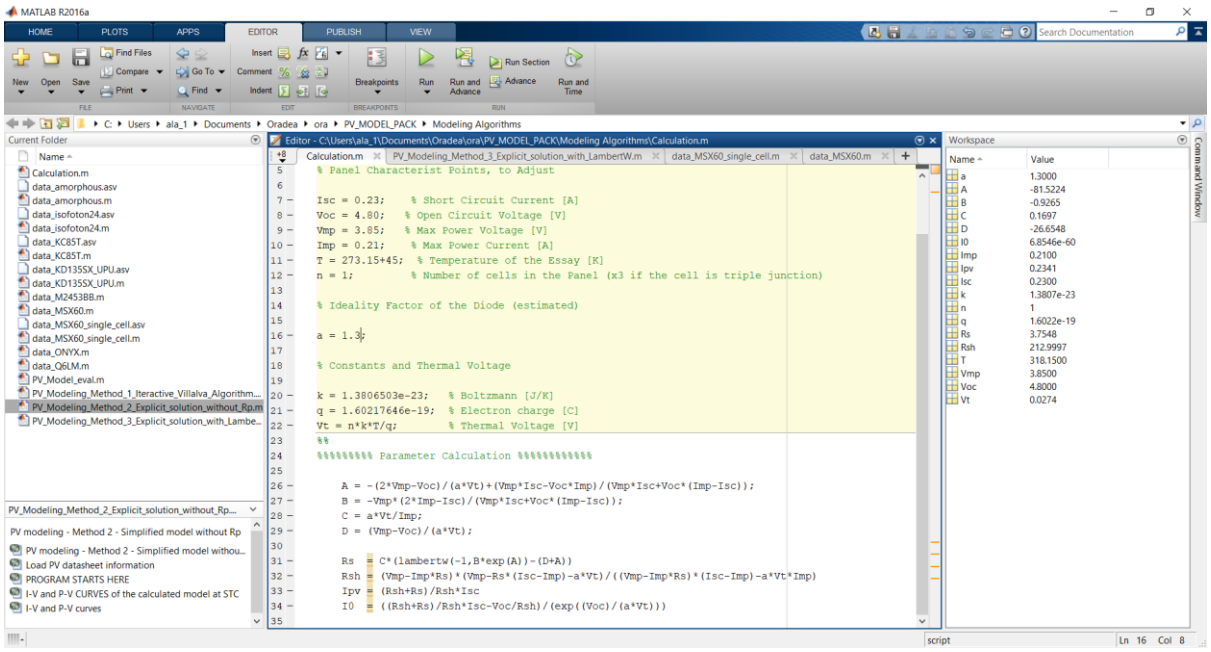

Figure 4.5: Screenshot from MATLAB for calculating required parameters through mathematical formulations

The calculated data for five unknown parameters for the equivalent circuit has been inserted in Table 4.2. This data will be used for modeling and simulation purposes as the required data towards the further building of the solar module.

Table 4.2: Calculated parameters of MC-SP0.8-NF-GCS from Multicomp

Parameters	Calculated Values
I_0	1.949e-30
Ipv	0.2303
Rs	0.3208
Rsh	235.142
a	1.3

4.3.4 Power Converter for Solar Energy Harvesting Module

Power management is required for the solar energy harvesting circuit, as the intermittent solar energy isn't enough to transfer it towards the load directly. Hence, PMIC is needed to transform the high impedance harvested energy into the desired output power. The COTS products are available for various energy sources, and we are not designing custom made PMIC or boost converter. The number of PMICs already discussed regarding their role in energy harvesting in Chapter 2, section 2.10, as both solar and thermal energy models require PMICs, and most of them support both sources. Therefore, regarding solar energy prerequisites, the chosen solar module is based on single photovoltaic cell for low-powered IoT applications, and in this regard, the most suitable PMIC for our research profile is LTC3105 [62] as shown in Figure 4.6. This PMIC, LTC3105, is particularly suited for boosting the output voltage and can start up at exceedingly low voltage, i.e., 0.25 V.

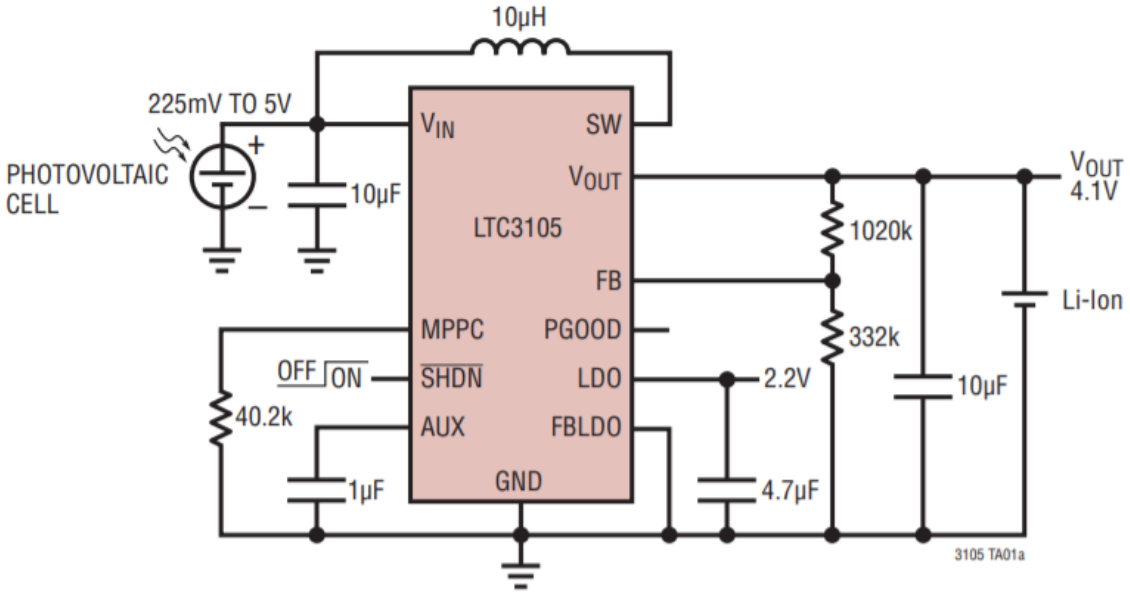

Figure 4.6: Typical application connected with LTC3105 with Photovoltaic Cell [62]

4.3.5 Solar Equivalent Circuit Modelling

After extraction of parameters, the selected solar model MC-SP0.8-NF-GCS will be modeled over the LTSpice simulator to analyze the real-time behavior of the solar module in terms of I – V and P – V characteristics. The simulation will be demonstrated in the next chapter. However, the commercial solar module is transformed into an electrical circuit configuration over the LTspice simulator, as shown in Figure 4.7.

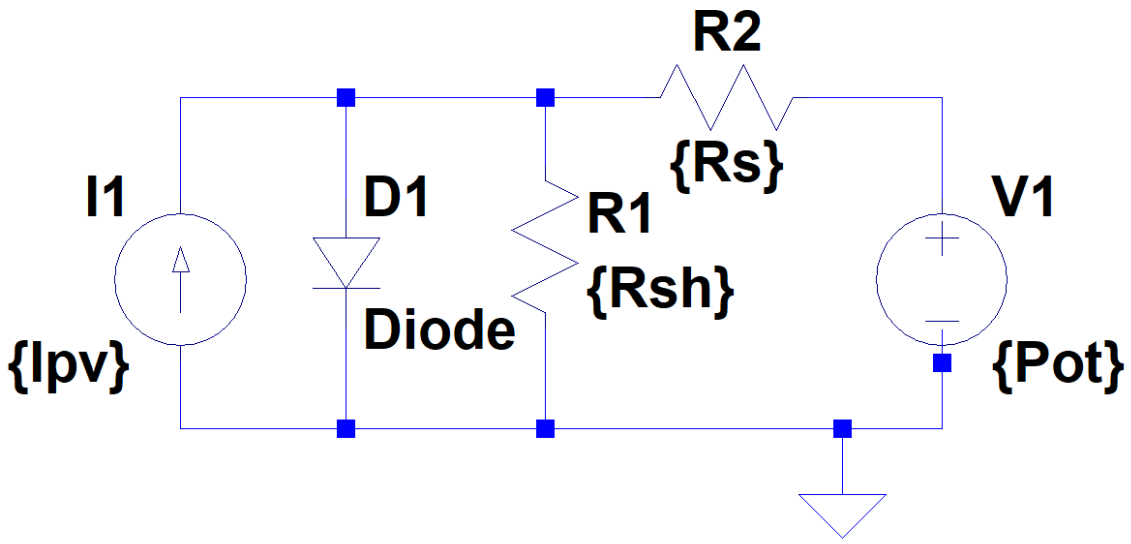

Figure 4.7: Solar equivalent circuit model for MC-SP0.8-NF-GCS

4.3.6 Proposed Solar Energy Harvesting Circuit with LTC3105

The commercial solar module MC-SP0.8-NF-GCS transformed into mathematical and electrical formulations can now be modeled with complete energy harvesting circuitry. The solar module will be combined with a step-up power management IC from Linear Technology, LTC3105. Hence the complete Solar Energy Harvesting Circuit (EHC) combined with LTC3105 PMIC ready for modeling and simulation is demonstrated in Figure 4.8.

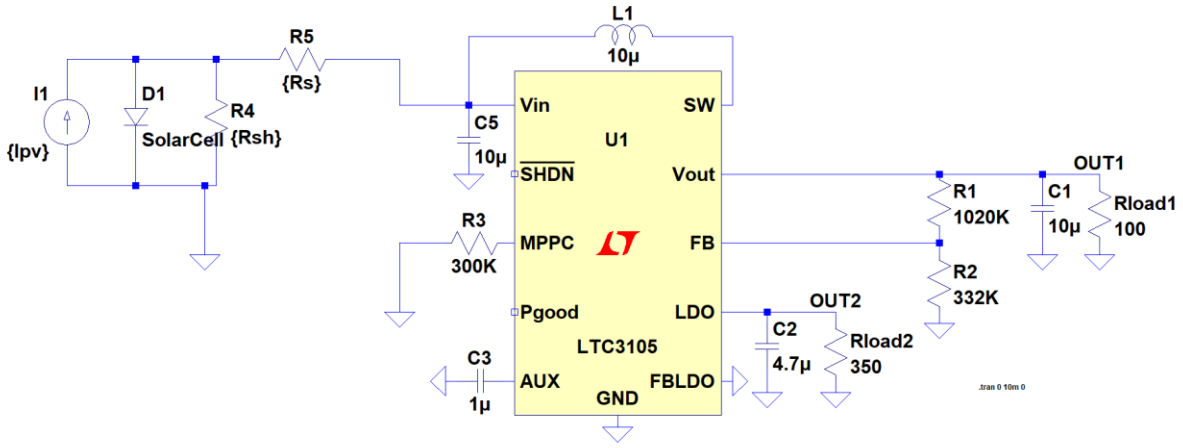

Figure 4.8: Solar Energy Harvesting Circuitry of MC-SP0.8-NF-GCS combined with LTC3105

4.4 Thermal Energy Harvesting Module

For building a thermal-based Energy harvesting simulation setup, the first characteristic is to harvest the thermal energy. One aspect to understand here is that it's a purely electrical circuit simulation analysis. Therefore, the selected commercial device will be modeled and simulated on the simulator according to the electrical perspective only. In terms of harvesting heat energy, the focus is on wearable devices from human body heat, as the basis for building this thermal-based energy harvesting module.

4.4.1 Selection of Commercially available Thermal Module

To harvest heat or thermal energy, it is required to have a transducer to transform heat energy into electrical energy. The detailed description and associated techniques and technologies are discussed in Chapter 3. Here, the selection of the module and related procedures are implemented after a thorough investigation of the thermal energy. In this regard, a commercial thermoelectric module TEC-12722 from Thermonamic [158] has been chosen, as shown in Figure 4.9. This model is selected to analyze the behavior of the module over the number of parameters. The module is explicitly supporting the IoT based application for wearable devices from human body heat. There are various reasons behind the selection of this module, which will be discussed in the next section.

Figure 4.9: Thermal module TEC-12722 from Thermonamic [158]

4.4.2 TEC and TEG

As the selection of the above model is based on a few critical parameters, and in this research profile, the power generation is the crucial parameter under investigation. Apart from this, the target applications are based on harvesting human body heat, which usually operates under lower temperature gradients. The selected module is thermoelectric cooler (TEC). However, TECs can be used as TEGs [144].

TEC is used in the reverse configuration of the TEG, where electric power is supplied to the TEM to cool down another system in the application of interest. However, two scenarios are behind this consideration.

(i) Size of heat sink and human body temperature for wearable:

One feature to consider is the temperature difference, which is reported only 5°C for human wearable energy harvesting [159]. In this paper, the authors demonstrated that temperature difference ranges from 1°C to 5°C for wearable devices. The reason for considering this lower

temperature difference is to make it in wearable form as the heat sink size was kept at 14x14 mm and natural human activity such as biking or running, which makes this lower temperature range till 5°C. If we would like to increase the temperature difference, in that case, either we must enhance the heat sink size or decrease the ambient temperature, i.e., 5°C or below that.

(ii) Comparison between TECs and TEGs based on simulation and experimental data for analyzing in terms of power generation and cost-effectiveness.

The experimental and simulation data has been conducted in which TECs and TEGs are analyzed based on similarities and differences for addressing the question that when it comes to power generation which one we should consider based on (a) at what temperature range (b) under which condition, expensive TEGs could be replaced with TECs.

Table 4.3 shows the differences and similarities in both TEC; TEC1-12706 [143] and TEG; GSM250-127-14-10 [160], where greyed cells are representing similarities and remaining cells are showing differences.

Table 4.3: Comparison of the selected TEC (TEC1-12706) and TEG (GM250-127-14-10). The Data are from the datasheets apart from the ceramic material for the TEG

Device	Dimensions	T_{hot}	$\Delta T_{max}/T_{cold}$	I_{max}/I_L	U_{max}/U_L	R_i	Q_{max}/Q	Number couples	Thermoelectric material	Ceramic material	Solder material
TEC1-12706	40x40x3.9 mm	50 °C	75 °C (ΔT_{max})	6.4 A (I_{max})	16.4 V (U_{max})	2.3 Ω	57 W (Q_{max})	127	Bi_2Te_3	Al_2O_3	BiSn (138 °C)
GM250-127-14-10	40x40x3.4 mm	250 °C	30 °C (T_{cold})	2 A (I_L)	4.96 V (U_L)	2.49 Ω	~ 198 W (Q)	127	Bi_2Te_3	Al_2O_3	N.N.

Then the power generation tests have been conducted to analyze how both TEC and TEG are generating power under the same conditions. It can be seen from the Figure 4.10, which represents the simulation and experimental data that the power generation curves for both devices are almost identical, and TEC is showing even more power at lower temperature difference.

The optimal result is that TECs can be used as TEGs for power generation in temperature range between 0°C to 100 °C. The results also prove that the performance of TECs is better at lower temperature range (20 °C to 40 °C) and is supporting a wide variety of applications for energy harvesting systems.

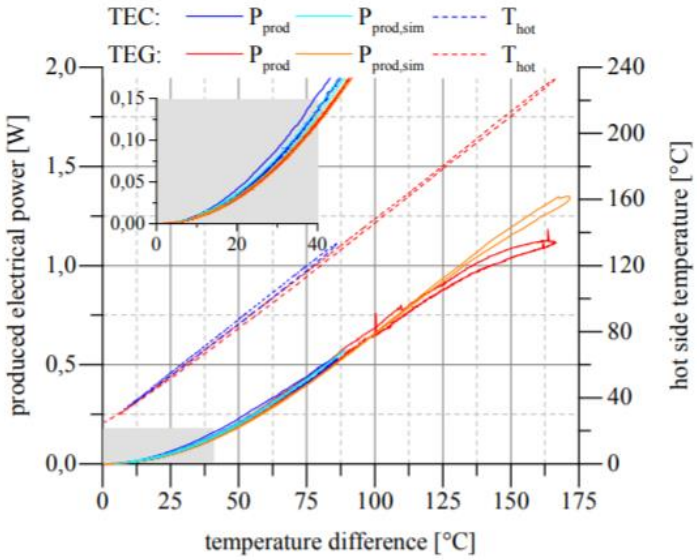

Figure 4.10: Comparison of the measured and simulated produced electrical power between TEG and TEC, plot against the temperature difference [144]

By considering the factors mentioned above, the selected model is from the same series of TEC, i.e., TEC1-12722.

4.4.3 Mathematical Modelling of Thermal Equivalent Circuit

For simulating the commercial thermal model on the simulator, it is required to transform the characteristics of the selected model in terms of electrical specifications over the simulator.

In this regard, the thermal equivalent model and respective SPICE models have been discussed in Chapters 3 and 4, along with their comprehensive derivations and limitations. The model which has been chosen for our research's scope will be discussed in a detailed manner, and the reasoning will be highlighted for the selection of this model.

The model chosen for our research requirement is Kubov's SPICE model based on the Peltier-Seebeck element due to its simplicity, and it contains a small set of variables specifically in power generation inside the thermoelectric module. This interconvertible model of the Peltier-Seebeck element converts electricity into heat and heat into electricity. The major limitation comes from the manufacturer's datasheet as the data isn't providing the information regarding output power generation of the TEC, which in our case is required to find out the maximum power generation of the system. However, the selection of the model is entirely based on the way parameters are extracted, which will lead to the efficiency of the selected thermoelectric module. This model is providing a straightforward approach and contains symmetric structure

of the electrical scheme; it also provides transparency in the SPICE model, which could be transferred and adapted in an extended version.

4.4.3.1 Mathematical Modelling of Peltier Seebeck Device

When the electric current flows in an electrical circuit, then the scenarios are developed as energy generation and energy absorption. Contemplating the mathematical conventions, the energy absorption relates to the positive sign, whereas the generation refers to the negative. The Peltier circuit consists of two voltage sources (V1, V2) and one internal resistance (R), as shown in Figure 4.11.

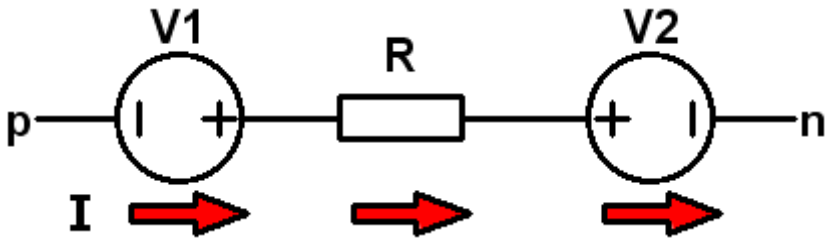

Figure 4.11: Two Peltier contacts with internal resistance

The model is based on two functionalities as follows:

- Considering the circuitry in terms of heat energy, then the element V1 will absorb from the environment and will cool down, whereas the element V2 will generate heat and energy, and the element R will produce Joule heating. This effect is called a Seebeck effect used for power generation due to temperature difference. It is used in TEGs.

- Considering the circuitry in terms of EMF of both element V1 and V2 and potential difference is similar for both voltage sources, and power from resistance is lesser than the power from both voltage sources, then this system is carrying a heat junction from V1 to V2, which is known as Peltier effect. This effect is used in TECs.

For modeling the Peltier Seebeck effect:

The output by heat which flows from cold to hot part of the element is given as:

$$P_Q = \Pi * \mathrm{I} \tag{4.13}$$

Here, the Peltier coefficient is represented by Π, and current is denoted by I. The thermal power balance equation can be represented by the same equation for generating cold and hot sides of the element.

$$P_Q = P_c = -P_h = \frac{P_c - P_h}{2} \tag{4.14}$$

Here, $P_{c,h} = \pm \Pi * I$, and sign conventions are determined by the direction of the current.

The equation for the potential difference which is generated by the temperature difference by both elements is given by:

$$V_s = \alpha * (T_h - T_c) \tag{4.15}$$

Here, α represents the Seebeck coefficient, and $T_{h,c}$ denotes the temperature on cold and hot sides.

The Peltier and Seebeck coefficients will be connected through Thompson equation, given as:

$$\Pi = \alpha * T \tag{4.16}$$

For designing the Peltier element with two voltage sources and different polarities along with temperature parts are derived as:

$$\Pi_{c,h} = \alpha * T_{c,h} \tag{4.17}$$

For making the equal description of Peltier and Seebeck effects, in terms of heat flux from cold to hot side will be transformed as:

$$P_Q = \frac{P_c - P_h}{2} = \alpha * I * \frac{T_h - T_c}{2} \tag{4.18}$$

The average value of the Peltier coefficient for two contacts is denoted by $\alpha * \frac{T_h - T_c}{2}$.

For determining the EMF for two opposite switched contacts by temperature difference as:

$$V_S = V_h + V_c = \alpha * T_h - \alpha * T_h = \alpha * (T_h - T_c) \tag{4.19}$$

The equations mentioned above are implemented over the LTspice model, as seen in Figure 4.12.

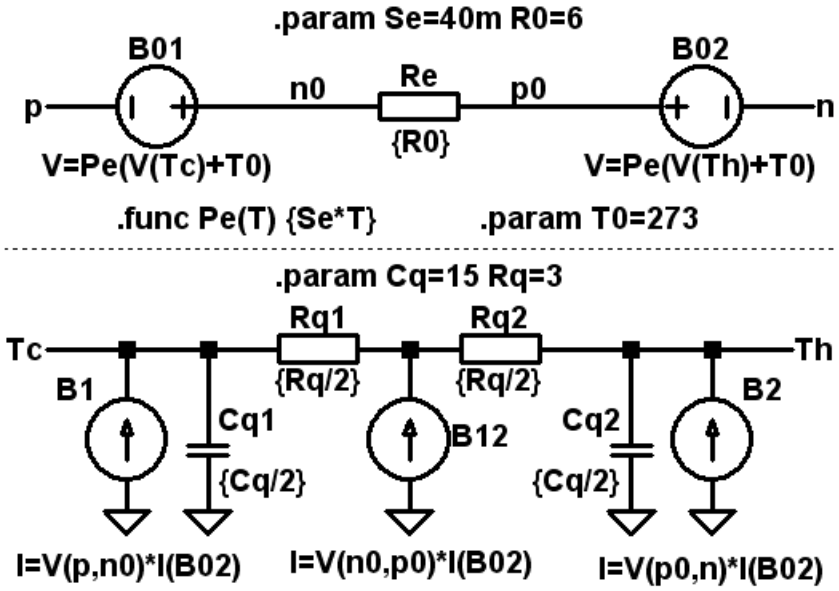

Figure 4.12: Kubov SPICE model for TEC/TEG [142]

The Kubov model has presented the thermal as well electrical simulation model in this paper, the upper part represents the electrical parameters, and the lower part is for thermal parameters.

The thermal part defines the current as an equivalent of thermal power, whereas voltage as a temperature equivalent. In this configuration, the electrical contact B01 is switched in reverse towards the current direction where it absorbs the heat, whereas contact B02 is in straight direction in which heat is generated. Therefore, heat is transferred from cold to hot side, and that heat is described as the Peltier coefficient.

The following equation defines the heat parameter as a Peltier coefficient (Pe) and it is enlisted inside the netlist of the simulation model on which it is working.

$$\text{.func } Pe\ (T)\{S_e * T\} \tag{4.20}$$

Here, *Se* represents the Seebeck coefficient and *T* – absolute temperature. For converting from the Celsius scale into the absolute temperature, the constant parameter is utilized as T0 = 273.

When current flows through resistance on element Re, joule heat is generated. Internal thermal resistance is modeled by element Rq. Thermal power sources are represented by current sources as B1, B2, B12, and heat capacity is denoted by two capacitors as Cq1 and Cq2.

4.4.4 Parameter Extraction for Commercial Thermoelectric Module

As mentioned in section 4.4.3, the factors behind the selection of the SPICE model and out of all other, one of them belongs to the parameter extraction of the thermal module as both (TEC/TEG model, parameter extraction) are closely related. How parameters are extracted and calculated in thermoelectric generators have been described thoroughly in Chapters 3 and 4, which were; *Extraction via Thermocouple scaling, Extraction via datasheet* and *device geometry, and extraction via datasheet only*. The associated extraction technique that will be applied in the selected model is based on the third category, which is *Extraction via the manufacturer's datasheet only*. The reason behind the selection of this category is due to small-scale users who rely entirely on the manufacturer's datasheet for electrical specifications of the thermoelectric module. Small-scale users can easily handle this technique because they do not need to have proper expertise and knowledge about digging into technicalities of exact parameter extraction. Only "Parameter extraction via the manufacturer's datasheet" technique could support them and the sole purpose of this research. This technique has been followed by the 7-step procedure towards the extraction of required data from limited manufacturer's datasheet for electrical parameters, whereas for thermal parameters, the experimental analysis has been observed. The visual representation of this significant step is highlighted in the following Figure 4.13.

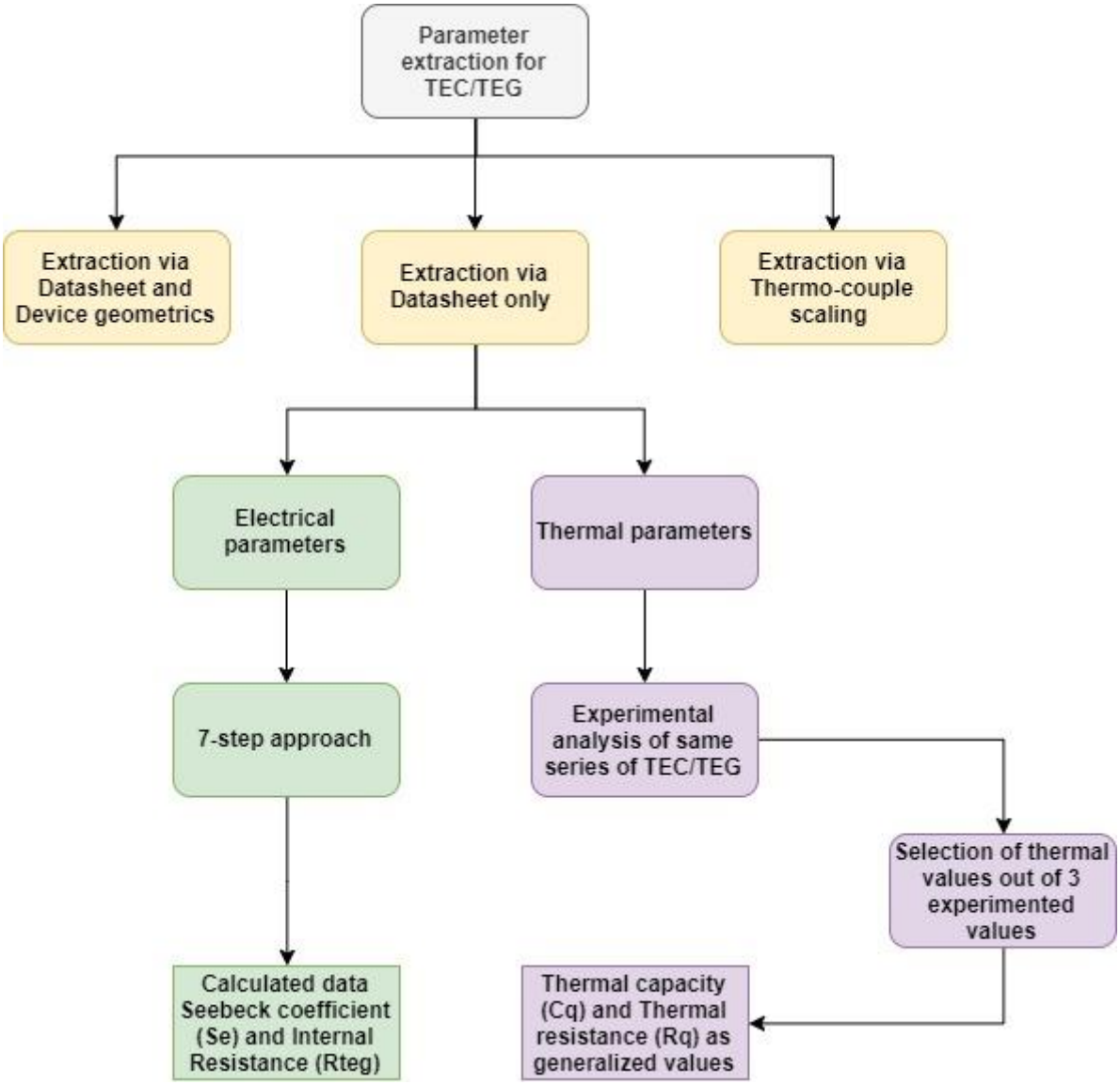

Figure 4.13: Comprehensive approach towards thermal module parameter extraction

Table 4.4 consists of the Performance characteristics of the selected module-12722 [158].

Table 4.4: Performance characteristics of TEC1-12722

Th (°C)	27	50	Dry air: Temperature of Hot side
DTmax (°C)	70	79	Temperature difference of hot and cold side of the module when cooling capacity is zero at cold side
Umax (V)	16	17.2	Voltage applied to the module at DTmax
Imax (A)	18.5	18.5	DC current through the module at DTmax
Q_{Cmax} (W)	185.3	202.5	Cooling capacity at cold side of the module at DT = 0°C
AC resistance (Ω)	0.68	0.74	The tested module resistance under AC
Tolerance (%)	± 10		For electrical and thermal parameters

Going back to the Peltier-Seebeck model described in Chapter 3 section 3.3.11, where it consists of two parts Thermal and Electrical, the required parameters also coming from these two configurations. In this manner, this model needed four parameters to process, which are Seebeck coefficient (Se), electrical resistance (R_{TEG}), thermal resistance (Rq), and heat capacity (Cq).

4.4.5 Parameter Extraction through Datasheet only

4.4.5.1 Extracting Electrical Parameters

The parameters belong to the electrical part are Seebeck coefficient (Se), electrical resistance (R_{TEG}). The entire research scope is based on electrical perspective and electrical circuit simulation. Therefore, the parameters of interest that have its place in this domain are Se and R_{TEG}. The calculation for electrical parameters follows a 7-step approach [161] will be elaborated shortly.

7-step approach

To determine numerous specific parameters such as Seebeck coefficient, electrical resistance and thermal resistance of the thermoelectric cooler, there are necessary calculations to be made. Upcoming series of calculations will allow and ensure ease throughout the simulation and modeling inside the LTspice module. Steps can be enumerated as:

1) Reading and observing maximum output voltage (V_{Opt}) of TEC-12722 from the Figure 4.14.

V_{Opt} value is 16V for $T_h = 27$ ℃

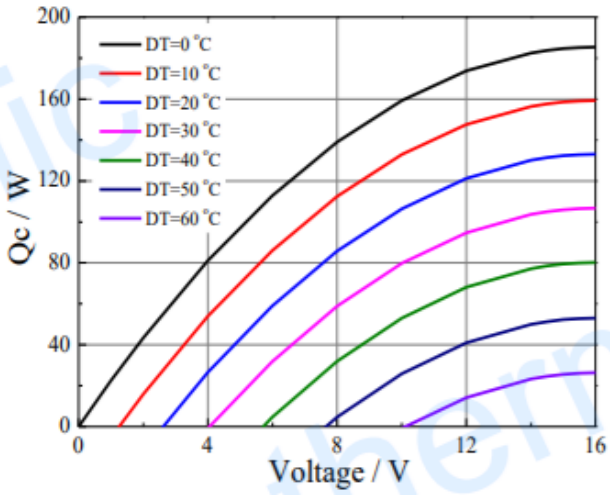

Figure 4.14: Performance curve at $T_h = 27$ ℃ for TEC1-12722 [158]

2) Calculating the Seebeck Coefficient with the formula:

$$Se = \frac{V_{Opt}\{V\}}{T_h\{K\}}$$

$$Se = \frac{V_{Opt}\{V\}}{T_h\{K\}} = \frac{16}{27+273} = 53\ mV/K$$

3) Determining the maximum performance for zero temperature difference which is Q_{Cold}.

$$Q_{Cold} = 185W$$

4) Calculating electrical resistance value with:

$$R_0 = \frac{{V_{Opt}}^2}{2.Q_{Cold}}$$

$$R_0 = \frac{{V_{Opt}}^2}{2.Q_{Cold}} = \frac{16^2}{2.185} = 0.692\Omega$$

5) Determining the maximum temperature difference between the cold and hot sides which is DT_{max} – the temperature which should secure the value for thermal performance returns to 0.

$$DT_{max} = 70℃$$

6) Determining the Quality Factor ($X = \left\{\frac{R_q}{R_0}\right\}$) which is the ratio between thermal resistance and electrical resistance, while using available parameters such as Seebeck Coefficient and DT_{max} from Figure 4.15.

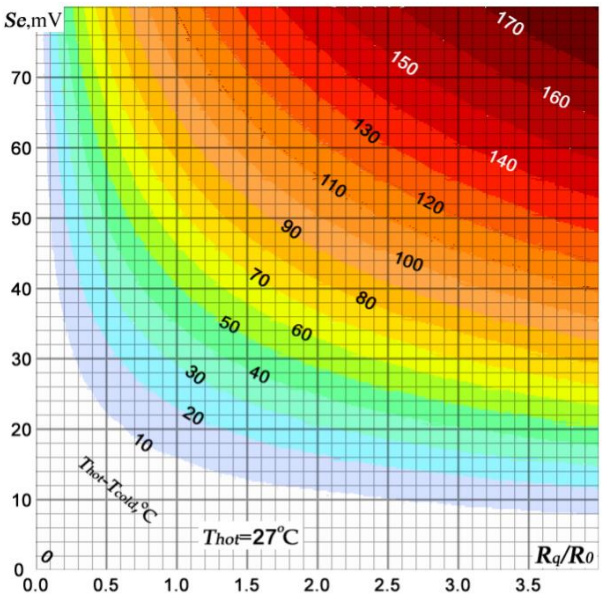

Figure 4.15: Relationship between Seebeck parameter and DT_{max} necessarily gathering results for thermal resistance for a wide range of variables [161]

By using Figure 4.15, after matching relevant values within each other, we get:

$$X = \left\{\frac{R_q}{R_0}\right\} = 0.95$$

7) Calculating the value of thermal resistance with $R_q = R_0.X$

$$R_q = R_0\, X = 0.692 \cdot 0.95 = 0.6574\ K/W$$

4.4.5.2 Extraction of Thermal Parameters

As this work is focused on electrical circuit perspective and thermal specifications weren't considered in a similar manner, but the model under analysis and used in the simulation have thermal characteristics and utilizing the thermal parameters in a generalized manner. The thermal part is also there, but as we have calculated electrical parameters from the manufacturer's datasheet, the thermal parameters weren't extracted in a similar manner. How thermal aspects reside in the model and the extraction for them is explained below:

Out of four required parameters for the equivalent model, the remaining two belong to the thermal domain, which is thermal resistance (Rq) and heat capacity (Cq). These values were selected as the generalized variables that were experimented and simulated by Kubov in this work [142].

However, the selection for thermal values is based on precise analysis typically based on temperature dependence and electrical resistance impacts on thermal parameters.

The nominal value for Cq and Rq is measured and experimented by the author in terms of 3 variations to see the impact of temperature dependence; the values were chosen as (lower, middle, higher). However, for internal thermal resistance; Rq = (1.5, 3.0, 6.0), the values were changed two times higher and two times lesser from the chosen one, i.e., Rq = 3.

The same calculations and experiments have been considered for thermal capacity Cq in 3 different variations as Cq = (7.5, 15, 30), the nominal values were changed two times higher and two times lesser than the chosen one Cq = 15.

Therefore, we considered the mid-range value as a general consideration for thermal resistance and heat capacity in our model.

Thus, parameters calculated for TEC1-12722 are tabulated in Table 4.5.

Table 4.5: Calculated Electrical and Thermal Parameters for TEC1-12722

Parameters		Calculated values	Units
Electrical	R_{TEG}	53	mV/K
	Se	0.692	Ω
Thermal	Cq	15	J/K
	Rq	3	K/W

4.4.6 Power Converter/PMIC for Thermal Energy Harvesting

The number of PMICs is already discussed in Chapter 2, section 2.10, and their role in energy harvesting, as both solar and thermal energy models, require PMICs, and most of them support both sources. Therefore, regarding thermal prerequisites and certain limitations discussed in terms of human body heat, the most suitable PMIC for our research profile is LTC3108 [63], as shown in Figure 4.16.

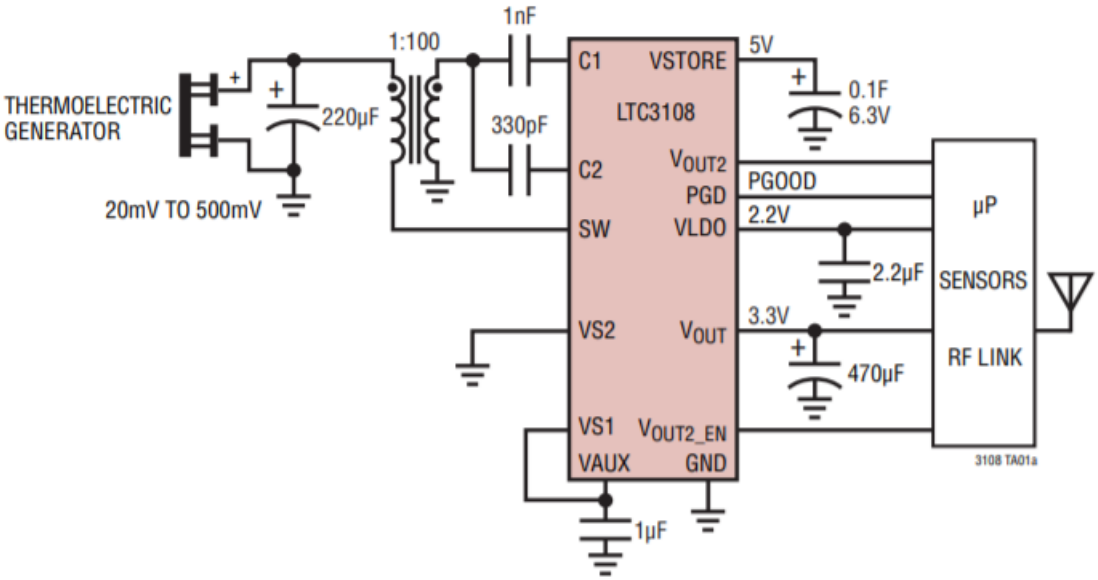

Figure 4.16: Typical application connected with LTC3108 along with TEG [63]

The crucial parameter for the selection of PMIC is the cold start activation voltage, as the temperature difference in steady-state between two sides of the TEG surface is small. Due to this issue, maintaining the voltage around 20mV is itself a challenge [159]. However, LTC3108 from Linear Technology supports in this manner but at the cost of efficiency, as this IC lacks the maximum power point tracking (MPPT) algorithm.

4.4.7 Thermal Circuit Modelling on LTspice

After extraction of parameters, the selected thermal model TEC1-12722 will be modeled over the LTspice simulator to analyze the real-time behavior of the thermal module in terms of I – V and P – V characteristics. The simulation will be demonstrated in the next chapter. However, the commercial thermal module is transformed into an electrical circuit configuration over the LTspice simulator, as shown in Figure 4.17.

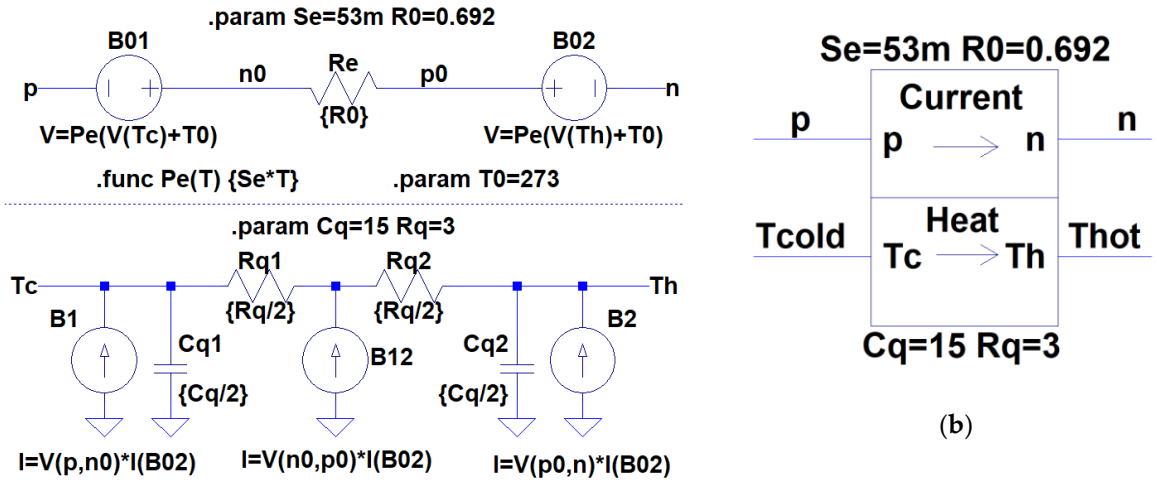

Figure 4.17: (a) Kubov's LTspice TEG model; (b) Subcircuit of TEC1-12722 along with calculated parameters

4.4.8 Proposed Model for Thermal Based Energy Harvesting Module

The commercial thermoelectric module TEC1-12722 transformed into mathematical and electrical formulations can now be modeled with complete energy harvesting circuitry. The thermal module will be combined with a step-up power management IC from Linear Technology, LTC3108. Hence the complete Thermal Energy Harvesting Circuit (EHC) combined with LTC3108 PMIC ready for modeling and simulation can be seen in Figure 4.18.

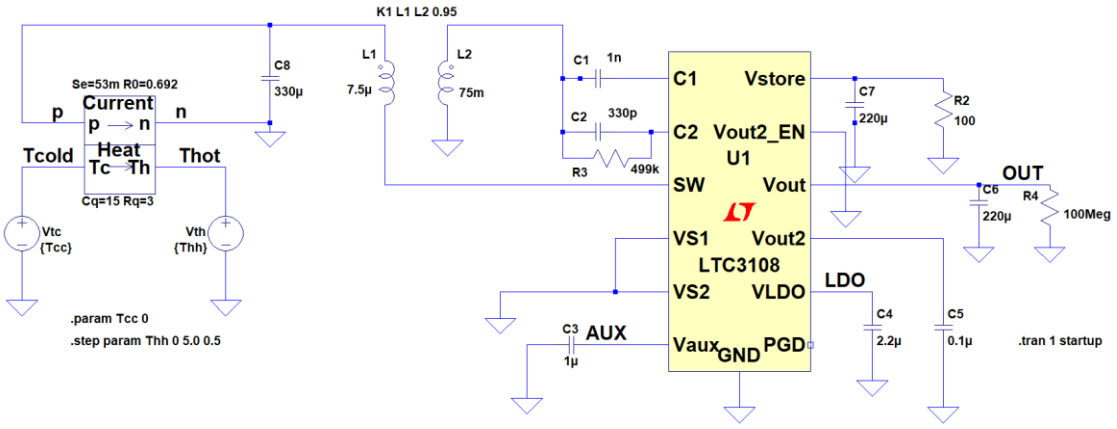

Figure 4.18: Thermal Energy Harvesting Circuit of TEC1-12722 with LTC3108 PMIC

4.5 Summary

This chapter aims to establish a proper understanding of the procedure and steps involved in achieving the research's major objectives. Starting from the selection of energy harvesting sources, which were solar and thermal/heat, have been chosen for investigating their associated techniques involved in power generation, energy extraction, and product selection, etc. The parameter extraction is itself a challenging aspect involved in both energy sources due to the limited amount of data available in the manufacturer's datasheet. As the end-user or small-scale users wholly solely rely on this particular piece of information for building their energy harvesting based system and economically maximizing the efficiency. In this chapter, the complete systematic methodology towards achieving the desired objectives has been discussed in a detailed manner, and in the next chapter, the implementation of the selected data and its implications will be analyzed, and the results of the simulation study will be elaborated.

5 Simulation Results and Comparative analysis: Results and Discussion

5.1 Introduction

Modeling requires two steps to follow the procedure: (a) Parameter extraction and (b) Modelling of the commercial module (Solar and Thermal). This chapter will elaborate simulation setup involved and generated results of proposed energy harvesting modules. In the end, the simulated results will be compared with already available experimented IoT modules.

5.2 Solar Energy Harvesting Modelling and Simulation in LTspice

The selected transducer for solar energy harvesting is MC-SP0.8-NF-GCS from Multicomp [151], whose parameters are extracted, and the solar equivalent model is constructed on LTspice, as shown in Figure 5.1.

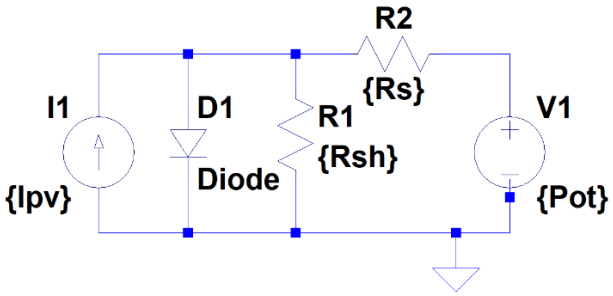

(a)

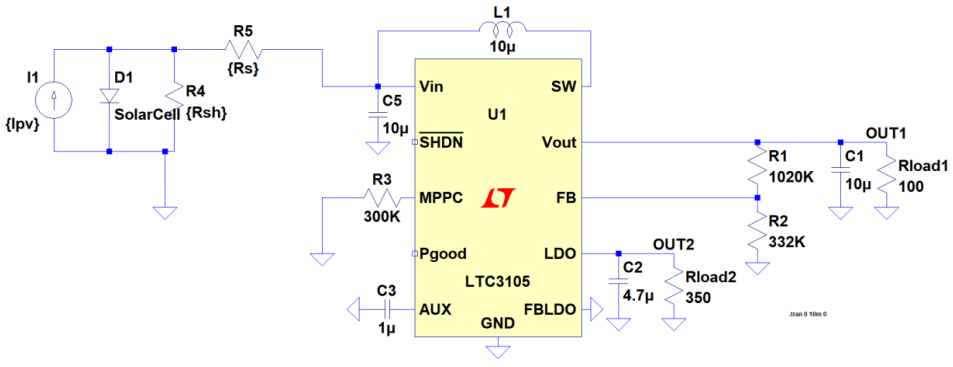

(b)

Figure 5.1: Simulation models constructed for Solar EHC Setup (a) Equivalent model, (b) complete EHC

5.2.1 Characterization of Solar Cell on LTspice Simulator

In order to analyze the selected solar module's characteristics and efficiency, it is mandatory to simulate the mathematically calculated system to analyze and compare the simulated data with the manufacturer's datasheet experimental result. Afterward, it could be confirmed that the calculated data for the solar equivalent circuit can predict the accurate or near to precise performance of the chosen module over the simulator.

For analyzing the performance of the module, it is essential to carry out a simulation-based study for current vs. voltage curves, i.e., I – V curves and power vs. voltage curves, i.e., P – V curves. The simulation will be performed for analyzing the system's efficiency under various levels of solar irradiation as well as the temperature levels for both I – V and P – V curves. This is how the temperature dependence and solar irradiation impacts will be shown and analyzed to see the maximum power generation under certain conditions of the solar module.

5.2.1.1 I – V curve and P – V Curve Simulation

The I – V and P – V curves for commercial solar cell have been generated on LTspice simulator, as shown in Figures 5.2 and 5.3. These simulations are mathematically formulated and are based on the manufacturer's datasheet information. These curves are based on standard test conditions (STC); for incident, normal radiance is 1000 W/m^2, Cell temperature is 25°C and Air Mass is AM 1.5g.

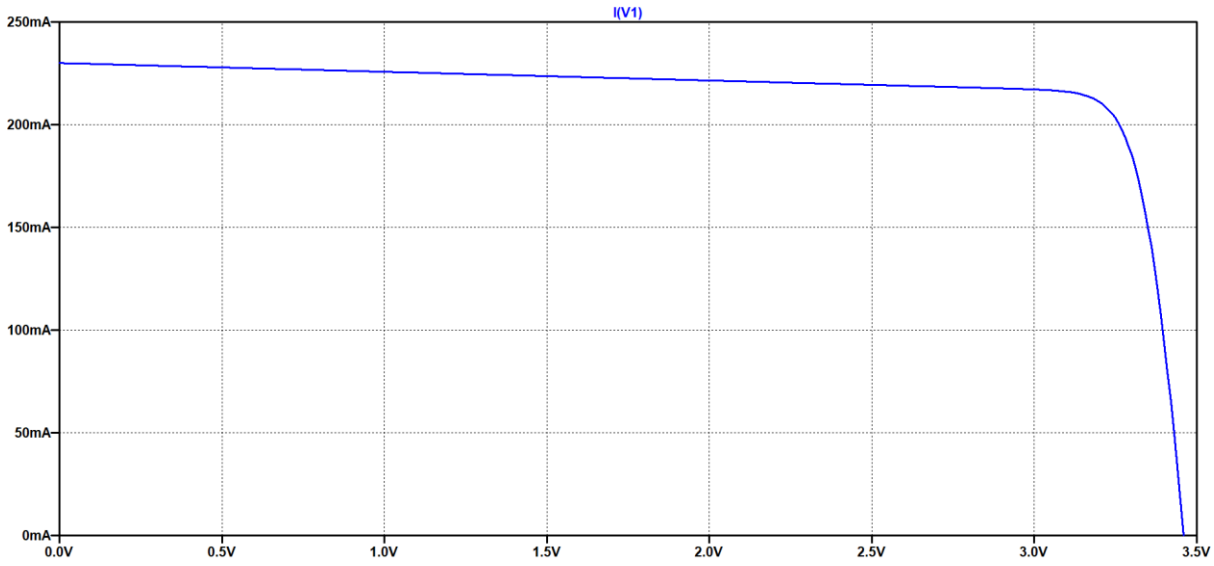

Figure 5.2: I – V curve of the Solar Equivalent circuit for MC-SP0.8-NF-GCS

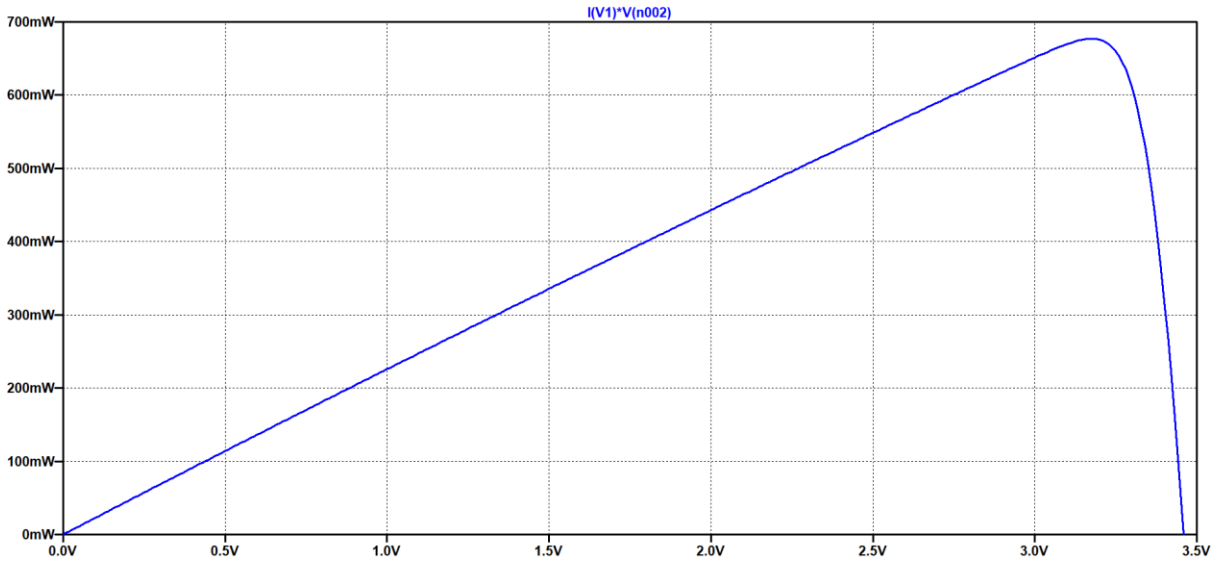

Figure 5.3: P – V curve of the Solar Equivalent circuit for MC-SP0.8-NF-GCS

5.2.1.2 Effect of Solar Irradiation on I – V and P – V curves of the Module

For analyzing the real-time behavior of the solar module, the environmental conditions must be inserted in the modeling setup for predicting the performance of solar module under different scenarios. As the photovoltaic structure is highly influenced by solar irradiation levels, such as the cloudy weather or rainy weather impact on the power generation, increment and decrement in temperature, plays a pivotal role in this phase. For modeling such segments, the variation in solar irradiation levels and different ranges of temperature are also introduced in modeling. However, the above I – V and P – V curves were calculated based on standard test conditions (STC). In this segment, the plots of characteristics curve have been established by varying solar irradiation parameters and keeping the temperature parameter as a constant at STC. The solar irradiance value G is being changed from 200 W/m^2 to 1000 W/m^2 and holding the temperature variable TEMP steady. Figures 5.4 and 5.5 have been demonstrating the impact of solar irradiation on I – V and P – V curves.

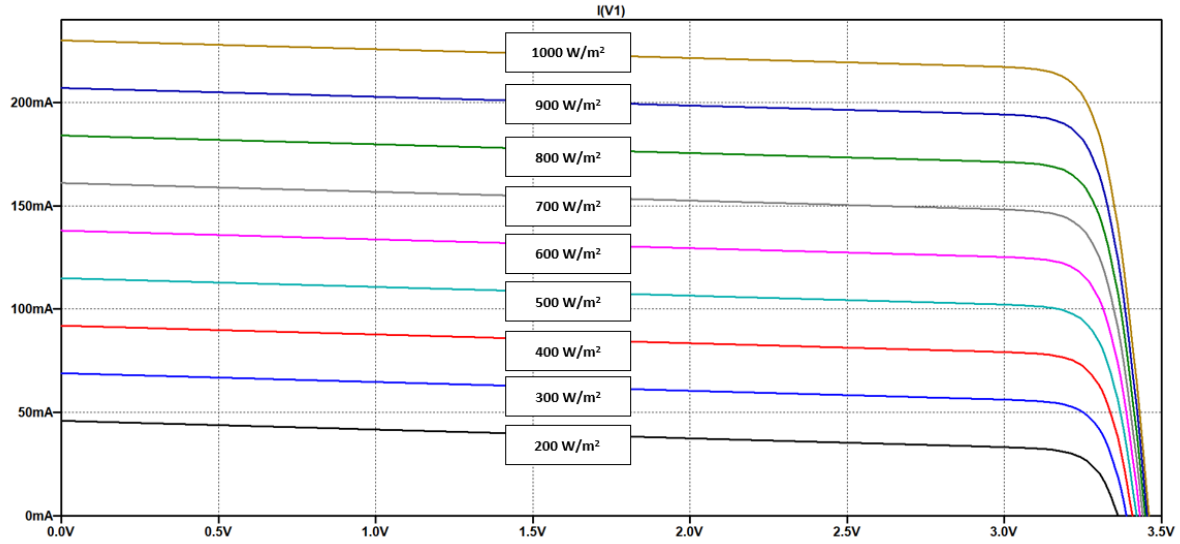

Figure 5.4: I – V curves of MC-SP0.8-NF-GCS for Solar irradiation levels from 200 W/m^2 to 1000 W/m^2 at 25°C

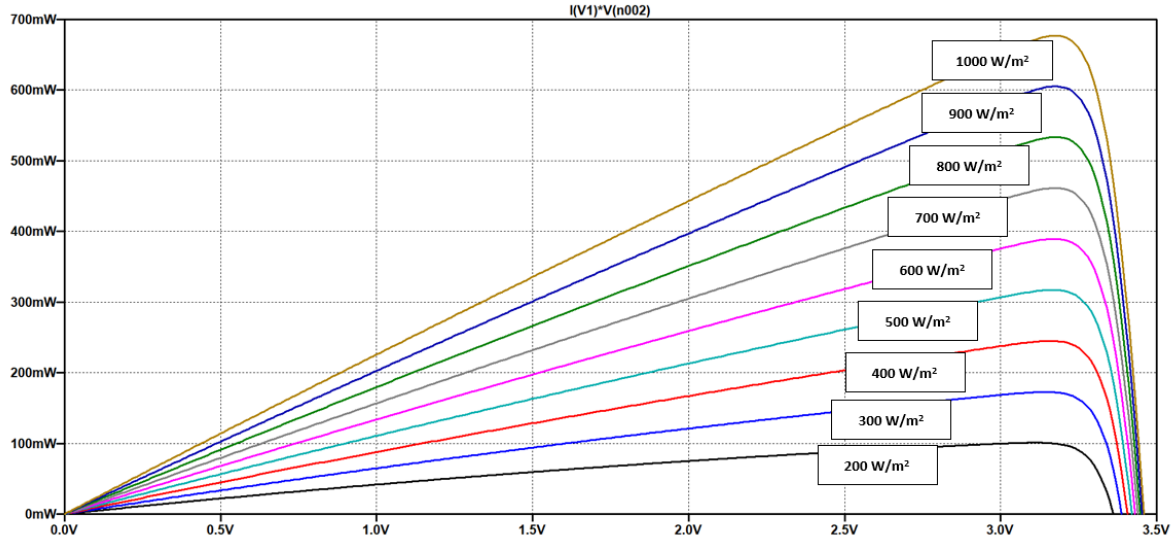

Figure 5.5: P – V curves of MC-SP0.8-NF-GCS for Solar irradiation levels from 200 W/m^2 to 1000 W/m^2 at 25°C

Analysis:

On observing these curves, it is indicated that by increasing the value of solar irradiation level G from 200 W/m^2 to 1000 W/m^2 has increased the cell current of the solar module proportionally; it can be defined in such a way that the incident light on the solar module profoundly influences the generation of current. As much as exposure to the incident light will generate cell current accordingly. Apart from this, the slight increment in the cell voltage is also noticed. The most important factor to analyze is the maximum power generation under

what circumstances can occur. In this regard, the maximum power generation by MC-SP0.8-NF-GCS module is approximately 765 mW at the highest irradiation level, i.e., 1000 W/m^2 at 25 °C and is decreased till 99 mW at 200 W/m^2, denoting the impact of highly cloudy and rainy weather.

5.2.1.3 Effect of Temperature variation on I – V and P – V Curves of the Module

In the same manner, the impact of temperature dependence will be observed by varying specific parameters on the simulator. For analyzing the influence of varying temperatures on the solar module, the temperature parameter TEMP will be varied from 15°C to 85°C by keeping the solar irradiation parameter G as a constant or STC, i.e., 1000 W/m^2. The generated plots for both I – V and P – V curves can be seen in Figures 5.6 and 5.7.

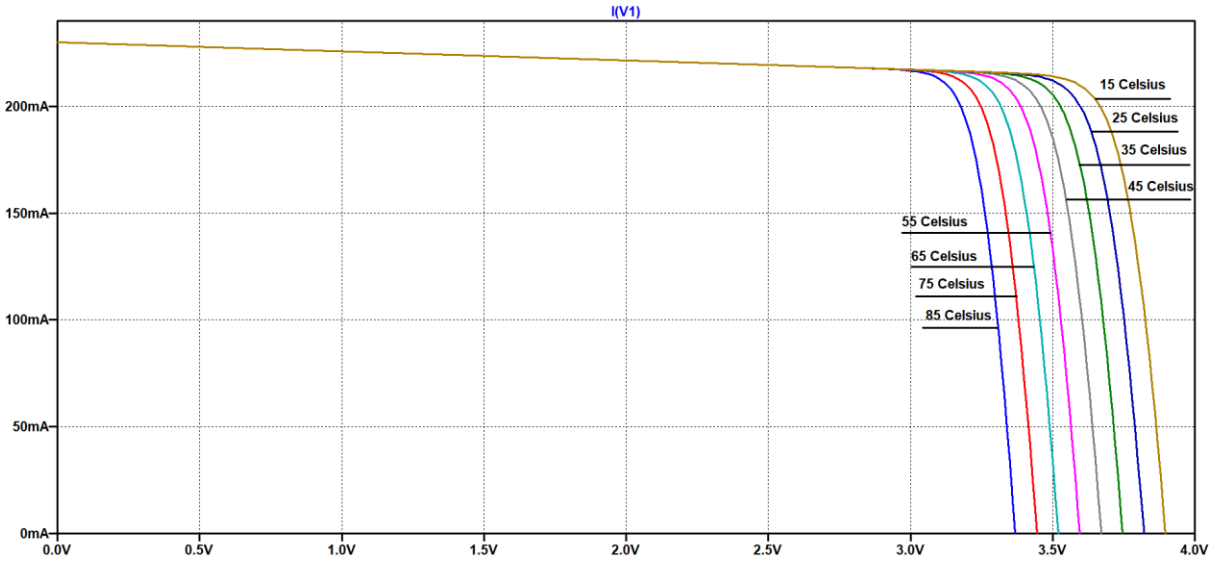

Figure 5.6: I – V curves of MC-SP0.8-NF-GCS for Temperature variation between 15°C to 85°C at 1000 W/m^2

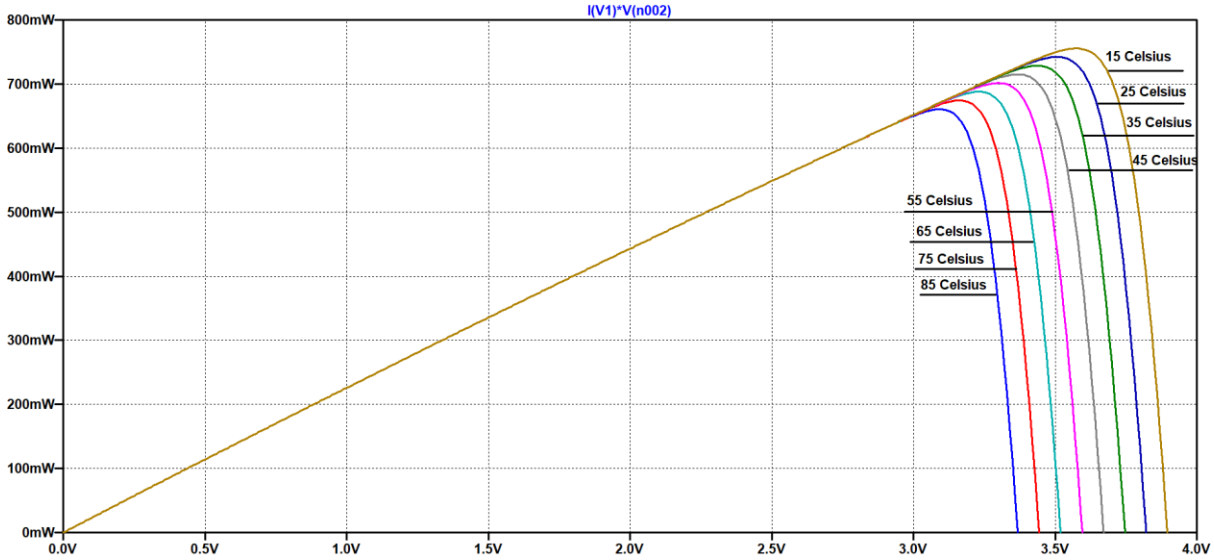

Figure 5.7: P – V curves of MC-SP0.8-NF-GCS for Temperature variation between 15°C to 85°C at 1000 W/m^2

Analysis

By observing the plots, it is analyzed that the increase in temperature is decreasing the cell voltage, hence effecting the output power, which is being decreased with an increase in temperature. For analyzing the maximum power condition under various temperature levels and at constant solar irradiation, the maximum power generated at 15°C is 772 mW and is decreased till 642 mW at 85°C.

The temperature impact is also there, but it's not entirely reducing the power generation of the solar module as the solar irradiation does on rainy weather, which highly decreases the power generation of the same module.

5.2.2 Comparative Analysis between Simulation and Experimental Results for Solar EHC

The generated results will now be compared with the experimental results of the manufacturer's datasheet in terms of characteristic curves. As the data provided in datasheet is demonstrating the plots for I – V curves under three different temperature levels; 25 °C, 50 °C, 75 °C as shown in Figure 5.8, whereas, for solar irradiance, the plots are represented under different levels as 200 W/m^2, 400 W/m^2, 600 W/m^2, 800 W/m^2, 1000 W/m^2 respectively as shown in Figure 5.9.

The simulation data and the experimental data are almost similar in terms of I – V curves under temperature variation, the simulation data has been reproduced to compare with the visually experimental data plots.

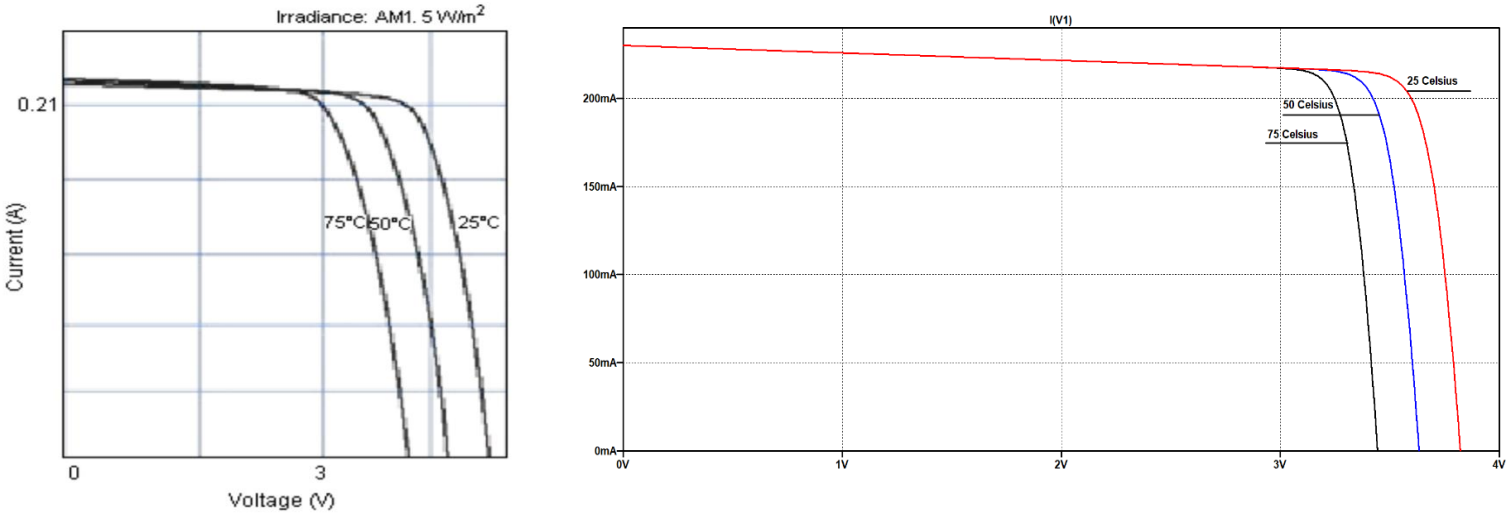

Figure 5.8: Comparative analysis between experimental and simulated results for I – V curves under different temperature levels

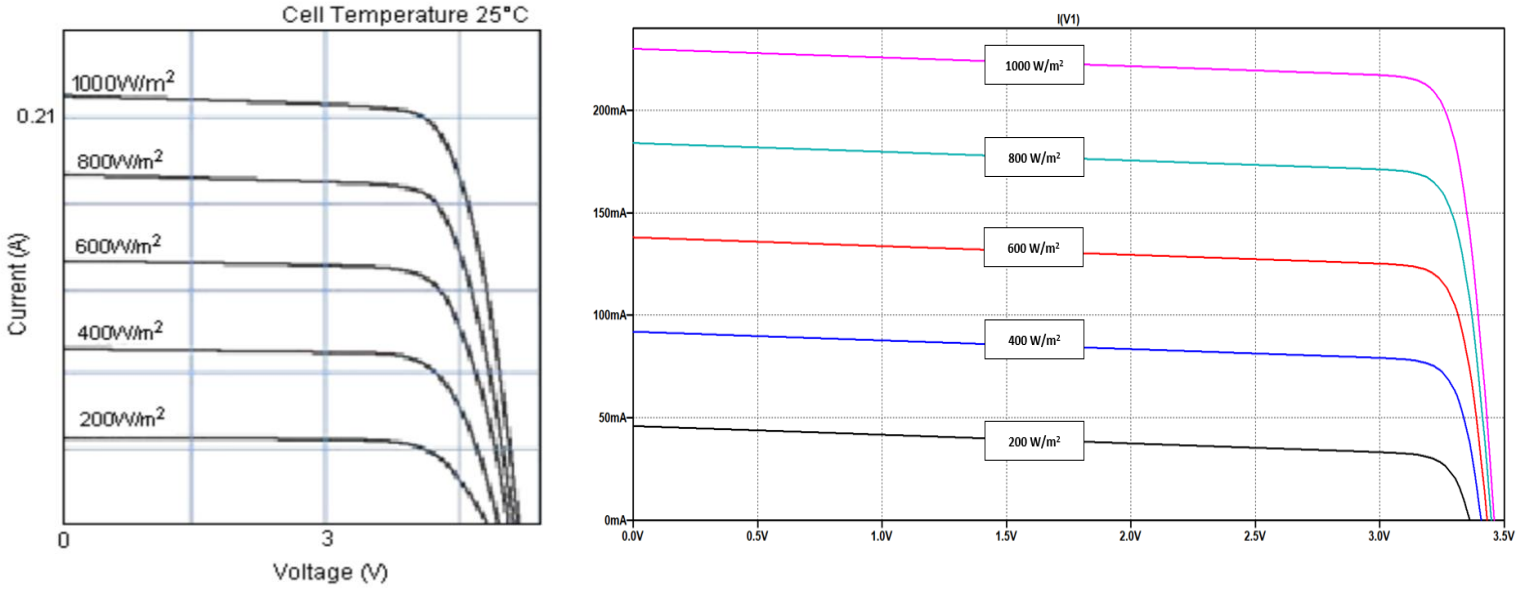

Figure 5.9: Comparative analysis between experimental and simulated results for I – V curves under different solar irradiation levels

5.2.3 Solar EHC Module Characterisation and Performance Curves

In this phase, the solar module, combined with LTC3105 PMIC, will be analyzed in a number of parameters to see the optimal power generation under these circumstances. The following settings have been initialized over the simulation setup, and with extensive simulation analysis, the data log has been generated for voltage, current, and power values, available in Appendix.

As from the above-analyzed characterization of the chosen module, it has been clearly identified that the solar irradiation or incident light profoundly influences the solar module for power generation, as cloudy or rainy weather will decrease the output power generation of the solar module due to impact of incident light which is directly proportional to the cell current, hence the cell current will decrease.

Irrespective of the STC conditions applied to the Solar EH based LTC3105 module; now, we will analyze the various solar irradiation levels for analyzing the behavior of the proposed module in terms of power generation.

Extensive simulations have been carried out to calculate the required data for power generation under different solar irradiations levels. The simulation settings are considered as follows:

The Vout setting for PMIC is calculated to make the stable output voltage on PMIC by setting the resistors R1 = 2.26 Meg and R2 = 1 Meg, which will stable the output voltage Vout = 3.3 V.

For analyzing the impact of various irradiation levels, the range will start from 1000 W/m^2 till 200 W/m^2 with the difference of 100 W/m^2 at every next simulation.

For first simulation the solar irradiation (G) will be kept at 1000 W/m^2 with varying load configurations (R_{LOAD}) which starts from 100 Ω till 500 Ω with a step size of 50 Ω; Which is constant Solar Irradiation (G) with varying R_{LOAD} situation at constant temperature 25°C.

After carefully analyzing the data and collecting in the log, the next simulation will be initiated for constant Solar Irradiation 900 W/m^2, with varying load R_{LOAD} configuration from 100 Ω till 500 Ω with a step size of 50 Ω at constant temperature 25°C.

The simulations are continued in the following manner till the last solar irradiation level, i.e., 200 W/m^2, varying Rload (100 Ω till 500 Ω, step size 50 Ω), at constant temperature 25°C.

In such a manner, the characteristics data have been analyzed, and the characteristics curves have been generated.

5.2.3.1 Effect of Solar Irradiation on Solar EHC Module: I – V curves

For analyzing the PMIC behavior, sustainability is main concern to understand that whether or not, under what circumstances, the PMIC could sustain the load. Apart from this, the MPPT algorithm also needed to be stabilized on PMIC, for which absolute values must be initialized to see the behavior of the whole system at the output. However, the number of parameters has been applied and initialized on the setup based on trial and error situation by taking care of the following perceptions:

(a) Analyzing the sustainability of PMIC under varying Rmppc values (for MPPT algorithm)

(b) Observing the output voltage stable conditions and unstable conditions

(c) Analyzing the maximum output power generation under varying solar irradiation levels and different load configurations

As soon as solar irradiation starts to decrease from 1000 W/m^2 till 200 W/m^2 then we can observe that the output voltage starts to drop from 3.3 V till 0.5 V

The generated I – V curves of the Solar EHC module can be seen in Figure 5.10. By observing these curves, we can say that the highest level of solar irradiation, i.e., 1000 W/m^2, has generated the highest level of current, i.e., 33.81 mA at R_{LOAD} configuration of 100 Ω. As soon as load starts to increase with a step size of 50 Ω, the generation of current starts to decrease. As an increase in load settings will directly impact on the current of the system. However, solar irradiation is the same throughout the initial circumstance. It means that on the sunny day or highest level of incident light being exposed to the solar module can have the impacts as mentioned above. If considering the increase in load, whereas, there's no change in the output voltage, as it remained stable at 3.3 V during the highest incident light conditions.

For solar radiation levels 1000 W/m^2 till 800 W/m^2, the output voltage remained constant at all load conditions from 100 Ω till 500 Ω. Whereas, from 700 W/m^2 till 500 W/m^2 the output voltage was unable to sustain at initial load conditions, but as soon as the load starts to increase, the output voltage is also increased and came to stable output at 3.3 V. Whereas, the lowest solar irradiation levels, 300 W/m^{2,} and 200 W/m^2 weren't able to sustain the output voltage till 3.3 V and went till 2.0 V for the highest given load settings.

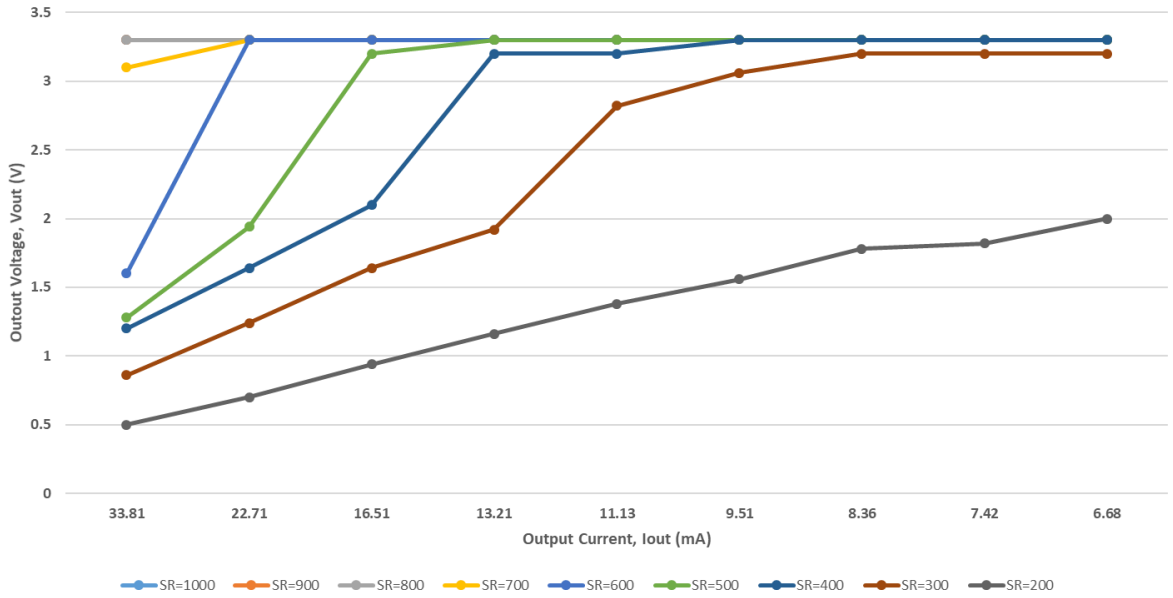

Figure 5.10: Solar EHC Output Voltage – Output Current curves at 3.3 V considering various levels of Solar irradiation under different load configurations

5.2.3.2 Effect of Solar Irradiation on Solar EHC Module: Power Curves

The power curves are arranged into two variations, which are P – I and P – V curves. As already mentioned, the sustainability of PMIC is a crucial concern, and precisely following the constraints and limitations based on output power and MPPT, we need to analyze the maximum power generation by Solar EHC module under different conditions.

The generated power curves are demonstrated in Figure 5.11; from this, we can analyze the response of the EHC module for generating maximal output power. By observing the initial curve, we can see that at maximum solar irradiation level, i.e., 1000 W/m^2, the maximum output power after following the MPPT algorithm is established at 108.60 mW under constant temperature 25°C and R_{LOAD} at minimum level, i.e., 100 Ω. This power starts to decrease with an increase in the R_{LOAD} values by reaching 22.28 mW at R_{LOAD} of 500 Ω. A similar situation is followed by the next solar irradiation levels (900, 800, 700) W/m^{2,} with a slight difference as a decreased value in output power. However, the exciting phase starts from Solar irradiation 600 W/m^2, where at the initial load setup, the generated power recorded is 28.6 mW, which is due to unstable voltage initiation at this particular solar irradiation phase, which however starts to stabilize after following load settings. The lowest possible generation of power is recorded at Solar irradiation of 200 W/m^2, R_{LOAD} = 500 Ω, which is 8.31 mW from the EHC module.

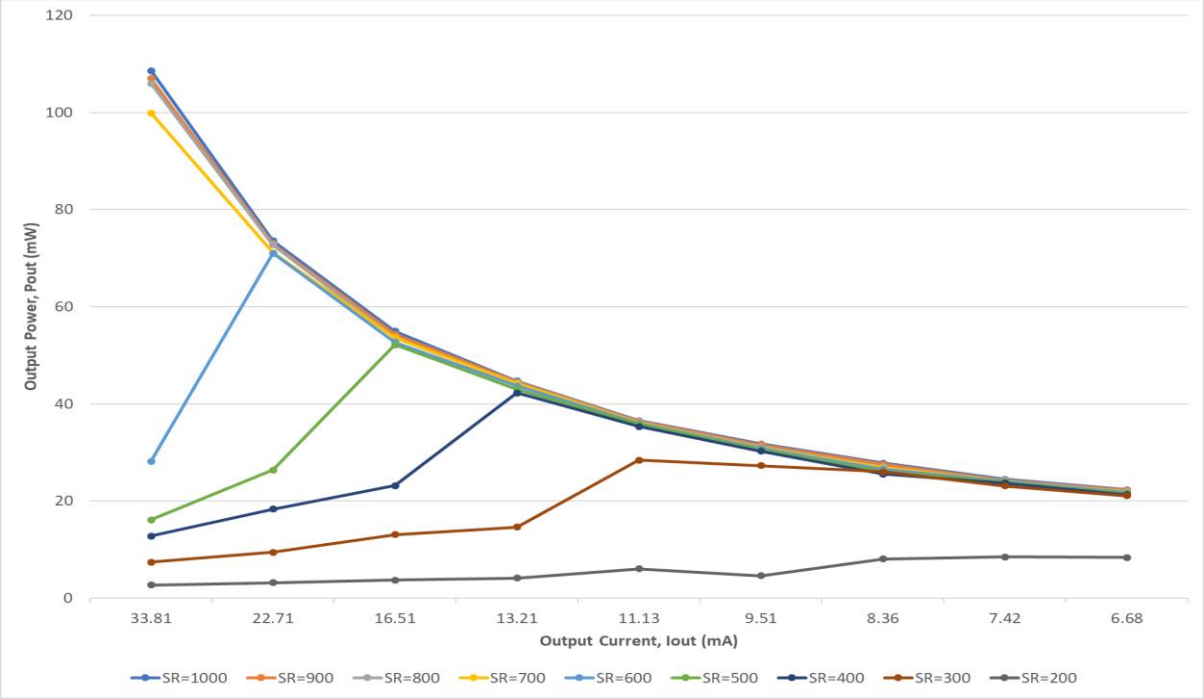

Figure 5.11: Solar EHC Output Power – Output Current curves at 3.3 V considering various levels of Solar irradiation under different load configurations

Figure 5.12 shows another way for representing power generation curves, where output power Pout as a function of output voltage Vout is parameterized under various solar irradiation levels.

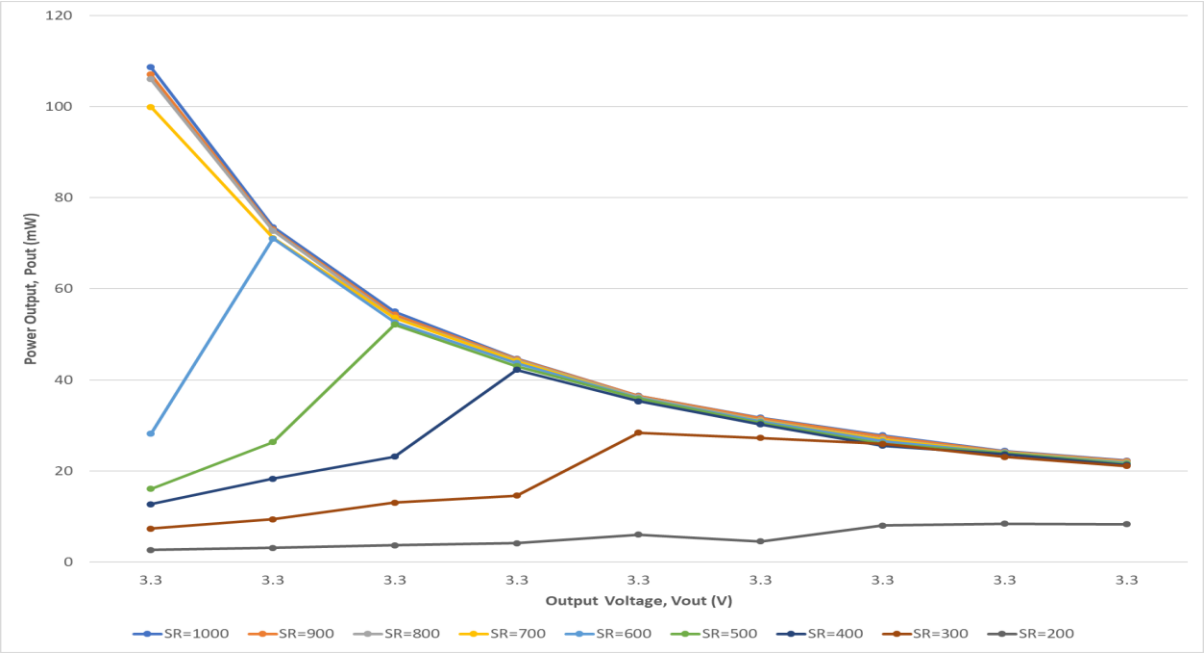

Figure 5.12: Solar EHC Output Power – Output Voltage curves at 3.3 V considering various levels of Solar irradiation under different load configurations

5.2.4 Maximum and Minimum Power Generation for Solar EHC Module

For more accessible analysis, only minimum and maximum power generation values have been considered in the following Table 5.1, which will be compared with IoT power requirements at the end of this chapter under comparative analysis for power generation and power consumption.

Table 5.1: Power generation of Solar EHC module at a minimum and maximum level

Solar EHC Power Generation (Pout)		
Solar irradiation W/m^2	Pmax under minimum load mW	Pmin at maximum load mW
1000	108.60	22.28
900	107	22.21
800	106.01	21.97
700	99.89	21.85
600	28.16	21.73
500	16.09	21.56
400	12.74	21.32
300	7.37	21.08
200	2.68	8.31

5.3 Thermal Energy Harvesting Modelling and Simulation in LTspice

In chapter 4, the methodology and approach towards the proposed Thermal based Energy Harvesting circuit (EHC) have been discussed. In this section, the complete step-by-step simulation setup will be highlighted along with achieved objectives for this study.

For modeling the commercial thermoelectric generator TEC1-12722 along with LTC3108 PMIC, the complete energy harvesting circuitry is transformed in terms of electrical circuitry, as seen in Figure 5.13.

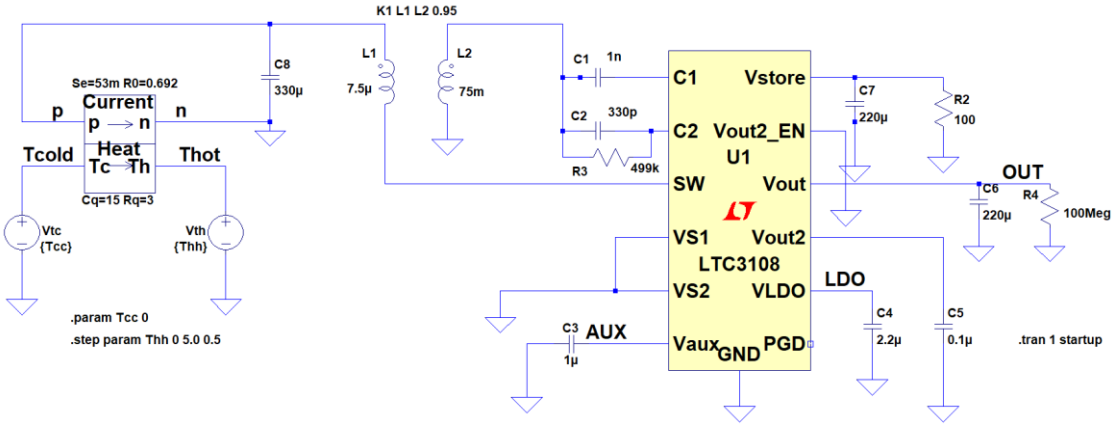

Figure 5.13: Thermal Energy Harvesting Circuit of TEC1-12722 with LTC3108 PMIC

In this setup, the extracted and calculated parameters of the chosen TEC1-12722 are initialized in the circuitry incorporated with PMIC, and before proceeding towards the characterization of TEG in terms of power generation, the first setting is to examine the open circuit testing for chosen thermal module for building the base towards further performance analysis.

Thermal transducer is incorporated with LTC3108 PMIC; there is a specific reason behind the selection of this PMIC as compared to others discussed in Chapter 4, as this power IC is explicitly designed for EHC modules for harvesting low efficient thermal energy and having the lowest cold start voltage as low as 20 mV. Other than that, this IC serves four different Vout settings, which makes it ideal for this research profile. As mentioned in the LTC3108 datasheet, the main output can be programmed to one of four fixed voltages for powering the sensor or wireless transmitter. However, our research profile has targeted two fixed voltages out of four (**2.3, 3.3**, 4.1, 5) for analyzing the performance curves regarding output power generation and the behavior of the PMIC. The central perspective taken under consideration for output voltage setting is that at what temperature range and at what load configuration the PMIC can sustain the output based on two fixed Vout settings; 2.3 V, 3.3 V.

The modeling and simulation analysis is based on the aspects mentioned above, considering two scenarios:

The Thermal EHC module performance curves will be examined as:

(a) Analyzing characteristics curves at Vout = 2.3 V

(b) Analyzing characteristics curves at Vout = 3.3 V

5.3.1 Thermal EHC Module Characterisation and Performance Curves

For analysis of thermal EHC module, the following settings will be initialized in the simulation environment: For simulating temperature difference or heat energy on EHC module the temperature experienced by TEC on both cold and hot sides is incorporated with two voltage supplies specified as Vtc (cold side) and Vth (hot side) linked with subcircuit of the module. Where Vtc is held at 0 °, C and Vth is swept in a linear step from 0 °C till 5 °C with the step size of 0.5 °C. The values for R_{LOAD} are tested and then selected based on the capability of the PMIC to sustain the load on two different V_{OUT} settings; 2.3 V, 3.3 V. There are three variations in the chosen range which are initialized as, smaller range [50 – 900; increment of 50], middle-range [1000 – 9000; increment of 1000], and the larger range [100 K – 500 K; increment of 100 K]. The next sections are dedicated to separate settings and observations related to open circuit testing and analyzing characteristic curves at two fixed output voltages.

5.3.2 TEG Modelling in LTspice: Open circuit testing

In order to analyze the accuracy of the TEG module, it is mandatory to simulate the open circuit testing before evaluating the further performance criterion.

The following simulation setup has been carried out to process the open-circuit conditions. The setup demonstrated on the LTspice simulator can be seen in Figure 5.14.

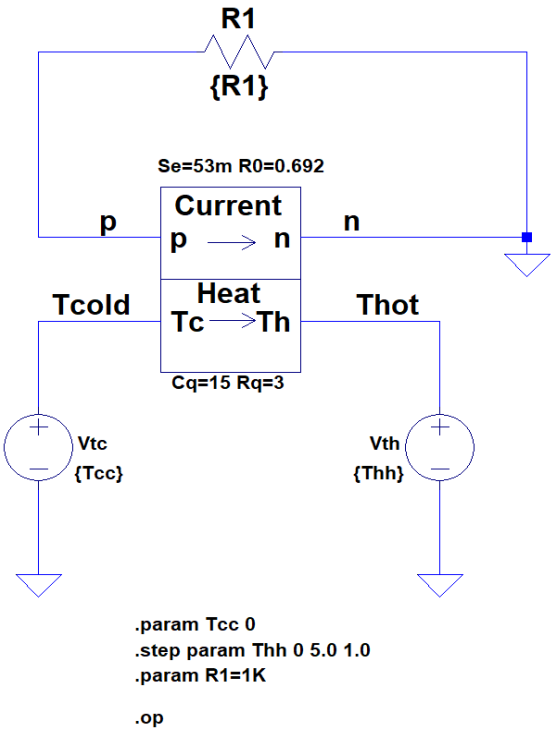

Figure 5.14: TEC1-12722 Open circuit test setup

The open-circuit consists of the temperature gradient, which is considered as an input, and the electrical output voltage will be measured without the load connection. For simulating the idling condition or open circuit situation, the values will be given as; for resistive value (R1) will be initialized as 1 KΩ, the thermal and electrical parameters are applied to the TEG module. The generated open circuit curve over temperature gradients can be seen in the Figure 5.15, where open circuit voltage is varied linearly with the increase in the temperature gradients (ΔT = (TH – TC (°C))).

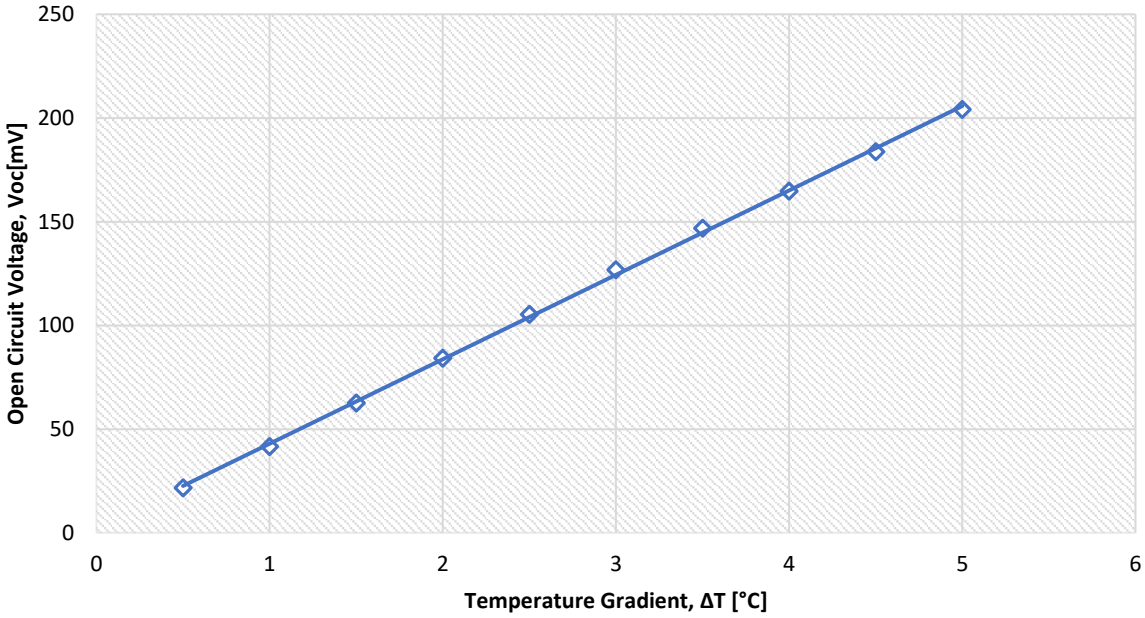

Figure 5.15: Open circuit testing Voc vs. Temperature gradients

5.3.3 Setup1: Setting V_{OUT} at 2.3 V for Thermal EHC Module

The calculated thermal and electrical parameters of TEC1-12722 mentioned in Table 4.5 have been initialized in the thermal EHC prototype; the output voltage will be programmed to remain at 2.3 V by setting the VS1 and VS2 pins to ground (GND) on the LTC3108 PMIC. One crucial aspect to consider here is that the temperature gradient ΔT will be scaled as low as possible, as already mentioned in Chapter 3 regarding the human body harvesting for wearables the observed temperature difference is quite small, and the maximum defined temperature difference across TEG is 5 °C. Hence, the simulation setting for temperature gradients ranged from 0.5 °C to 5.0 °C, with an incremental step size of 0.5°C.

5.3.3.1 EHC Module I – V curves at V_{OUT} = 2.3

For observing the current versus voltage (I – V) curves for Thermal EHC, the temperature difference ΔT starts from 0.5 °C until the output voltage comes at stable or fixed output voltage setting, while, the series of resistive load (R_{LOAD}) is implemented for measuring the values for output current (I_{OUT}) and output voltage (V_{OUT}). The generated I – V curves can be seen in Figure 5.16.

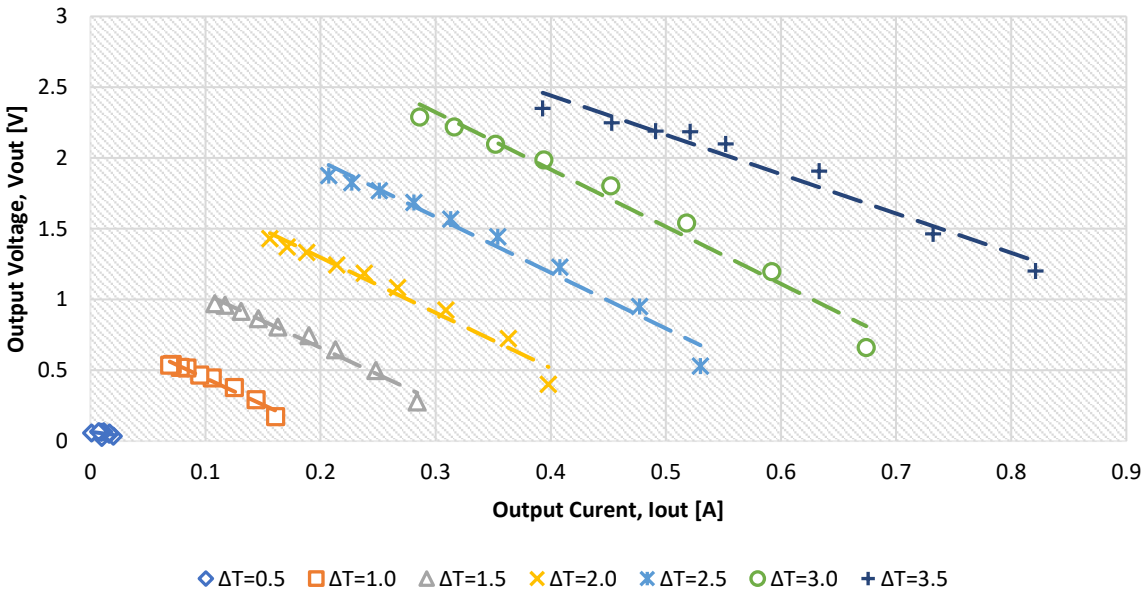

Figure 5.16: Thermal EHC Output Voltage – Current curve at 2.3 V

5.3.3.2 EHC Module Power Curves at V_{OUT} = 2.3

The output power generation for the Thermal EHC module will be analyzed; in this regard, the open circuit testing data collected will be utilized. The direct proportional relation is established between the generated power and the temperature gradient due to already examined data collected from the voltage (V_{OUT}) versus current (I_{OUT}) curves by applying a fixed resistive load. The output power (P_{OUT}) as a function of output current (I_{OUT}) parametrized in the temperature gradients (ΔT) is demonstrated as the generated characteristic curves of Thermal EHC, as shown in Figure 5.17.

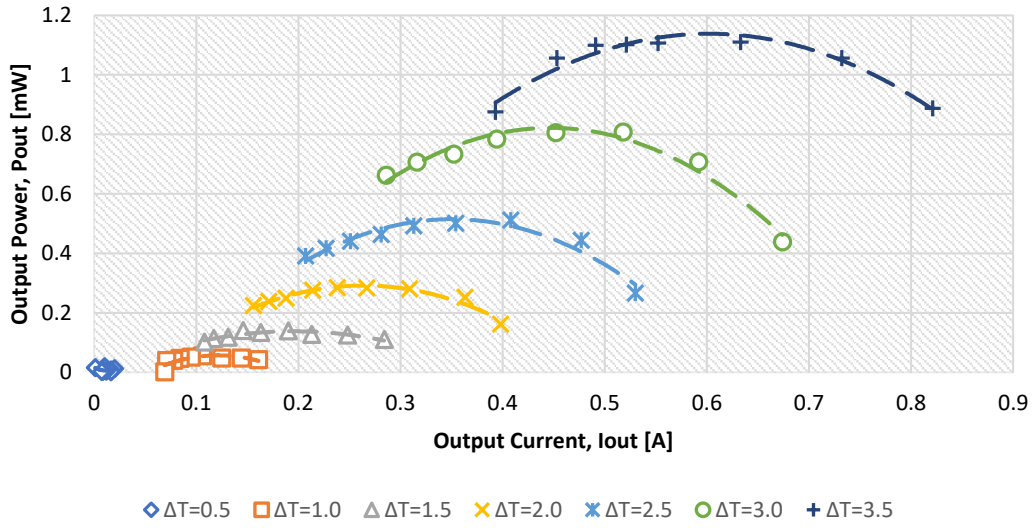

Figure 5.17: Thermal EHC Output Power – Output Current curve at 2.3V

By observing the curves, it is evident that the increase in temperature has significantly raised the output power generation of the module, hence following a highly quadratic nature.

The alternative way for representing power generation is essential in terms of output voltage (V_{OUT}) is demonstrated in Figure 5.18, which gives a proper insight of the impact of temperature on the voltage and taking more temperature and time for stabilizing the voltage.

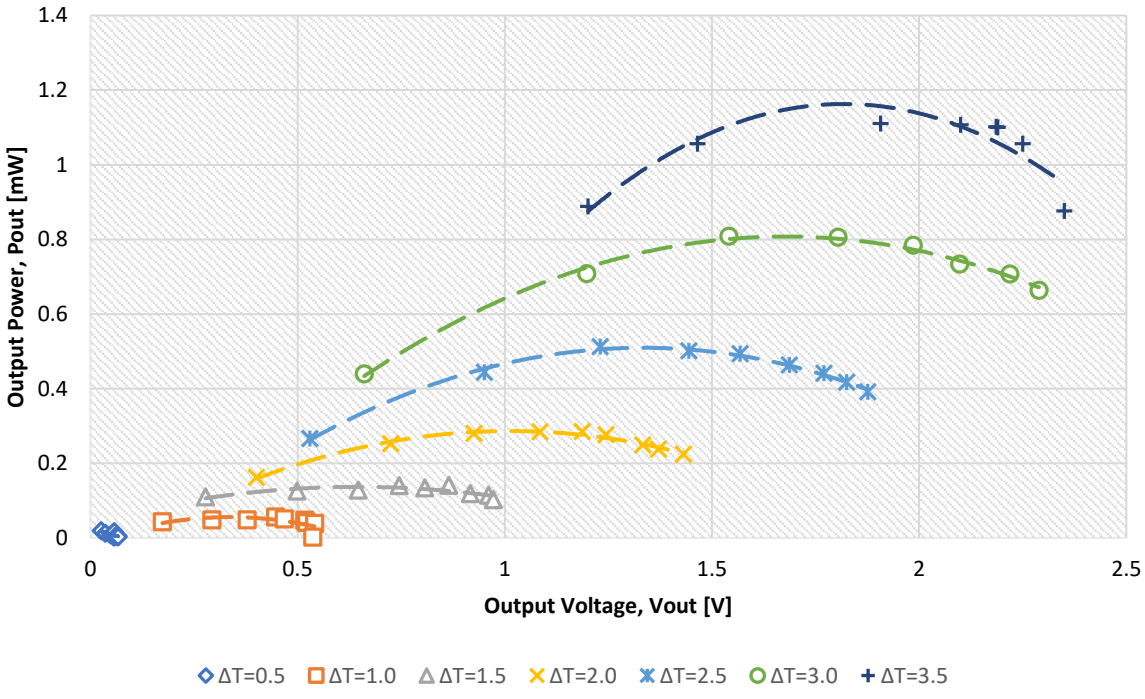

Figure 5.18: Thermal EHC Output Power – Output Voltage curve at 2.3 V

5.3.4 Setup 2: Setting V_{OUT} at 3.3 V for Thermal EHC Module

The already calculated parameters will be applied as an input for another setup of Thermal EHC at 3.3 V. For setting the output voltage V_{OUT} at 3.3 V, the VS1 pin will be connected with VAUX pin and VS2 with GND.

5.3.4.1 EHC Module I – V Curves at V_{OUT} = 3.3

The current versus voltage curves will be analyzed for the Thermal EHC module at 3.3 V setting in PMIC. The generated curves can be seen in Figure 5.19, which represents the existence of the linear relationship between output voltage (V_{OUT}) and output current (I_{OUT}). Other than this, this setup requires more temperature gradients to reach the stable output voltage as compared to the 2.3 V setup.

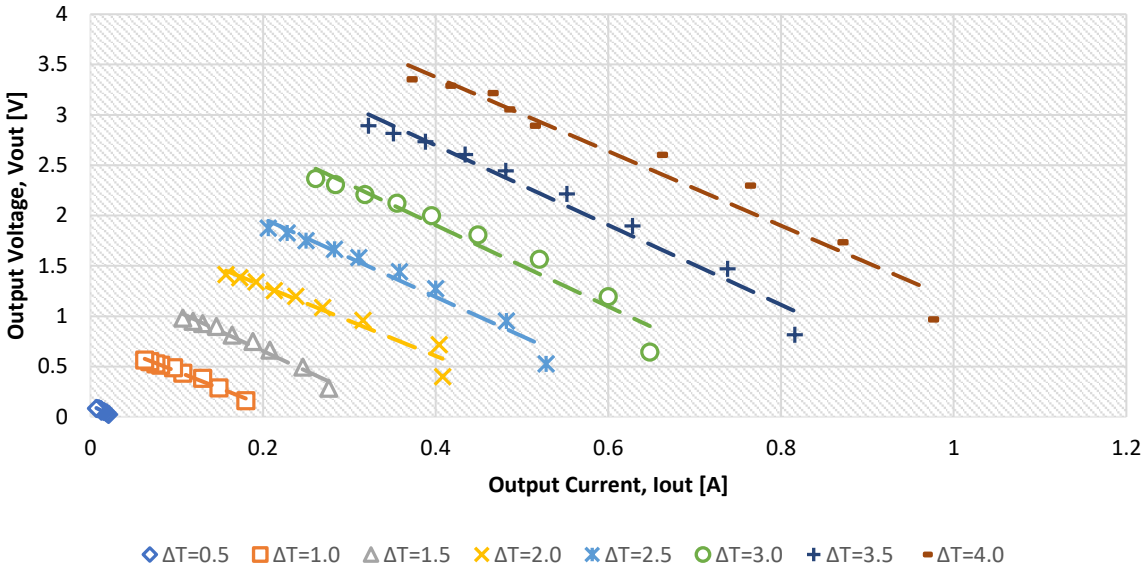

Figure 5.19: Thermal EHC Output Voltage – Current curve at 3.3 V

5.3.4.2 EHC Module Power Curves at V_{OUT} = 3.3

The same parameters will be applied here except the output voltage setting, as V_{OUT} = 3.3 V. The results generated from I – V curves made a basis for direct proportional relation between the power supplied for a fixed load and temperature gradients. Since the power dissipation in the external load will be based on the general theory of electrical circuit analysis i.e. $P = R_L I^2_{OUT}$. By applying this formulation, the generated power curves are obtained as the P_{OUT} as the function of I_{OUT} and V_{OUT} carrying various resistive loads. The generated curves can be seen in Figure 5.20, showing the maximum power generation as compared to the previous setup.

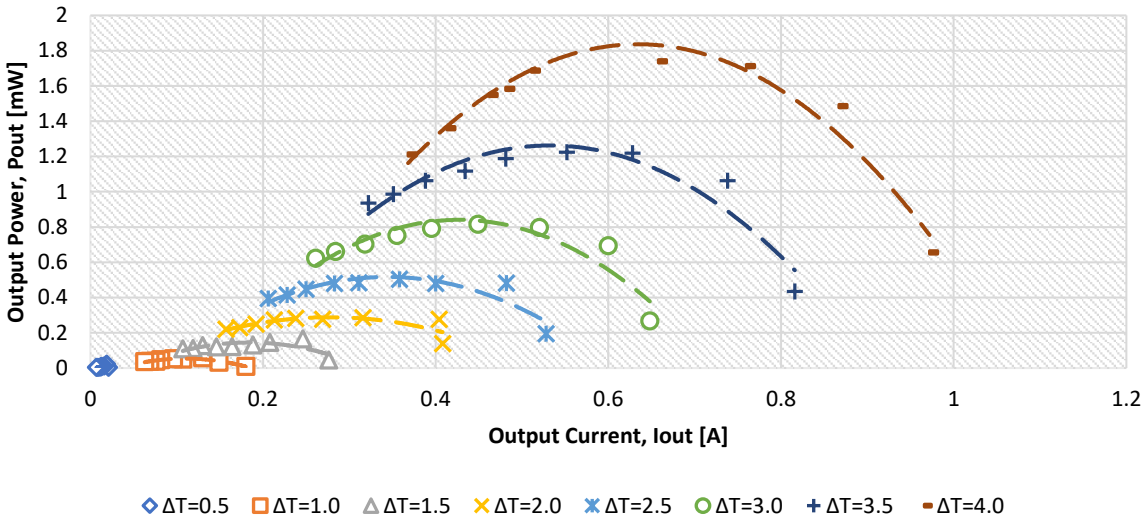

Figure 5.20: Thermal EHC Output Power – Current curve at 3.3 V

By carefully inspecting the generated power curves in Figure 5.21, it is evident that the maximal output power (P_{OUT}) is approximately half of the maximal output voltage (V_{OUT}), and this voltage is equal to half of the open circuit output. Hence, in this regard, it has verified the formula for TEG at the maximum power transfer moment [137].

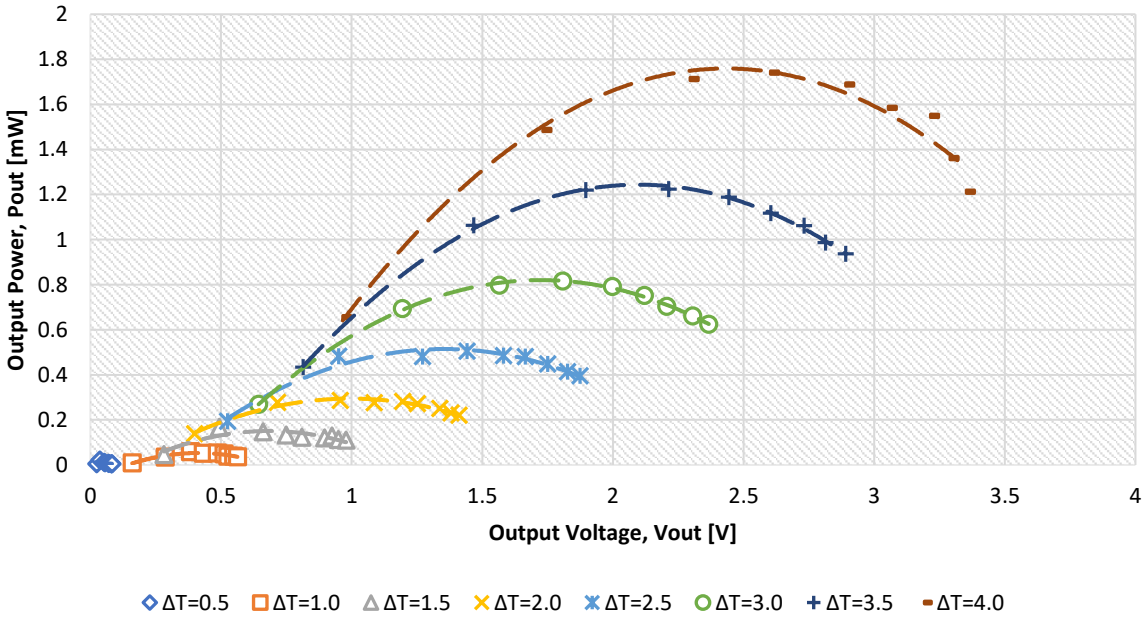

Figure 5.21: Thermal EHC Output Power – Voltage curve at 3.3 V

5.3.5 Maximum and Minimum Power Generation for Thermal EHC

For more accessible analysis, only minimum and maximum power generation values have been considered in the following Table 5.2, which will be compared with IoT power requirements

at the end of this chapter under comparative analysis for power generation and power consumption.

Table 5.2: Power generation of Thermal EHC module at a minimum and maximum level

Thermal EHC Power generation (P_{OUT})		
Power generation at 2.3 V_{OUT}		
Temperature (°C)	**P_{OUT} at R_{LOAD} Minimum (mW)**	**P_{OUT} at R_{LOAD} Maximum (mW)**
3.5	0.688	1.098
Power generation at 3.3 V_{OUT}		
Temperature (°C)	**P_{OUT} at R_{LOAD} Minimum (mW)**	**P_{OUT} at R_{LOAD} Maximum (mW)**
4.0	1.529	1.719

5.3.6 Comparative Analysis between Simulation and Experimental Results for Thermal EHC: Discussion

The results are assessed for verifying the characteristics and performance of the chosen Thermal module TEC1-12722 under two different setups. In the first scenario, the performance current and voltage curves were collected till 3.5 °C according to the LTC3108 PMIC capability, in which the programmed output voltage setting at 2.3 V became stabilized till this temperature range. Hence, the maximum power generation following these settings went till P_{MAX} = 1.098 mW (I_{MAX} = 0.467 mA, V_{MAX} = 2.353 mV). The second scenario took 4.0 °C to stabilize the programmed output voltage at 3.3 V; hence by observing the generated maximum power curves, we found out that maximum power P_{MAX} reached till 1.719 mW (I_{MAX} = 0.521 mA, V_{MAX} = 3.3 V).

Currently, this is purely simulation-based study before moving towards the prototyping of the stated model, and for the sake of making a basis, we have followed and analyzed the already available research on the same series of TEC incorporated with LTC3108 PMIC as benchmarking the hypothesis of our analysis.

In the already available module, the commercially available TEC used for simulation purpose is TEC-12706 as the same series of TEC is being used in our study, various literature and prototypes have been analyzed which utilizes TEC-127 series along with PMIC LTC3108, to see the output power generation. But they weren't available in terms of spice simulation study

connected with PMIC to analyze output power. So, based on literature and analysis, we have followed their output result and have set them as a benchmark with the output of our research. One critical thing to consider here is that the nature of our research is different (Power generation P – V curves) than the ones we are following to see the output power generation at the end.

However, we have tried to set a reference point based on the following.

(i) The focus is on TEG as a wearable EHS with lower temperature difference, i.e., 0 to 5°C, Considering the average output power for a wearable TEG using state-of-the-art TE materials with ZT=1 is approximately 30μW/cm^2 [162].

(ii) In terms of efficiency, TEC 127 with PMIC was compared along with other converters to analyze the lowest temperature range, where the author claims to get 55% efficiency, as shown in Figure 5.22, with constant output power of 719 μW [163].

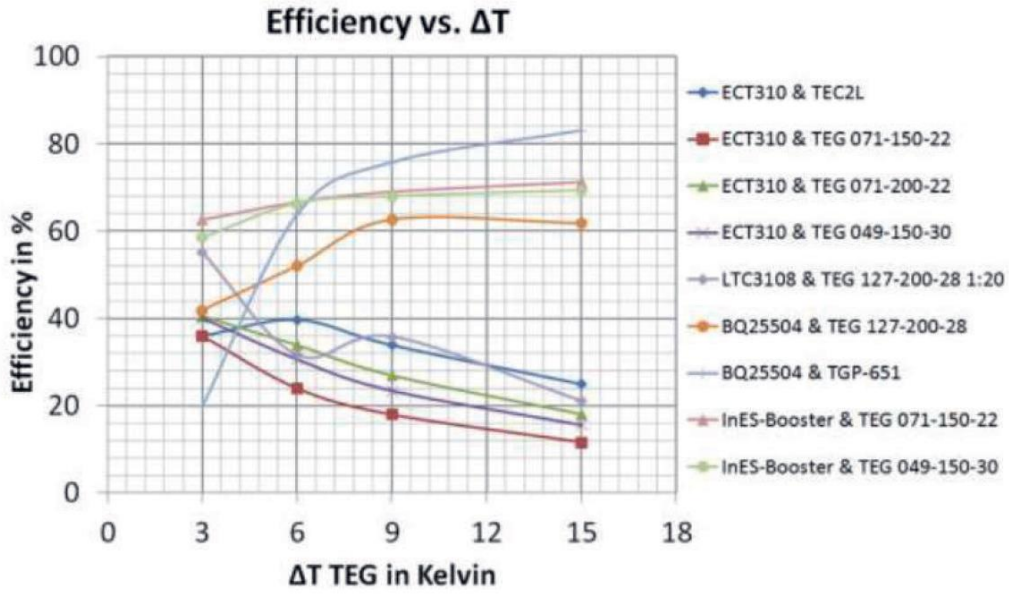

Figure 5.22: Efficiency comparison of different PMIC combinations in TEG [163]

(iii) A thesis result has been analyzed, which practically implemented TEC1-12706 with LTC3108; here, the authors claim to charge a wearable device from human body temperature [164].

(iv) The author presented a prototype for Autonomous Wireless Sensor with a Low-Cost TEG for Application in Automobile Vehicles, in which TEC1-12706 has been experimented along

with 5 different step-up converters, amongst all, LTC3108 has provided the optimal result for powering the autonomous sensor [165].

5.4 IoT Power Constraints

The major objective after analysis and power generation by solar and thermal modules is based on IoT power requirements. The established study of power generation will be compared with the power consumption of typical IoT devices, specific components, etc., to see whether the approach for implementing energy harvesting on IoT is feasible or not. In this regard, it is mandatory to determine the basis for comparison and understanding of the IoT power criteria. The average power consumption will be highlighted in three different phases given as:

(a) Average power requirement of various sensors

(b) Average power requirement of different Microcontroller units (MCU)s

(c) Average power consumption of typical IoT applications

Before contemplating the complete IoT application, the vital thing to consider is that the essential element of any IoT device is a sensor and a microcontroller unit (MCU). There are various types of sensors having their specific power consumption, as demonstrated in Table 5.3 [166], and a variety of MCUs with their operating frequencies and powering requirements as shown in Table 5.4 [167].

Table 5.3: Sensor types and its powering requirements.

Sensor Type	Power Consumption
Gas sensor	500mW – 800mW
Image sensor	150mW
Pressure sensor	10mW – 15mW
Acceleration sensor	3mW
Temperature sensor	0.5mW – 5mW

Table 5.4: Comparison of average power consumption for MCUs.

Performance Metrics	NV-MCU	JSSC2017	ISSCC2016	VLSI2015	ISSCC2015	ISSCC2014
Architecture	Cortex-M0 32 bit	Cortex-M0 32 bit	8051 8 bit	MSP430 16 bit	MSP430 16 bit	MSP430 16 bit
Frequency [MHz]	200	30	100	25	16	20
Active power [μW/Mhz]	26.7	28.92	33	33	28.3	145

Standby power [μW]	0.7	0.009	N/A	0.7	0.32	1.2
Average power@ intermittent operation[μW]	47.14	143.3	>2900	583.2	499.8	2560

The power consumption related to specific IoT applications along with their states and all related components will be highlighted to have better insight regarding each and every element powering requirement while combined as a single application. The following data presented in Table 5.5 for average power consumption of typical IoT application is taken from the annual report [168] presented by 4E (Energy Efficient End-use Equipment) International agency regarding Energy harvesting technologies for IoT edge devices.

Table 5.5: Average power consumption of several IoT applications

Product	**User Link**	**Product Link**	**Battery type**	**Peak Power consumption (W)**					**Average power consumption (W)**
				Initial Pairing	**Network mode 1**	**Network mode 2**	**Initialize actuators, sensors**	**Power consumption during Rx/Tx**	
Tracking device	Bluetooth Low Energy (BLE)	Bluetooth Low Energy (BLE)	1x CR2025 ½ years	0.17	0.12	0.12	0.17	0.001-0.003 (2500 ms)	n/a
Fire detector	WiFi 802.11b/g/n	-Wi-Fi 802.11b/g/n -Wireless Interconnect (IEEE 802.15.4) -Bluetooth Low Energy (BLE)	6x AA (lithium) 5 years	1.8	0.12	0.12	1.8	0.02 (10 s)	0.61
Smart Home Thermostat	WiFi 802.11b/g/n	868 MHz Band	2x AAA (alkaline)	0.46	0.06-0.1	0.06-0.1	0.25-0.4	0.003 (500 ms)	0.15
Smart Home Door/Window	WiFi 802.11b/g/n	868 MHz Band	1x AAA (alkaline)	0.15	0.1	0.1	0.17	0.003 (500 ms	0.15
Sensor Node Thermometer	Bluetooth Low Energy (BLE)	Bluetooth Low Energy (BLE)	1x CR2025 up to 3 months	1.1 (speaker)	0.08	0.08	Not applicable	0.001 (2500 ms)	0.1

Measuring power consumption and defining certain limits is always critical. However, it is pointless to set a general threshold regarding the powering requirements of IoT devices. These typical applications are dynamic in nature and are in different states, which are continuously variable depending upon the system design and purpose of the required use. But for the sake of making analysis and comparison with this study, these thresholds are always acceptable with tolerance ratio.

5.5 Solar and Thermal Power Generation and Comparative Analysis for IoT

For solar power generation, the conditions under which analysis has been carried out are dynamic; the power levels could be intermittent due to environmental factors impacting directly to the power generation of the module. In this research, the Solar EHC prototype for commercial solar transducer MC-SP0.8-NF-GCS has generated certain levels of power generation under various environmental and temperature dependence, for the sake of easier grip on analysis the minimum and maximum power levels have been tabulated from entire collected simulation data. The range varies between 2.68 mW (minimum generated power) till 108.60 mW (maximum generated power), specifically, under various solar irradiation levels and load configurations. The above-generated data can be compared with the power consumption data accumulated in Tables 5.1 and 5.2, where we can loosely relate the power generation and power consumption. However, mostly the Solar EHC prototype can sustain the required power consumption criteria for IoT components as well as wearable IoT devices; in our case, considering all mentioned examples of IoT application in Table 5.5. Hence this simulation also compared with experimental analysis conducted by manufacturers have proved at a certain point that this prototype could be used as an EH based module for IoT application.

Considering the thermal EHC module, there are two factors in comparison; firstly, the power generation and power consumption, secondly, the performance analysis and selection of TEG, is also an important decision that will directly influence the whole design of the system.

The power generation by Thermal EHC is demonstrated in Table 5.2, where the minimum and maximum power output is listed for an easier understanding of the whole situation. As there were two programmed output voltages (2.3 V, 3.3 V), and accordingly, the power has been generated. Due to the target applications require lesser temperature gradients such as human body heat harvesting for wearables; therefore, the temperature gradients were till 3.5°C and 4.0°C. The minimum power generated for TEC1-12722 fused as a Thermal EHC prototype went till 0.688 mW and maximum reached at 1.719 mW. By comparing the generated thermal power with the required power for IoT; It is evident that TEG can generate that much power, which can make the IoT device operational, considering the specific sensors in Table 5.3 and some of the MCUs in Table 5.4. Other than that, the above mentioned IoT application could be powered up by this thermal EHC prototype.

Comparing the simulation data for performance efficiency as well for selection of TEG, the factors that profoundly affects the performance and efficiency of TEG are the temperature

difference ΔT between the cold and hot side of the device and the material and specifically for lower temperature difference (BiTe) or (PbTe) are used.

For wearable, the typical TEG will work below their optimal efficiency due to lower temperature difference, and TEGs are mostly providing their higher efficiency at higher temperature levels.

The commercially available TEGs are analyzed in terms of efficiency and to understand the suitability of these TEGs when it comes to support EH based wearable devices. This paper [169] has demonstrated the three different types of TEGs in which each model is pertaining to a specific combination of temperature, resistance, and voltage values. They are given as:

(a) TEG2-126LDT (BiTeTEG) optimised for lower temperature differences [170]
(b) TEG2-07025HT-SS (BiTe TEG) optimised for liquid-to-liquid applications [61]
(c) TEG1-PB-12611-6.0 (BiTe and PbTe hybrid) capable of withstanding higher temperature differences (up to 360 °C) [23].
Based upon the measurement results and the power needs of wearable devices, it is concluded that commercially available TEGs, especially those optimized for low-temperature applications – such as the TEG2-126LDT device, enable providing power levels suitable to power typical wearable medical devices.
Therefore, according to the available reported prototypes, mostly used TEC1-12706 presented their results in terms of suitability and efficiency, whereas, TEG2-126LDT which is specially prepared for lower temperature difference, also proved to be an efficient solution for wearable devices.

Therefore, the results obtained from the simulation authenticated the hypothesis and proposed prototypes for both solar and thermal modules that the commercially selected devices (MC-SP0.8-NF-GCS, TEC1-12722) could fulfill this demand as a power source.

6 Conclusion and Future Research Directions

In this chapter, the entire contributions of the dissertation will be summarized and will discuss the future directions and open research issues related to the energy harvesting and IoT to extend this work further.

6.1 Conclusion and Discussion

By the advent of the Internet of Things (IoT), which entirely changed the way to communicate, interact, connect, operate, and exchange the data around the globe, from smartwatches to medical implant devices, from self-directed car parking till industrial smart machines; IoT is getting pervasive. Despite of enormous technological advancement, IoT is still at a slower pace due to battery and power obstacles. To cope with this hurdle, Energy harvesting (EH) comes to rescue and can provide solutions to these problems; but surely, it's a long way to go. Nevertheless, researchers have bloomed both IoT and EH by their tremendous contributions and have been successfully moving out of this critical phase. Currently, the situation is still at an infancy position when it comes to design an EH based IoT application or any product by an end-user. There's no availability of any standard version or a guideline to follow up the procedure specifically for those small-scale users who would like to build their own EH system for their IoT projects and would like to save cost on electricity consumption. Other than that, there's a lack of modeling tool which is highly required for prototyping and analyzing the complex EH setup and various parameters involved for capturing the intermittent ambient energy source, transforming into usable output and considering numerous heterogenous factors in designing the system.

This dissertation has addressed the issues mentioned above related to the enormous necessity towards a proper guideline and step-by-step approach in building any EH based IoT application by end-users. This study has provided a simulation-based method by modeling the whole EH setup and analyzing the performance and behavior of the system under numerous stringent conditions. Such detailed understanding is necessarily required before the implementation of the entire system into the physical EH module. For proving the authenticity of the simulation study and acquired results, the proposed modules have been compared with the available EH based systems as well as the power generation perspective in terms of power consumption, related to IoT products. However, the results have made a basis that the proposed modules could fulfill the powering requirement of the available IoT devices.

The contributions related to each and every step will be provided in the upcoming section with brief analysis and publications for achieving all steps at the same time.

Scientific contributions of Doctoral dissertation:

Thesis I:

The comprehensive steps towards building an Energy Harvesting (EH) based Internet of Things (IoT) has been defined through extensive literature review and provided insight regarding the selection of all blocks required in that system.

- **IoT prerequisite and power consumption threshold have been specified.**
- **Analyzed and Highlighted the factors involved in the selection of EH transducers and their efficiency by specific algorithms**
- **Worked on EH based PMICs regarding power management and sustainability issues**

Related publications: [P5, P10, P16]

1. This dissertation has demonstrated the necessity of comprehensive guidelines for building an Energy harvesting based prototype for powering low-powered devices, IoT, or wearable devices. As IoT is the major basis for powering its components or a complete application through ambient Energy harvesting sources. The most critical phase is to establish the basis and understanding of fundamentals and their associated issues which could be settled by alternatives. In this regard, IoT design considerations have been studied and analyzed in terms of energy harvesting sources, IoT components, IoT communication protocols, and most importantly the power consumption analysis has been carefully investigated.

2. A systematic literature review regarding all ambient energy harvesting sources have been carried out by observing the actual power generation of the transducers and associated techniques required to enhance the efficiency of the energy harvesters. Analyzing the specific transducers and their selections play a pivotal role in enhancing the efficiency of the harvesters, which is comprehensively addressed, analyzed and published, also a thorough review is conducted for available battery characteristics in terms of their support for IoT and EH based products.

3. The general steps have been configured for building an EH based self-powered IoT devices, the required components, their necessity, and understanding the balance between the power generation and power consumption, which is a critical measure to take care. However, power management is the mandatory element, and the number of power management ICs have been analyzed and reviewed, which accurately follows the working principle of energy harvesting and supporting the IoT devices.

4. Out of various energy harvesting sources, the most abundantly available sources, Solar and Heat/Thermal energy, have been investigated for building a prototype as an Energy harvesting circuitry (EHC) based on Solar and Thermal sources. These prototypes were tested under a number of parameters as both sources are highly dependent on environmental conditions.

Thesis II

Transforming the commercial Solar and Heat/Thermal module into an electrical SPICE model have been analyzed and defined according to the manufacturer's datasheet (techniques supporting limited data revealed by manufacturer's)

- ***The Solar parameter extraction techniques experimented with mathematical formulations have been analyzed and presented another version with modification in ideality factor for solar module and then presented according to the accurate results produced***
- ***The Thermal parameter extraction containing both thermal and electrical aspects have been analyzed and chosen along with related techniques to configure after careful analysis and simulation of parameters***

Related Publications: [P1, P4, P9, P13]

5. The most critical challenge is to transform the commercially selected transducers for both solar and thermal sources into an electrical perspective. And that's why this study is interesting and highly required, as end-users don't have access to experimental equipment for deciding the efficiency factor and performance of the chosen transducer, without such setup the only thing which can give a little piece of information is the manufacturer's datasheet. The challenge resides in extracting the electrical parameters from limited information are discussed. In this regard, the number of parameters

extraction techniques for both transducers have been investigated and, at the same time, verified on simulation for getting the accurate result for both transducers. The mathematical formulations for both modules, according to their various equivalent circuits, have been derived and calculated.

6. Related to the modeling of both modules, the number of available models has been examined, as consideration of the solar and thermal model is again a challenge, and this step will ultimately impact the parameter extraction techniques. However, various equivalent circuit models and related mathematical formulation were investigated, and the ones that closely matched our research profile were chosen, which is purely electrical and for small-scale users.

7. The number of PMICs has been analyzed in terms of energy harvesting sources, and for both transducers, the PMIC has been selected accordingly. The detailed analysis has been conducted and highlighted the factors involving in selection of PMIC as this element includes numerous tasks for enhancing the efficiency of the harvested power, and how the output voltage will be considered according to the IoT voltage ratings.

Thesis III

The Solar Energy Harvesting Circuitry (EHC), along with commercial-off-the-shelf (COTS) PMIC; LTC3105 have been proposed for supporting IoT applications.

- ***The entire EHC setup has been experimented with several environmental conditions; Solar irradiation and Temperature dependence, as well as three different load setups, have been set up.***
- ***The sustainability of PMIC has been analyzed after extensive simulation by varying the number of parameters, more specifically under various load configurations, for maximum power generation, power management, and accuracy of the system.***
- ***This prototype can be reused and reprogrammed by other researchers and engineers according to their prerequisite of the EH based IoT system.***

Related Publications: [P4, P5, P9, P12]

8. The proposed Solar EHC module has been characterized for analyzing the number of parameters inside the EHC. More specifically, the power generation is the main concern which will be compared with the power consumption of IoT. The environmental conditions (solar irradiation, temperature) have been induced to see the performance and behavior of the whole system when all components are combined. The trial and error based extensive simulation have been carried out, and all parameters and their associated responses were recorded as data logging, and graphical representation has been developed for more straightforward analysis. The generated simulated data are compared with the experimental data from the manufacturer's datasheet, and it produced almost identical results with a minor error ratio.

Thesis IV

The Thermal Energy Harvesting Circuitry (EHC) along with commercial-off-the-shelf (COTS) PMIC; LTC3108 have been proposed for supporting IoT applications.

- ***The entire EHC setup has been experimented with two programmed output settings (2.3 V, 3.3 V) and temperature gradients scaled from 0.5°C to 5.0°C (for human body heat wearable applications); also three different variations of load setups have experimented.***
- ***The sustainability of PMIC has been analyzed after extensive simulation by varying the number of parameters, more specifically under various load configurations for maximum power generation, power management, and accuracy of the system.***
- ***This prototype can be reused and reprogrammed by other researchers and engineers according to their prerequisite of the EH based IoT system.***

Related Publications: [P1, P5]

9. The proposed Thermal EHC module has been characterized for investigating the various factors involved and their influence on the system. As the power generation of the thermal module is the actual factor under consideration as well as the smaller temperature difference (0°C till 5°C) is the focal study due to the target human body heat wearables. The analysis is carried out based on trial and error situations under the number of parameters to see the performance of the whole system. The generated data

have been logged, and the desired graphical representation has been produced to make analysis easier. The measured data is also compared with already available thermal EH modules and was used as a benchmark for associating this prototype for already experimented modules. Other than that, the feasibility of the thermoelectric material was also considered and has been under analysis regarding performance and which thermoelectric cooler or generator to select for IoT applications.

Thesis V

The trial and error case study generated for efficient and maximum power output has been compared with already experimented IoT components in terms of power consumption. The comparative analysis has proved the authenticity of all steps involved in the proposed Solar and Thermal EHC for supporting IoT power demands.

Related Publications: [P1, P5, P9, P12]

10. In both modules, the power generation data was carefully recorded, and for the sake of analysis on the power consumption of IoT, the data is compared to see whether the prototypes can produce the required power levels, which can make IoT product operational.

11. The acquired results have been compared with IoT components such as sensors, Microcontroller unit (MCU)s, and the complete IoT applications. Hence, the measured results produced typical power levels that could be suitable for some of the IoT components and applications. Consequently, this simulation-based analysis towards building an EH based IoT system could be used as a point of reference and provides an insight towards a fundamental step-by-step basis for developing any Solar or Thermal found IoT prototype for specific applications.

6.2 Future Research direction

The major goal of this study was to establish a proper guideline towards building an energy harvesting based IoT device. This thesis has addressed the necessity of modeling tool and has produced the prototypes for solar and thermal sources for optimal power generation. The comparative analysis has been carried out for authenticating the power generation from

harvesters and power consumption of IoT devices. However, various issues are still there, which require further research contributions. However, this practical study can be considered as the initial point of reference in multiple domains. The future directions for this research include the following:

- Similar investigations could be performed with different types of transducers in both solar and thermal, as PV and TEC/TEG efficiency relies on the material used in the modules. In this manner, any discrepancies or inaccuracies in modeling will then be highlighted. Later, the performance of different PV and TEC/TEG along with PMICs, and their respective results should be studied meticulously. Accordingly, this study will help in deciding on the selection of transducers in terms of their performance and efficiency regarding LTspice modeling.

- Combining two different energy harvesting sources and analyzing the performance of the entire EH setup, as heterogeneity and harvesting transformation techniques are different such as AC-AC, AC-DC. To analyze the impact of having two various energy sources on the system and at the output power generation. Not all PMICs can take two different energy sources as an input. However, there are some of the available products like MAXIM 17710, which can provide the capacity of inducing more than one energy harvesting sources.

- Combining the same energy harvesting sources in series and parallel to see the impact of the output power generation with PMIC, whether the PMIC can sustain that much input or not. This study could help to seek the issues related to PMIC and could suggest the limitations associated as well as compatibility.

- Finally, we propose a thorough and comprehensive investigation of the cost-effectiveness of multiple energy sources in comparison, which will guide the user to select the transducers and related components accordingly. These investigations could lead towards the development of better models for multiple energy sources and better insight for modeling tools, which could support the building of cost-effective powering solutions for typical IoT devices.

7 References

[1] ‘An IoT Data Flood. Are we ready? (Intro)’, *Denis Canty*, 23-Feb-2015. [Online]. Available: https://deniscanty.com/2015/02/23/an-iot-data-flood-are-we-ready-intro/. [Accessed: 22-Nov-2019].

[2] S. C. Mukhopadhyay and N. K. Suryadevara, ‘Internet of Things: Challenges and Opportunities’, in *Internet of Things: Challenges and Opportunities*, S. C. Mukhopadhyay, Ed. Cham, The Netherlands: Springer International Publishing, 2014, pp. 1–17.

[3] ‘Internet of Things (IoT) Market Size, Share, Trends, Opportunities & Forecast’, *Verified Market Research*. [Online]. Available: https://www.verifiedmarketresearch.com/product/global-internet-of-things-iot-market-size-and-forecast-to-2026/. [Accessed: 22-Nov-2019].

[4] H. Jayakumar, K. Lee, W. S. Lee, A. Raha, Y. Kim, and V. Raghunathan, ‘Powering the Internet of Things’, in *2014 IEEE/ACM International Symposium on Low Power Electronics and Design (ISLPED)*, 2014, pp. 375–380, doi: 10.1145/2627369.2631644.

[5] B. Aksanli, T. S. Rosing, and I. Monga, ‘Benefits of Green Energy and Proportionality in High Speed Wide Area Networks Connecting Data Centers’, in *Proceedings of the Conference on Design, Automation and Test in Europe, Dresden, Germany, 12-16 March 2012*, San Jose, CA, USA, 2012, pp. 175–180, doi: 10.1109/date.2012.6176458.

[6] ‘The Internet of Things (IoT) Starts with Intel Inside®’, *Intel*. [Online]. Available: https://www.intel.com/content/www/us/en/internet-of-things/overview.html. [Accessed: 22-Nov-2019].

[7] S. Sarkar, ‘Chapter 11 - Internet of Things—robustness and reliability’, in *Internet of Things: Principles and Paradigms*, R. Buyya and A. Vahid Dastjerdi, Eds. Burlington, MA, USA: Morgan Kaufmann, 2016, pp. 201–218.

[8] I.-I. of Things, ‘Gartner Says the Internet of Things Will Transform the Data Center’, *IoT - Internet of Things*, 19-Mar-2014. [Online]. Available: https://iot.do/gartner-says-internet-things-will-transform-data-center-2014-03. [Accessed: 22-Nov-2019].

[9] ‘3GPP Low Power Wide Area Technologies White Paper’, *Internet of Things*. [Online]. Available: https://www.gsma.com/iot/resources/3gpp-low-power-wide-area-technologies-white-paper/. [Accessed: 22-Nov-2019].

[10] R. V. Prasad, S. Devasenapathy, V. S. Rao, and J. Vazifehdan, ‘Reincarnation in the Ambiance: Devices and Networks with Energy Harvesting’, *IEEE Communications Surveys & Tutorials*, vol. 16, no. 1, pp. 195–213, First Quarter 2014, doi: 10.1109/SURV.2013.062613.00235.

[11] P. Gautam, S. Kumar, and S. Lokhandwala, ‘Chapter 11 - Energy-Aware Intelligence in Megacities’, in *Current Developments in Biotechnology and Bioengineering*, S. Kumar, R. Kumar, and A. Pandey, Eds. Elsevier, 2019, pp. 211–238.

[12] E. Stephens *et al.*, ‘Future prospects of microalgal biofuel production systems’, *Trends Plant Sci.*, vol. 15, no. 10, pp. 554–564, Oct. 2010, doi: 10.1016/j.tplants.2010.06.003.

[13] H. Wang, A. Jasim, and X. Chen, ‘Energy harvesting technologies in roadway and bridge for different applications – A comprehensive review’, *Applied Energy*, vol. 212, pp. 1083–1094, Feb. 2018, doi: 10.1016/j.apenergy.2017.12.125.

[14] ‘17MAD216_EM - Electronic Products & Technology’. [Online]. Available: https://www.ept.ca/features/energy-harvesting-greener-environment/17mad216_em/. [Accessed: 22-Nov-2019].

[15] F. K. Shaikh and S. Zeadally, ‘Energy harvesting in wireless sensor networks: A comprehensive review’, *Renewable and Sustainable Energy Reviews*, vol. 55, pp. 1041–1054, Mar. 2016, doi: 10.1016/j.rser.2015.11.010.

[16] P. Jiao, W. Borchani, H. Hasni, and N. Lajnef, ‘Enhancement of quasi-static strain energy harvesters using non-uniform cross-section post-buckled beams’, *Smart Material Structures*, vol. 26, p. 085045, Aug. 2017, doi: 10.1088/1361-665X/aa746e.

[17] P. Hersch, K. Zweibel, and S. E. R. Institute, ‘Basic Photovoltaic Principles and Methods’, p. 71.

[18] F. Yildiz, ‘Potential Ambient Energy-Harvesting Sources and Techniques’, *Journal of Technology Studies*, vol. 35, no. 1, pp. 40–48, 2009.
[19] S. Galmés and S. Escolar, ‘Analytical Model for the Duty Cycle in Solar-Based EH-WSN for Environmental Monitoring’, *Sensors (Basel)*, vol. 18, no. 8, p. 2499, Aug. 2018, doi: 10.3390/s18082499.
[20] P. G. V. Sampaio and M. O. A. González, ‘Photovoltaic solar energy: Conceptual framework’, *Renewable and Sustainable Energy Reviews*, vol. 74, no. C, pp. 590–601, 2017, doi: 10.1016/j.rser.2017.02.08.
[21] J. Halme, P. Vahermaa, K. Miettunen, and P. Lund, ‘Device Physics of Dye Solar Cells’, *Advanced Materials*, vol. 22, no. 35, pp. E210–E234, 2010, doi: 10.1002/adma.201000726.
[22] T. M. Clarke and J. R. Durrant, ‘Charge photogeneration in organic solar cells’, *Chem. Rev.*, vol. 110, no. 11, pp. 6736–6767, Nov. 2010, doi: 10.1021/cr900271s.
[23] T. Ibn-Mohammed *et al.*, ‘Perovskite solar cells: An integrated hybrid lifecycle assessment and review in comparison with other photovoltaic technologies’, *Renewable and Sustainable Energy Reviews*, vol. 80, pp. 1321–1344, Dec. 2017, doi: 10.1016/j.rser.2017.05.095.
[24] M. N. Bhukya and V. R. Kota, ‘A quick and effective MPPT scheme for solar power generation during dynamic weather and partial shaded conditions’, *Engineering Science and Technology, an International Journal*, vol. 22, no. 3, pp. 869–884, Jun. 2019, doi: 10.1016/j.jestch.2019.01.015.
[25] A. S. Andrenko, Xianyang Lin, and Miaowang Zeng, ‘Outdoor RF spectral survey: A roadmap for ambient RF energy harvesting’, in *TENCON 2015 - 2015 IEEE Region 10 Conference*, 2015, pp. 1–4, doi: 10.1109/TENCON.2015.7373140.
[26] X. Lu, P. Wang, D. Niyato, D. I. Kim, and Z. Han, ‘Wireless Networks With RF Energy Harvesting: A Contemporary Survey’, *IEEE Communications Surveys Tutorials*, vol. 17, no. 2, pp. 757–789, Secondquarter 2015, doi: 10.1109/COMST.2014.2368999.
[27] D. Mishra, S. De, S. Jana, S. Basagni, K. Chowdhury, and W. Heinzelman, ‘Smart RF energy harvesting communications: challenges and opportunities’, *IEEE Communications Magazine*, vol. 53, no. 4, pp. 70–78, Apr. 2015, doi: 10.1109/MCOM.2015.7081078.
[28] S. N. Daskalakis, S. D. Assimonis, E. Kampianakis, and A. Bletsas, ‘Soil moisture wireless sensing with analog scatter radio, low power, ultra-low cost and extended communication ranges’, in *2014 IEEE SENSORS*, 2014, pp. 122–125, doi: 10.1109/ICSENS.2014.6984948.
[29] S. K. Divakaran, D. D. Krishna, and Nasimuddin, ‘RF energy harvesting systems: An overview and design issues’, *International Journal of RF and Microwave Computer-Aided Engineering*, vol. 29, no. 1, p. e21633, 2019, doi: 10.1002/mmce.21633.
[30] Y. Zeng, B. Clerckx, and R. Zhang, ‘Communications and Signals Design for Wireless Power Transmission’, *arXiv:1611.06822 [cs, math]*, Nov. 2016.
[31] F. Yildiz and K. L. Coogler, ‘Low Power Energy Harvesting with a Thermoelectric Generator through an Air Conditioning Condenser’, 2014.
[32] M. D. Vithanage, X. Fafoutis, C. B. Andersen, and N. Dragoni, ‘Medium access control for thermal energy harvesting in advanced metering infrastructures’, in *Eurocon 2013*, 2013, pp. 291–299, doi: 10.1109/EUROCON.2013.6624999.
[33] H. Kuttarmare *et al.*, ‘ Fabrication of Peltier Cooling System: Alternative for Refrigeration ’, *IJARIIE*, vol. 2, pp. 260–264, May 2016.
[34] G. J. Snyder, ‘Small thermoelectric generators’, *Electrochemical Society Interface*, vol. 17, pp. 54–56, Sep. 2008.
[35] D. K. Aswal, R. Basu, and A. Singh, ‘Key issues in development of thermoelectric power generators: High figure-of-merit materials and their highly conducting interfaces with metallic interconnects’, *Energy Conversion and Management*, vol. 114, pp. 50–67, Apr. 2016, doi: 10.1016/j.enconman.2016.01.065.
[36] H. J. Goldsmid, A. R. Sheard, and D. A. Wright, ‘The performance of bismuth telluride thermojunctions’, *British Journal of Applied Physics*, vol. 9, p. 365, Sep. 1958, doi: 10.1088/0508-3443/9/9/306.
[37] A. J. Minnich *et al.*, ‘Modeling study of thermoelectric SiGe nanocomposites’, *Phys. Rev. B*, vol. 80, no. 15, p. 155327, Oct. 2009, doi: 10.1103/PhysRevB.80.155327.

[38] W.-S. Liu, B.-P. Zhang, L.-D. Zhao, and J.-F. Li, ‘Improvement of Thermoelectric Performance of CoSb3−xTex Skutterudite Compounds by Additional Substitution of IVB-Group Elements for Sb’, *Chem. Mater.*, vol. 20, no. 24, pp. 7526–7531, Dec. 2008, doi: 10.1021/cm802367f.
[39] T. Ikeda, L. A. Collins, V. A. Ravi, F. S. Gascoin, S. M. Haile, and G. J. Snyder, ‘Self-Assembled Nanometer Lamellae of Thermoelectric PbTe and Sb2Te3 with Epitaxy-like Interfaces’, *Chem. Mater.*, vol. 19, no. 4, pp. 763–767, Feb. 2007, doi: 10.1021/cm062121p.
[40] J. J. Pulikkotil *et al.*, ‘Doping and temperature dependence of thermoelectric properties in Mg${}_{2}$(Si,Sn)’, *Phys. Rev. B*, vol. 86, no. 15, p. 155204, Oct. 2012, doi: 10.1103/PhysRevB.86.155204.
[41] X. Guo *et al.*, ‘Thermoelectric transport properties and crystal growth of BiSbTe3 bulk materials produced by a unique high-pressure synthesis’, *CrystEngComm*, vol. 15, no. 36, pp. 7236–7242, Aug. 2013, doi: 10.1039/C3CE40780B.
[42] H. Kim, Y. Tadesse, and S. Priya, ‘Piezoelectric Energy Harvesting’, in *Energy Harvesting Technologies*, S. Priya and D. J. Inman, Eds. Boston, MA: Springer US, 2009, pp. 3–39.
[43] H. S. Kim, J.-H. Kim, and J. Kim, ‘A review of piezoelectric energy harvesting based on vibration’, *Int. J. Precis. Eng. Manuf.*, vol. 12, no. 6, pp. 1129–1141, Dec. 2011, doi: 10.1007/s12541-011-0151-3.
[44] V. E and S. Rajakumar, ‘Performance improvement of piezoelectric materials in energy harvesting in recent days – A review’, *Journal of Vibroengineering*, vol. 20, Nov. 2018, doi: 10.21595/jve.2018.19434.
[45] Y.-F. Lin, J. Song, Y. Ding, S.-Y. Lu, and Z. L. Wang, ‘Alternating the Output of a CdS Nanowire Nanogenerator by a White-Light-Stimulated Optoelectronic Effect’, *Adv. Mater.*, vol. 20, no. 16, pp. 3127–3130, Aug. 2008, doi: 10.1002/adma.200703236.
[46] M.-G. Kang *et al.*, ‘Enhanced piezoelectric properties of vertically aligned single-crystalline NKN nano-rod arrays’, *Sci Rep*, vol. 5, p. 10151, May 2015, doi: 10.1038/srep10151.
[47] G. Zhu, R. Yang, S. Wang, and Z. L. Wang, ‘Flexible High-Output Nanogenerator Based on Lateral ZnO Nanowire Array’, *Nano Lett.*, vol. 10, no. 8, pp. 3151–3155, Aug. 2010, doi: 10.1021/nl101973h.
[48] Y. Duan, Y. Huang, Z. Yin, N. Bu, and W. Dong, ‘Non-wrinkled, highly stretchable piezoelectric devices by electrohydrodynamic direct-writing’, *Nanoscale*, vol. 6, no. 6, pp. 3289–3295, Feb. 2014, doi: 10.1039/C3NR06007A.
[49] Y.-F. Lin, J. Song, Y. Ding, S.-Y. Lu, and Z. L. Wang, ‘Piezoelectric nanogenerator using CdS nanowires’, *Appl. Phys. Lett.*, vol. 92, no. 2, p. 022105, Jan. 2008, doi: 10.1063/1.2831901.
[50] C.-T. Huang *et al.*, ‘GaN Nanowire Arrays for High-Output Nanogenerators’, *J. Am. Chem. Soc.*, vol. 132, no. 13, pp. 4766–4771, Apr. 2010, doi: 10.1021/ja909863a.
[51] S. Cao and J. Li, ‘A survey on ambient energy sources and harvesting methods for structural health monitoring applications’, *Advances in Mechanical Engineering*, vol. 9, no. 4, p. 1687814017696210, Apr. 2017, doi: 10.1177/1687814017696210.
[52] A. Harb, ‘Energy harvesting: State-of-the-art’, *Renewable Energy*, vol. 36, no. 10, pp. 2641–2654, 2011.
[53] J.-H. Lee, J. Kim, T. Y. Kim, S. A. Hossain, S.-W. Kim, and J. H. Kim, ‘All-in-one energy harvesting and storage devices’, 2016.
[54] F. Bordry and D. Aguglia, ‘Definition of Power Converters’, *arXiv:1607.01538 [physics]*, 2015, doi: 10.5170/CERN-2015-003.15.
[55] A. Vinco, R. Siddique, D. Brunelli, and W. Wang, ‘AA-Battery Sized Energy Harvesting Power Management Module for Indoor Light Wireless Sensor Applications’, in *Applications in Electronics Pervading Industry, Environment and Society: APPLEPIES 2014*, A. De Gloria, Ed. Cham: Springer International Publishing, 2016, pp. 91–97.
[56] M. K. Stojčev, M. R. Kosanović, and L. R. Golubović, ‘Power management and energy harvesting techniques for wireless sensor nodes’, in *2009 9th International Conference on Telecommunication in Modern Satellite, Cable, and Broadcasting Services*, 2009, pp. 65–72, doi: 10.1109/TELSKS.2009.5339410.
[57] M. K. Kim, M. S. Kim, S. E. Jo, H. L. Kim, S. M. Lee, and Y. J. Kim, ‘Wearable thermoelectric generator for human clothing applications’, in *2013 Transducers Eurosensors*

XXVII: The 17th International Conference on Solid-State Sensors, Actuators and Microsystems (TRANSDUCERS EUROSENSORS XXVII), 2013, pp. 1376–1379, doi: 10.1109/Transducers.2013.6627034.
[58] 'Choosing Power Management IC for Energy-Harvesting | DigiKey'. [Online]. Available: https://www.digikey.hu/en/articles/techzone/2013/may/choosing-a-power-management-ic-for-energy-harvesting-applications. [Accessed: 23-Nov-2019].
[59] 'MAX17710 Energy-Harvesting Charger and Protector - Maxim'. [Online]. Available: https://www.maximintegrated.com/en/products/power/battery-management/MAX17710.html. [Accessed: 23-Nov-2019].
[60] 'BQ25504 Ultra Low Power Boost Converter with Battery Management for Energy Harvester | Nano-Power Management | TI.com'. [Online]. Available: http://www.ti.com/product/BQ25504?keyMatch=BQ25504&tisearch=Search-EN-everything&usecase=part-number. [Accessed: 23-Nov-2019].
[61] 'SPV1050', *STMicroelectronics*. [Online]. Available: https://www.st.com/en/power-management/spv1050.html. [Accessed: 23-Nov-2019].
[62] 'LTC3105 Datasheet and Product Info | Analog Devices'. [Online]. Available: https://www.analog.com/en/products/ltc3105.html. [Accessed: 23-Nov-2019].
[63] 'LTC3108 Dual TEG Energy Harvester (3.3V/2.2V) Operates from Temperature Differentials of Either Polarity Circuit Collection | Analog Devices'. [Online]. Available: https://www.analog.com/en/design-center/reference-designs/circuit-collections/ltc3108-dual-teg-energy-harvester-3-3v-2-2v-operates-from-temperature-differentials-of-either.html#cc-documentation. [Accessed: 10-Jul-2019].
[64] N. Ertugrul, 'Battery storage technologies, applications and trend in renewable energy', in *2016 IEEE International Conference on Sustainable Energy Technologies (ICSET)*, 2016, pp. 420–425, doi: 10.1109/ICSET.2016.7811821.
[65] 'Will Secondary Batteries replace Primaries? – Battery University'. [Online]. Available: https://batteryuniversity.com/learn/archive/will_secondary_batteries_replace_primaries. [Accessed: 23-Nov-2019].
[66] J. Taneja, J. Jeong, and D. Culler, 'Design, Modeling, and Capacity Planning for Micro-solar Power Sensor Networks', in *2008 International Conference on Information Processing in Sensor Networks (ipsn 2008)*, 2008, pp. 407–418, doi: 10.1109/IPSN.2008.67.
[67] 'Summary and Comparison of Battery Characteristics | PVEducation'. [Online]. Available: https://www.pveducation.org/pvcdrom/battery-characteristics/summary-and-comparison-of-battery-characteristics. [Accessed: 23-Nov-2019].
[68] F. Akhtar and M. H. Rehmani, 'Energy replenishment using renewable and traditional energy resources for sustainable wireless sensor networks: A review', *Renewable and Sustainable Energy Reviews*, vol. 45, pp. 769–784, May 2015, doi: 10.1016/j.rser.2015.02.021.
[69] J. Libich, J. Máca, J. Vondrák, O. Čech, and M. Sedlaříková, 'Supercapacitors: Properties and applications', *Journal of Energy Storage*, vol. 17, pp. 224–227, Jun. 2018, doi: 10.1016/j.est.2018.03.012.
[70] 'Supercapacitor vs Battery - Ultracapacitor Pros & Cons', *Arrow.com*. [Online]. Available: https://www.arrow.com/en/research-and-events/articles/supercapacitor-vs-battery-ultracapacitor-pros-and-cons. [Accessed: 23-Nov-2019].
[71] R. J. M. Vullers, R. van Schaijk, I. Doms, C. Van Hoof, and R. Mertens, 'Micropower energy harvesting', *Solid State Electronics*, vol. 53, p. 684, Jul. 2009, doi: 10.1016/j.sse.2008.12.011.
[72] 'Energy Harvesting Powers Wireless Sensors'. [Online]. Available: https://www.psma.com/HTML/newsletter/Q2_2012/page8.html. [Accessed: 23-Nov-2019].
[73] Y. Lee, D. Blaauw, and D. Sylvester, 'Ultralow Power Circuit Design for Wireless Sensor Nodes for Structural Health Monitoring', *Proceedings of the IEEE*, vol. 104, no. 8, pp. 1529–1546, Aug. 2016, doi: 10.1109/JPROC.2016.2547946.
[74] H.-C. Chung, T. Enomoto, K. Loh, and M. Shinozuka, 'Real-time visualization of bridge structural response through wireless MEMS sensors', *Proc SPIE*, vol. 5392, Jul. 2004, doi: 10.1117/12.539263.
[75] Vijay Raghunathan, A. Kansal, J. Hsu, J. Friedman, and Mani Srivastava, 'Design considerations for solar energy harvesting wireless embedded systems', in *IPSN 2005. Fourth*

International Symposium on Information Processing in Sensor Networks, 2005., 2005, pp. 457–462, doi: 10.1109/IPSN.2005.1440973.
[76] J. Polastre, R. Szewczyk, and D. Culler, 'Telos: enabling ultra-low power wireless research', in *IPSN 2005. Fourth International Symposium on Information Processing in Sensor Networks, 2005.*, 2005, pp. 364–369, doi: 10.1109/IPSN.2005.1440950.
[77] K. Lin *et al.*, *Heliomote: Enabling long-lived sensor networks through solar energy harvesting*. 2005.
[78] J. L. Hill and D. E. Culler, 'Mica: a wireless platform for deeply embedded networks', *IEEE Micro*, vol. 22, no. 6, pp. 12–24, Nov. 2002, doi: 10.1109/MM.2002.1134340.
[79] S. Nazir, H. Hamdoun, F. Verdicchio, and G. Fairhurst, 'Autonomous monitoring of critical infrastructures', in *2015 International Conference on Computing, Control, Networking, Electronics and Embedded Systems Engineering (ICCNEEE)*, 2015, pp. 236–241, doi: 10.1109/ICCNEEE.2015.7381369.
[80] A. Ravinagarajan, D. Dondi, and T. S. Rosing, 'DVFS based task scheduling in a harvesting WSN for Structural Health Monitoring', in *2010 Design, Automation Test in Europe Conference Exhibition (DATE 2010)*, 2010, pp. 1518–1523, doi: 10.1109/DATE.2010.5457052.
[81] M. Renaud, K. Karakaya, T. Sterken, P. Fiorini, C. Van Hoof, and R. Puers, 'Fabrication, modelling and characterization of MEMS piezoelectric vibration harvesters', *Sensors and Actuators A: Physical*, vol. 145–146, pp. 380–386, Jul. 2008, doi: 10.1016/j.sna.2007.11.005.
[82] J.-Q. Liu *et al.*, 'A MEMS-based piezoelectric power generator array for vibration energy harvesting', *Microelectronics Journal*, vol. 39, no. 5, pp. 802–806, May 2008, doi: 10.1016/j.mejo.2007.12.017.
[83] G. De Pasquale, Mian Wei, A. Soma, and Jing Wang, 'Capacitive MEMS energy harvesters for structural monitoring: Design and fabrication', in *2009 International Semiconductor Conference*, 2009, vol. 1, pp. 211–214, doi: 10.1109/SMICND.2009.5336566.
[84] J. Kymissis, C. Kendall, J. Paradiso, and N. Gershenfeld, 'Parasitic power harvesting in shoes', in *Digest of Papers. Second International Symposium on Wearable Computers (Cat. No.98EX215)*, 1998, pp. 132–139, doi: 10.1109/ISWC.1998.729539.
[85] Z. L. Wang and J. Song, 'Piezoelectric Nanogenerators Based on Zinc Oxide Nanowire Arrays', *Science*, vol. 312, no. 5771, p. 242, Apr. 2006, doi: 10.1126/science.1124005.
[86] S. Lee *et al.*, 'Super-Flexible Nanogenerator for Energy Harvesting from Gentle Wind and as an Active Deformation Sensor', *Advanced Functional Materials*, vol. 23, no. 19, pp. 2445–2449, May 2013, doi: 10.1002/adfm.201202867.
[87] L. Lin *et al.*, 'Transparent flexible nanogenerator as self-powered sensor for transportation monitoring', *Nano Energy*, vol. 2, no. 1, pp. 75–81, Jan. 2013, doi: 10.1016/j.nanoen.2012.07.019.
[88] S. Roundy, 'Energy Scavenging for Wireless Sensor Nodes with a Focus on Vibration to Electricity Conversion', University of California, 2003.
[89] C. Cepnik and U. Wallrabe, 'A flat high performance micro energy harvester based on a serpentine coil with a single winding', in *2011 16th International Solid-State Sensors, Actuators and Microsystems Conference*, 2011, pp. 661–664, doi: 10.1109/TRANSDUCERS.2011.5969839.
[90] J. M. Donelan, Q. Li, V. Naing, J. A. Hoffer, D. J. Weber, and A. D. Kuo, 'Biomechanical energy harvesting: generating electricity during walking with minimal user effort', *Science*, vol. 319, no. 5864, pp. 807–810, Feb. 2008, doi: 10.1126/science.1149860.
[91] D. Samson, M. Kluge, Th. Becker, and U. Schmid, 'Wireless sensor node powered by aircraft specific thermoelectric energy harvesting', *Sensors and Actuators A: Physical*, vol. 172, no. 1, pp. 240–244, Dec. 2011, doi: 10.1016/j.sna.2010.12.020.
[92] Y. J. Kim *et al.*, 'High-performance self-powered wireless sensor node driven by a flexible thermoelectric generator', *Energy*, vol. 162, pp. 526–533, Nov. 2018, doi: 10.1016/j.energy.2018.08.064.
[93] B. Iezzi, K. Ankireddy, J. Twiddy, M. D. Losego, and J. S. Jur, 'Printed, metallic thermoelectric generators integrated with pipe insulation for powering wireless sensors', *Applied Energy*, vol. 208, pp. 758–765, Dec. 2017, doi: 10.1016/j.apenergy.2017.09.073.

[94] M. Thielen, L. Sigrist, M. Magno, C. Hierold, and L. Benini, ‘Human body heat for powering wearable devices: From thermal energy to application’, *Energy Conversion and Management*, vol. 131, Nov. 2016, doi: 10.1016/j.enconman.2016.11.005.
[95] K. Kumar and M. Hemalatha, ‘Designing EM energy harvesting antenna to give power support to embedded sensor’, *International Journal of Applied Engineering Research*, vol. 9, pp. 1565–1574, Jan. 2014.
[96] S. Kim *et al.*, ‘Ambient RF Energy-Harvesting Technologies for Self-Sustainable Standalone Wireless Sensor Platforms’, *Proceedings of the IEEE*, Oct. 2014, doi: 10.1109/JPROC.2014.2357031.
[97] ‘Powerharvester Receivers’, *Powercast Co.* [Online]. Available: https://www.powercastco.com/products/powerharvester-receivers/. [Accessed: 23-Nov-2019].
[98] A. M. Zungeru, L.-M. Ang, S. R. S. Prabaharan, and K. P. Seng, ‘Radio Frequency Energy Harvesting and Management for Wireless Sensor Networks’, *arXiv:1208.4439 [cs]*, pp. 341–368, Mar. 2012, doi: 10.1201/b10081-16.
[99] T. D. Nguyen, J. Y. Khan, and D. T. Ngo, ‘A Self-Sustainable RF Energy Harvesting Algorithm for WSN-Based IoT Applications’, *GLOBECOM 2017 - 2017 IEEE Global Communications Conference*, pp. 1–6, 2017, doi: 10.1109/GLOCOM.2017.8253962.
[100] B. Nasreddine, ‘Matlab-Simulink of photovoltaic system based on a two-diode model simulator with shaded solar cells’, *Revue des Energies Renouvelables*, vol. 16, p. 65, Mar. 2013.
[101] J. A. Gow and C. D. Manning, ‘Development of a model for photovoltaic arrays suitable for use in simulation studies of solar energy conversion systems’, in *1996 Sixth International Conference on Power Electronics and Variable Speed Drives (Conf. Publ. No. 429)*, 1996, pp. 69–74, doi: 10.1049/cp:19960890.
[102] A. Karafil, ‘Temperature and Solar Radiation Effects on Photovoltaic Panel Power’, *Journal of New Results in Science*, vol. 5, pp. 48–58, 2016.
[103] S. Bana and R. P. Saini, ‘A mathematical modeling framework to evaluate the performance of single diode and double diode based SPV systems’, *Energy Reports*, vol. 2, pp. 171–187, Nov. 2016, doi: 10.1016/j.egyr.2016.06.004.
[104] E. Rodrigues, R. Melicio, V. M. F. Mendes, and J. Catalão, *Simulation of a Solar Cell considering Single-Diode Equivalent Circuit Model*. 2011.
[105] H. S. Rauschenbach, *Solar Cell Array Design Handbook: The Principles and Technology of Photovoltaic Energy Conversion*. Springer Netherlands, 1980.
[106] B. Alsayid, ‘Modeling and simulation of photovoltaic cell/module/array with two-diode model’, *International Journal of Computer Technology and Electronics Engineering*, vol. 1, pp. 6–11, Jan. 2012.
[107] F. Rasool, M. Drieberg, N. Badruddin, B. Singh, and M. Singh, ‘Modeling of PV panels performance based on datasheet values for solar micro energy harvesting’, in *2016 6th International Conference on Intelligent and Advanced Systems (ICIAS)*, 2016, pp. 1–5, doi: 10.1109/ICIAS.2016.7824072.
[108] S. Yilmaz, A. Yılmaz, M. Gunes, and H. Özçalık, ‘Two-Diode Model Performance Analysis of Photovoltaic Panels’, *International Journal of Engineering Trends and Technology (IJETT)*, vol. 4, May 2013.
[109] V. Tamrakar, S. C. Gupta, and Y. Sawle, ‘Single-Diode Pv Cell Modeling And Study Of Characteristics Of Single And Two-Diode Equivalent Circuit’, *Electrical and Electronics Engineering: An International Journal*, vol. 4, pp. 13–24, Aug. 2015, doi: 10.14810/elelij.2015.4302.
[110] M. F. AlHajri, K. M. El-Naggar, M. R. AlRashidi, and A. K. Al-Othman, ‘Optimal extraction of solar cell parameters using pattern search’, *Renewable Energy*, vol. 44, pp. 238–245, Aug. 2012, doi: 10.1016/j.renene.2012.01.082.
[111] M. A. de Blas, J. L. Torres, E. Prieto, and A. García, ‘Selecting a suitable model for characterizing photovoltaic devices’, *Renewable Energy*, vol. 25, no. 3, pp. 371–380, Mar. 2002, doi: 10.1016/S0960-1481(01)00056-8.

[112] J. Cubas, S. Pindado, and C. D. Manuel, ‘Explicit Expressions for Solar Panel Equivalent Circuit Parameters Based on Analytical Formulation and the Lambert W-Function’, *Energies*, vol. 7, no. 7, pp. 1–18, 2014.
[113] C. Zhang, J. Zhang, Y. Hao, Z. Lin, and C. Zhu, ‘A simple and efficient solar cell parameter extraction method from a single current-voltage curve’, *Journal of Applied Physics*, vol. 110, no. 6, p. 064504, Sep. 2011, doi: 10.1063/1.3632971.
[114] M. R. AlRashidi, K. M. El-Naggar, and M. F. AlHajri, ‘Heuristic Approach for Estimating the Solar Cell Parameters’, in *Proceedings of the 5th WSEAS Congress on Applied Computing Conference, and Proceedings of the 1st International Conference on Biologically Inspired Computation*, Stevens Point, Wisconsin, USA, 2012, pp. 80–83.
[115] A. Jain and A. Kapoor, ‘Exact analytical solutions of the parameters of real solar cells using Lambert W-function’, *Solar Energy Materials and Solar Cells*, vol. 81, no. 2, pp. 269–277, Feb. 2004, doi: 10.1016/j.solmat.2003.11.018.
[116] R. Pradhan, ‘Development of new parameter extraction schemes and maximum power point controllers for photovoltaic power systems’, PhD, National Institute of Technology, Rourkela, 2004.
[117] A. Mohapatra, B. K. Nayak, and K. B. Mohanty, ‘Comparative study on single diode photovoltaic module parameter extraction methods’, in *2013 International Conference on Power, Energy and Control (ICPEC)*, 2013, pp. 30–34, doi: 10.1109/ICPEC.2013.6527619.
[118] K. Ishaque, Z. Salam, and H. Taheri, ‘Accurate MATLAB Simulink PV System Simulator Based on a Two-Diode Model’, vol. 11, Mar. 2011, doi: 10.6113/JPE.2011.11.2.179.
[119] R. Tamrakar, ‘A Review: extraction of solar cell modelling parameters’, *ijireeice*.
[120] R. Khezzar, M. Zereg, and A. Khezzar, ‘Comparative study of mathematical methods for parameters calculation of current-voltage characteristic of photovoltaic module’, in *2009 International Conference on Electrical and Electronics Engineering - ELECO 2009*, 2009, pp. I-24-I–28, doi: 10.1109/ELECO.2009.5355236.
[121] M. Zagrouba, A. Sellami, M. Bouaïcha, and M. Ksouri, ‘Identification of PV solar cells and modules parameters using the genetic algorithms: Application to maximum power extraction’, *Solar Energy*, vol. 84, no. 5, pp. 860–866, May 2010, doi: 10.1016/j.solener.2010.02.012.
[122] M. Alrashidi, K. El-Naggar, and M. AlHajri, *Extraction of Photovoltaic Characteristics Using Simulated Annealing*. 2014.
[123] J. Ma, T. O. Ting, K. L. Man, N. Zhang, S.-U. Guan, and P. W. H. Wong, ‘Parameter Estimation of Photovoltaic Models via Cuckoo Search’, *Journal of Applied Mathematics*, vol. 2013, p. 8, 2013.
[124] H. Qin and J. W. Kimball, ‘Parameter determination of Photovoltaic Cells from field testing data using particle swarm optimization’, in *2011 IEEE Power and Energy Conference at Illinois*, 2011, pp. 1–4, doi: 10.1109/PECI.2011.5740496.
[125] M. Ketkar and A. Chopde, ‘Efficient Parameter Extraction of Solar Cell using Modified ABC’, *International Journal of Computer Applications*, vol. 102, pp. 1–6, Sep. 2014, doi: 10.5120/17776-8535.
[126] J. K. Maherchandani, C. Agarwal, and M. Sahi, ‘Estimation of Solar Cell Model Parameter by Hybrid Genetic Algorithm Using MATLAB’, 2012.
[127] I. Banu and M. Istrate, ‘Modeling and simulation of photovoltaic arrays’, *Buletinul AGIR, World Energy Systems. Towards Sustainable and Integrated Energy Systems - Proceedings of the 9th International World Energy System Conference (WESC2012), June 28-30, 2012, Suceava, Romania*, pp. 161–166, Jun. 2012.
[128] F. Adamo, F. Attivissimo, A. Di Nisio, and M. Spadavecchia, ‘Characterization and Testing of a Tool for Photovoltaic Panel Modeling’, *IEEE Transactions on Instrumentation and Measurement*, vol. 60, no. 5, pp. 1613–1622, May 2011, doi: 10.1109/TIM.2011.2105051.
[129] D. Rekioua and E. Matagne, *Optimization of Photovoltaic Power Systems: Modelization, Simulation and Control*. London: Springer-Verlag, 2012.
[130] H. Yatimi and E. Aroudam, ‘A Detailed Study and Modeling of Photovoltaic Module under Real Climatic Conditions’, *International Journal of Electronics and Electrical Engineering*, vol. 3, Jan. 2014, doi: 10.12720/ijeee.3.3.171-176.

[131] D. Rekioua, ‘Regular paper Experimental Study of a PV Water Pumping System’, *J. Electrical Systems*, vol. 9, pp. 212–222, Jan. 2013.
[132] S. R. Pendem and S. Mikkili, ‘Modeling, simulation and performance analysis of solar PV array configurations (Series, Series–Parallel and Honey-Comb) to extract maximum power under Partial Shading Conditions’, *Energy Reports*, vol. 4, pp. 274–287, Nov. 2018, doi: 10.1016/j.egyr.2018.03.003.
[133] S. Beeby and N. White, ‘Energy Harvesting for Autonomous Systems’, vol. 308, Jan. 2010.
[134] M. Chen, L. A. Rosendahl, T. J. Condra, and J. K. Pedersen, ‘Numerical Modeling of Thermoelectric Generators With Varing Material Properties in a Circuit Simulator’, *IEEE Transactions on Energy Conversion*, vol. 24, pp. 112–124, 2009, doi: 10.1109/tec.2008.2005310.
[135] M. Freunek, M. Müller, T. Ungan, W. Walker, and L. M. Reindl, ‘New Physical Model for Thermoelectric Generators’, *Journal of Elec Materi*, vol. 38, no. 7, pp. 1214–1220, Jul. 2009, doi: 10.1007/s11664-009-0665-y.
[136] M. Bond and J.-D. Park, ‘Current-Sensorless Power Estimation and MPPT Implementation for Thermoelectric Generators’, *IEEE Transactions on Industrial Electronics*, vol. 62, no. 9, pp. 5539–5548, Sep. 2015, doi: 10.1109/TIE.2015.2414393.
[137] A. Montecucco and A. R. Knox, ‘Maximum Power Point Tracking Converter Based on the Open-Circuit Voltage Method for Thermoelectric Generators’, *IEEE Transactions on Power Electronics*, vol. 30, no. 2, pp. 828–839, Feb. 2015, doi: 10.1109/TPEL.2014.2313294.
[138] V. Leonov, P. Fiorini, T. Torfs, R. J. M. Vullers, and C. Van Hoof, ‘Thermal matching of a thermoelectric energy harvester with the environment and its application in wearable self-powered wireless medical sensors’, in *2009 15th International Workshop on Thermal Investigations of ICs and Systems*, 2009, pp. 95–100.
[139] M. Lossec, B. Multon, and H. Ben Ahmed, ‘Sizing optimization of a thermoelectric generator set with heatsink for harvesting human body heat’, *Energy Conversion and Management*, vol. 68, pp. 260–265, Apr. 2013, doi: 10.1016/j.enconman.2013.01.021.
[140] Y. Moumouni and R. Jacob Baker, ‘Concise thermal to electrical parameters extraction of thermoelectric generator for spice modeling’, in *2015 IEEE 58th International Midwest Symposium on Circuits and Systems (MWSCAS)*, 2015, pp. 1–4, doi: 10.1109/MWSCAS.2015.7282014.
[141] ‘2411G-7L31-15CX1 ThermoElectric Generator 56 x 56mm’. [Online]. Available: https://customthermoelectric.com/2411g-7l31-15cx1-thermoelectric-generator-56-x-56mm.html. [Accessed: 23-Nov-2019].
[142] V. I. Kubov, Y. Y. Dymytrov, and R. M. Kubova, ‘LTspice-model of thermoelectric Peltier-Seebeck element’, in *2016 IEEE 36th International Conference on Electronics and Nanotechnology (ELNANO)*, Kiev, Ukraine, 19-21 April, 2016, pp. 47–51, doi: 10.1109/ELNANO.2016.7493007.
[143] ‘Thermoelectric Cooler TEC1-12706’, *Hebei I.T Shanghai*. .
[144] M. Nesarajah and G. Frey, ‘Thermoelectric power generation: Peltier element versus thermoelectric generator’, in *IECON 2016 - 42nd Annual Conference of the IEEE Industrial Electronics Society*, 2016, pp. 4252–4257, doi: 10.1109/IECON.2016.7793029.
[145] M. Chen, L. A. Rosendahl, I. Bach, T. Condra, and J. K. Pedersen, ‘Transient Behavior Study of Thermoelectric Generators through an Electro-thermal Model Using SPICE’, in *2006 25th International Conference on Thermoelectrics*, 2006, pp. 214–219, doi: 10.1109/ICT.2006.331335.
[146] J. A. Chavez, J. A. Ortega, J. Salazar, A. Turo, and M. J. Garcia, ‘SPICE model of thermoelectric elements including thermal effects’, in *Proceedings of the 17th IEEE Instrumentation and Measurement Technology Conference [Cat. No. 00CH37066]*, 2000, vol. 2, pp. 1019–1023 vol.2, doi: 10.1109/IMTC.2000.848895.
[147] S. Lineykin and S. Ben-Yaakov, ‘Modeling and Analysis of Thermoelectric Modules’, *IEEE Transactions on Industry Applications*, vol. 43, no. 2, pp. 505–512, Mar. 2007, doi: 10.1109/TIA.2006.889813.

[148] A. Mirocha and P. Dziurdzia, ‘Improved electrothermal model of the thermoelectric generator implemented in SPICE’, in *2008 International Conference on Signals and Electronic Systems*, 2008, pp. 317–320, doi: 10.1109/ICSES.2008.4673424.
[149] M. O. Cernaianu, C. Cirstea, and A. S. Gontean, ‘Thermoelectrical energy harvesting system: Modelling, simulation and implementation’, *2012 10th International Symposium on Electronics and Telecommunications*, pp. 67–70, 2012, doi: 10.1109/ISETC.2012.6408047.
[150] Y. Moumouni and R. J. Baker, ‘Improved SPICE modeling and analysis of a thermoelectric module’, in *2015 IEEE 58th International Midwest Symposium on Circuits and Systems (MWSCAS)*, Fort Collins, CO, USA, 2-5 August, pp. 1–4, doi: 10.1109/MWSCAS.2015.7282015.
[151] ‘MC-SP0.8-NF-GCS - 800mW Solar Panel’. [Online]. Available: https://uk.farnell.com/multicomp/mc-sp0-8-nf-gcs/solar-panel-0-8w-4v-no-frame/dp/1852494. [Accessed: 23-Nov-2019].
[152] T. C. Banwell and A. Jayakumar, ‘Exact analytical solution for current flow through diode with series resistance’, *Electronics Letters*, vol. 36, no. 4, pp. 291–292, Feb. 2000, doi: 10.1049/el:20000301.
[153] A. Jain, S. Sharma, and A. Kapoor, ‘Solar cell array parameters using Lambert W-function’, *Solar Energy Materials and Solar Cells*, vol. 90, no. 1, pp. 25–31, Jan. 2006, doi: 10.1016/j.solmat.2005.01.007.
[154] L. Peng, Y. Sun, Z. Meng, Y. Wang, and Y. Xu, ‘A new method for determining the characteristics of solar cells’, *Journal of Power Sources*, vol. 227, pp. 131–136, Apr. 2013, doi: 10.1016/j.jpowsour.2012.07.061.
[155] M. G. Villalva, J. R. Gazoli, and E. R. Filho, ‘Comprehensive Approach to Modeling and Simulation of Photovoltaic Arrays’, *IEEE Transactions on Power Electronics*, vol. 24, no. 5, pp. 1198–1208, May 2009, doi: 10.1109/TPEL.2009.2013862.
[156] M. G. Villalva, J. R. Gazoli, and E. R. Filho, ‘Modeling and circuit-based simulation of photovoltaic arrays’, in *2009 Brazilian Power Electronics Conference*, 2009, pp. 1244–1254, doi: 10.1109/COBEP.2009.5347680.
[157] P. M. Cuce and E. Cuce, ‘A novel model of photovoltaic modules for parameter estimation and thermodynamic assessment’, *International Journal of Low-Carbon Technologies*, vol. 7, no. 2, pp. 159–165, Nov. 2011, doi: 10.1093/ijlct/ctr034.
[158] ‘Thermonamic Module: TEC1-12722’. [Online]. Available: http://www.thermonamic.com/TEC1-12722-English.pdf. [Accessed: 15-Jul-2019].
[159] M. Magno *et al.*, ‘InfiniTime: Multi-sensor wearable bracelet with human body harvesting’, *Sustainable Computing: Informatics and Systems*, vol. 11, pp. 38–49, 2016, doi: https://doi.org/10.1016/j.suscom.2016.05.003.
[160] ‘Thermoelectric Generator Module: GM250-127-14-10’,. [Online]. Available: https://www.europeanthermodynamics.com/products/datasheets/GM250-127-14-10-v2.pdf. [Accessed: 15-Jul-2019].
[161] Y. Dymytrov and V. Kubov, ‘Simple method of thermoelectric cooler (Peltier device) parameters determination based on datasheet and modeling results’, May 2017.
[162] V. Leonov and R. Vullers, ‘Wearable Thermoelectric Generators for Body-Powered Devices’, *Journal of Electronic Materials*, vol. 38, pp. 1491–1498, 2009, doi: 10.1007/s11664-008-0638-6.
[163] J.-M. Gruber and S. Mathis, ‘Efficient Boost Converter for Thermoelectric Energy Harvesting’, *Proceedings Sensor 2017*, pp. 642–645, May 2017, doi: http://dx.doi.org/10.5162/sensor2017/P3.6.
[164] A. Raheem, R. D Sai, R. K Srinivasa, and S. K, ‘Wireless Charge of Wearable device Using Human warmth’, V.R. SIDHARTHA ENGINEERING COLLEGE, Kanuru, Vijayawada, Andhra Pradesh, India, 2019.
[165] A. Costa, D. Costa, J. Morgado, H. Santos, and C. Ferreira, ‘Autonomous Wireless Sensor with a Low Cost TEG for Application in Automobile Vehicles’, *Procedia Engineering*, vol. 87, pp. 1226–1229, Jan. 2014, doi: 10.1016/j.proeng.2014.11.404.

[166] D. Boyle, R. Kolcun, and E. Yeatman, ‘Energy-Efficient Communication in Wireless Networks’, *ICT - Energy Concepts for Energy Efficiency and Sustainability*, Mar. 2017, doi: 10.5772/65986.
[167] M. Natsui *et al.*, ‘12.1 An FPGA-Accelerated Fully Nonvolatile Microcontroller Unit for Sensor-Node Applications in 40nm CMOS/MTJ-Hybrid Technology Achieving 47.14μW Operation at 200MHz’, in *2019 IEEE International Solid- State Circuits Conference - (ISSCC)*, San Francisco, CA, USA, 17-21 February, 2019, pp. 202–204, doi: 10.1109/ISSCC.2019.8662431.
[168] ‘4E - Energy Efficient End-use Equipment - IEA Technology Collaboration Programme’. [Online]. Available: https://www.iea-4e.org/. [Accessed: 23-Nov-2019].
[169] P. Gljuscic, S. Zelenika, and E. Kamenar, ‘Characterisation of Performances of Thermoelectric Generators for Energy Harvesting Applications’, in *DAAAM Proceedings*, 1st ed., vol. 1, B. Katalinic, Ed. DAAAM International Vienna, Austria, 2018, pp. 0025–0030.
[170] ‘TEG2-126LDT for Body & Sensor Power Thermoelectric Harvesting Applications’. [Online]. Available: https://tecteg.com/wp-content/uploads/2015/01/TEG1-PB-12611-6.0_CBH-1-Final-November-17th-update.pdf. [Accessed: 02-Sep-2019].
[171] ‘TEG2-07025HT-SS liquid to liquid applications.’ [Online]. Available: https://espressomilkcooler.com/wp-content/uploads/2014/05/Spec-TEG2-07025HT-SS-rev1.pdf. [Accessed: 02-Sep-2019].
[172] ‘TEG1-PB-12611-6.0_CBH-1 TECTEG Power Generation’. [Online]. Available: https://tecteg.com/wp-content/uploads/2015/01/TEG1-PB-12611-6.0_CBH-1-Final-November-17th-update.pdf. [Accessed: 02-Sep-2019].

8 Publications

P1. **Syeda, Adila Afghan** ; Husi, Géza
Modelling and Analysis of Energy Harvesting in Internet of Things (IoT): Characterization of a Thermal Energy Harvesting Circuit for IoT based Applications with LTC3108
ENERGIES 12 : 20 pp. 1-13. Paper: 3873 , 13 p. (2019)
DOI Google scholar
Journal Article/Article (Journal Article)/Scientific [30844694] [Admin approved]

P2. Almusawi, Husam ; **Afghan, Syeda Adila** ; Géza, Husi
Designing the Mechanical Parts of a Low-Cost Hand Rehabilitation CPM Device for Stroke Patients
In: Machado, José; Soares, Filomena; Veiga, Germano (eds.) Innovation, Engineering and Entrepreneurship. HELIX 2018. Lecture Notes in Electrical Engineering
[s. l.] - Nemzetközi, International : Springer International Publishing, (2019) pp. 60-66. , 7 p.
DOI Scopus Google scholar
Chapter in Book/Conference paper (Chapter in Book)/Scientific [3382260] [Admin approved]

P3. Alsebai, A ; **Afghan, S**
Designing and Implementing Control panel for Diesel generator
IOP CONFERENCE SERIES: MATERIALS SCIENCE AND ENGINEERING 568 p. 012107 (2019)
DOI Egyéb URL
Journal Article/Conference paper in journal (Journal Article)/Scientific [30813395] [Admin approved]

P4. **Syeda, Adila Afghan** ; Husam, Almusawi ; Husi, Géza
Simulating the Electrical Characteristics of Solar Panels Based on Practical Single-Diode Equivalent Circuit Model: Analyzing the Influence of Environmental Parameters on Output Power
In: Machado, José; Soares, Filomena; Veiga, Germano (eds.) Innovation, Engineering and Entrepreneurship. HELIX 2018. Lecture Notes in Electrical Engineering
[s. l.] - Nemzetközi, International : Springer International Publishing, (2019) pp. 67-74. , 8 p.
DOI Scopus Google scholar
Chapter in Book/Conference paper (Chapter in Book)/Scientific [3382263] [Admin approved]

P5. **Afghan, Syeda Adila** ; Almusawi, Husam ; Géza, Husi
Towards the self-powered Internet of Things (IoT) by energy harvesting: Trends and technologies for green IoT
In: IEEE (eds.) 2nd International Symposium on Small-scale Intelligent Manufacturing Systems (SIMS), 2018
New York, United States of America * : IEEE, (2018) pp. 1-6. , 6 p. DOI IEEE Xplore WoS Scopus Google scholar
Chapter in Book/Conference paper (Chapter in Book)/Scientific [3369383] [Admin approved]

External citations: 13, Self citations: 0, Unhandled citations: 0, All citations: 13

P6. Akbar, Husna ; **Afghan, Syeda Adila** ; Jokhio, Sana Hoor ; Jokhio, Imran Ali
Secure multi-level Cluster based wireless sensor network
RECENT INNOVATIONS IN MECHATRONICS 5 : Klnsz. pp. 1-7. , 7 p. (2018) DOI Google scholar
Journal Article/Article (Journal Article)/Scientific [3384410] [Admin approved]

P7. Almusawi, Husam AbdulKareem ; **Afghan, Syeda Adila** ; Géza, Husi
Recent trends in robotic systems for upper-limb stroke recovery: A low-cost hand and wrist rehabilitation device
In: IEEE (eds.) 2nd International Symposium on Small-scale Intelligent Manufacturing Systems (SIMS), 2018
New York, United States of America * : IEEE, (2018) pp. 1-6. , 6 p. DOI IEEE Xplore WoS Scopus Google scholar
Chapter in Book/Conference paper (Chapter in Book)/Scientific [3369389] [Admin approved]
External citations: 2, Self citations: 0, Unhandled citations: 0, All citations: 2

P8. Bano, Shahzadi ; **Afghan, Syeda Adila** ; Jokhio, Sana Hoor ; Talpur, Shahnawaz ; Jokhio, Imran Ali
Lightweight multi-agent framework for a cluster-based wireless sensor network
RECENT INNOVATIONS IN MECHATRONICS : Klnsz. pp. 1-7. , 7 p. (2018) DOI
Journal Article/Article (Journal Article)/Scientific [3384404] [Admin approved]

P9. **Afghan, Syeda Adila** ; Géza, Husi
Modelling and Simulating Photovoltaic Energy Harvesting Circuit: An Analysis based on Trial and Error approximation for Optimal Output Power of a Harvester
In: IEEE (eds.) 2017 International Conference on Engineering, Technology and Innovation (ICE/ITMC): Proceedings of the 23rd ICE/IEEE International Conference on Engineering Technology and Innovation
[s. l.], International : IEEE, (2017) pp. 504-508. , 5 p. DOI IEEE Xplore WoS Scopus Google scholar
Chapter in Book/Conference paper (Chapter in Book)/Scientific [3246148] [Admin approved]

P10. **Afghan, Syeda Adila** ; Almusawi, Husam ; Husi, Géza
Approximating the minimum output power for energy harvesting prototype: a case study of cell phone specifications = Minimális kimeneti teljesítmény meghatározása energy harvesting prototípushoz: egy esettanulmány mobiltelefon specifikációkra In: Bitay, Enikő (eds.) A XXII. Fiatal Műszakiak Tudományos Ülésszak előadásai : Proceedings of the XXII-th International Scientific Conference of Young Engineers
Kolozsvár, Romania : Óbudai Egyetem, Erdélyi Múzeum Egyesület (EME), (2017) pp. 55-58. , 4 p.
Teljes dokumentum Google scholar
Chapter in Book/Conference paper (Chapter in Book)/Scientific [3201428] [Admin approved]

P11. Almusawi, Husam ; **Afghan, Syeda Adila** ; Husi, Géza ; Molnár, Zsolt ; Erdei, Timotei István

Reviewing the notable progress of e"ective techniques in the development of stroke hand rehabilitation devices = A stroke-t kapott egyének rehabilitációs eszközeiben jelentős fejlődést mutató hatékony technikák áttekintése
In: Bitay, Enikő (eds.) A XXII. Fiatal Műszakiak Tudományos Ülésszak előadásai : Proceedings of the XXII-th International Scientific Conference of Young Engineers
Kolozsvár, Romania : Óbudai Egyetem, Erdélyi Múzeum Egyesület (EME), (2017) pp. 63-66. , 4 p.
Teljes dokumentum Google scholar
Chapter in Book/Conference paper (Chapter in Book)/Scientific [3201431] [Admin approved]
External citations: 0, Self citations: 3, Unhandled citations: 0, All citations: 3

P12. **Syeda, Adila Afghan** ; Husam, Almusawi ; Husi, Geza
Simulating the electrical characteristics of a photovoltaic cell based on a single- diode equivalent circuit model
MATEC WEB OF CONFERENCES 126 p. 03002 Paper: 03002 , 6 p. (2017)
DOI Scopus Teljes dokumentum Google scholar
Journal Article/Conference paper in journal (Journal Article)/Scientific [3283182] [Admin approved]

P13. **Syeda, Adila Afghan** ; Husam, Almusawi ; Husi, Geza
Simulating the electrical characteristics of a photovoltaic cell based on a single- diode equivalent circuit model
ANALELE UNIVERSITATII DIN ORADEA FASCIOLA MANAGEMENT SI INGINERIE
TEHNOLOGICA / ANNALS OF THE UNIVERSITY OF ORADEA FASCICLE OF MANAGEMENT AND TECHNOLOGICAL ENGINEERING 16 (26) : 1 pp. 91-96. , 6 p.
(2017)
Google scholar
Journal Article/Article (Journal Article)/Scientific [3235588] [Admin approved]

P14. **Syeda, Adila Afghan** ; Husam, Almusawi ; Géza, Husi
Simulating the Eletrical Characteristics of a Photovoltaic Cell Based on a Single-Diode Equivalent Cicuit Model
In: Calin, Baban; Florin, Sandu Blaga; Gavril, Grebenisan; Alexandru-Viorel, Pele; Mircea, Teodor Pop; Alexandru, Rus; Radu, Catalin Tarca (eds.) "Imt Oradea" - 2017 : Proceedings of the Annual Seesion of Scientific Papers
Oradea, Romania : University of Oradea Publishing House, (2017) pp. 181-186. , 6 p.
Chapter in Book/Conference paper (Chapter in Book)/Scientific [3230342] [Admin approved]

P15. Husam, Almusawi ; **Syeda, Adila Afghan** ; Géza, Husi
Technological Advancements in Stroke Hand Rehabilitation Devices: A Review In: Adrienn, Dineva; István, Nagy (eds.) Proceedings of 4th INTERNATIONAL MECHATRONICAL STUDENT micro-CONFERENCE
Budapest, Hungary : Óbudai Egyetem, (2016) pp. 80-90. , 11 p.
Chapter in Book/Conference paper (Chapter in Book)/Scientific [3241206] [Admin approved]

P16. **Syeda, Adila Afghan** ; Husam, Almusawi ; Sana, Hoor Jokhio ; Géza, Husi
Estimation of minimum output power threshold for energy harvesting module: An inspection of battery and charging parameters of cell phones
In: Adrienn, Dineva; István, Nagy (eds.) Proceedings of 4th INTERNATIONAL MECHATRONICAL STUDENT micro-CONFERENCE
Budapest, Hungary : Óbudai Egyetem, (2016) pp. 56-71. , 16 p. Chapter in Book/Conference paper (Chapter in Book)/Scientific [3241204] [Admin approved]
External citations: 0, Self citations: 3, Unhandled citations: 0, All citations: 3

9 Appendix

Experimenting Commercial Solar Module: (Generated results under various parameters)

Vin	Vout	Rmppc	Iout	Pout	Rload
3.3. 1.77	4.2, 3.82	100K	38.01mA	145.76mw	100
3.3	4.2	100K	27.24	111.02	150
3.3	4.2	100K	20.64	84.08	200
3.3	4.2	100K	16.27	67.45	250
3.3	4.2	100K	13.61	55.92	300
3.3	4.2	100K	11.71	48.20	350
3.3	4.2	100K	10.3	42.11	400

100K TILL 300K VOUT SUSTAINED

Vin	Vout	Rmppc	Iout	Pout	Rload	Solar
3.43	*3.3*	*100K*	*33.80*	*108.60*	*100*	*1000*
3.3	*3.3*	*100K*	*32.81*	*107*	*100*	*900*
3.3	*3.3*	*100K*	*32.61*	*106*	*100*	*800*
3.3	3.1	100K	31.21	99.89	100	700
3.3	1.6	100K	17.01	28.16	100	600
3.3	1.28	100K	13.81	16.09	100	500
3.3	1.08	100K	10.06	12.74	100	400
3.3	0.86	100K	8.21	7.37	100	300
3.3	0.5	100K	4.41	2.68	100	200

Vin	Vout	Rmppc	Iout	Pout	Rload	Solar
3.43	*3.3*	*100K*	*22.71*	*73.56*	*150*	*1000*
3.3	*3.3*	*100K*	*22.13*	*73.01*	*150*	*900*
3.3	*3.3*	*100K*	*21.87*	*72.76*	*150*	*800*
3.3	3.3	100K	21.13	71.15	150	700
3.3	3.3	100K	21.01	71.01	150	600
3.3	1.94	100K	13.33	26.37	150	500
3.3	1.64	100K	10.93	18.32	150	400
3.3	1.24	100K	8.27	9.39	150	300
3.3	0.7	100K	5.21	3.13	150	200

Vin	Vout	Rmppc	Iout	Pout	Rload	Solar
3.43	*3.3*	*100K*	*16.51*	*54.97*	*200*	*1000*
3.3	*3.3*	*100K*	*16.31*	*54.31*	*200*	*900*
3.3	*3.3*	*100K*	*16.29*	*53.67*	*200*	*800*
3.3	3.3	100K	16.01	53.63	200	700
3.3	3.3	100K	15.98	52.67	200	600
3.3	3.2	100K	15.87	52.13	200	500
3.3	2.1	100K	10.81	23.13	200	400
3.3	1.64	100K	08.01	13.07	200	300

3.3	0.94	100K	04.81	3.69	200	200

Vin	Vout	Rmppc	Iout	Pout	Rload	Solar
3.43	*3.3*	*100K*	*13.21*	*44.69*	*250*	*1000*
3.3	*3.3*	*100K*	*13.15*	*44.53*	*250*	*900*
3.3	*3.3*	*100K*	*13.08*	*44.34*	*250*	*800*
3.3	3.3	100K	13.01	44.15	250	700
3.3	3.3	100K	12.98	43.67	250	600
3.3	3.3	100K	12.87	43.01	250	500
3.3	3.2	100K	12.41	42.23	250	400
3.3	1.92	100K	7.81	14.58	250	300
3.3	1.16	100K	04.81	4.13	250	200

Vin	Vout	Rmppc	Iout	Pout	Rload	Solar
3.43	*3.3*	*100K*	*9.51*	*31.71*	*350*	*1000*
3.3	*3.3*	*100K*	*9.41*	*31.56*	*350*	*900*
3.3	*3.3*	*100K*	*9.34*	*31.13*	*350*	*800*
3.3	3.3	100K	9.31	30.97	350	700
3.3	3.3	100K	9.27	30.87	350	600
3.3	3.3	100K	9.25	30.56	350	500
3.3	3.2	100K	9.22	30.23	350	400
3.3	3.06	100K	8.89	27.28	350	300
3.3	1.56	100K	04.56	7.01	350	200

Vin	Vout	Rmppc	Iout	Pout	Rload	Solar
3.43	*3.3*	*100K*	*8.36*	*27.82*	*400*	*1000*
3.3	*3.3*	*100K*	*8.31*	*27.56*	*400*	*900*
3.3	*3.3*	*100K*	*8.27*	*27.01*	*400*	*800*
3.3	3.3	100K	8.25	26.87	400	700
3.3	3.3	100K	8.24	26.54	400	600
3.3	3.3	100K	8.23	26.01	400	500
3.3	3.3	100K	8.21	25.53	400	400
3.3	3.2	100K	7.96	25.98	400	300
3.3	1.78	100K	04.54	8.04	400	200

Vin	Vout	Rmppc	Iout	Pout	Rload	Solar
3.43	*3.3*	*100K*	*7.42*	*24.44*	*450*	*1000*
3.3	*3.3*	*100K*	*7.32*	*24.22*	*450*	*900*
3.3	*3.3*	*100K*	*7.29*	*24.13*	*450*	*800*
3.3	3.3	100K	7.28	24.01	450	700
3.3	3.3	100K	7.26	23.97	450	600
3.3	3.3	100K	7.23	23.87	450	500
3.3	3.3	100K	7.21	23.68	450	400
3.3	3.2	100K	7.15	23.08	450	300
3.3	1.82	100K	04.15	8.45	450	200

Experimenting Commercial Thermal Module: (Generated results under various parameters)

Smaller load configuration

Tc	Th	Pout	Iout	Vout	Rload
0	0.5	31.34Nw	24.77(0.028mA)	1.34mV	50
0	1.0	1.348uW	167.68(0.163)	8.21	50
0	1.5	3.90	279.60(0.278)	14.01	50
0	2.0	8.16	409.92(0.409)	20.02	50
0	2.5	13.94	0.536	26.79	50
0	3.0	22.50	0.679	34.07	50
0	3.5	33.81	0.829	41.28	50
0	4.0	48.47	0.982	49.10	50
Tc	**Th**	**Pout**	**Iout**	**Vout**	**Rload**
0	0.5	0.085uW	0.028	3.04	100
0	1.0	2.643uW	0.160	16.52	100
0	1.5	7.99	0.283	28.26	100
0	2.0	16.80	0.402	40.00	100
0	2.5	28.80	0.532	53.48	100
0	3.0	44.80	0.670	66.98	100
0	3.5	66.80	0.824	81.74	100
0	4.0	95.20	0.974	98.26	100
Tc	**Th**	**Pout**	**Iout**	**Vout**	**Rload**
0	0.5	0.60uW	0.028	3.91Mv	150
0	1.0	4.80	0.028	24.78	150
0	1.5	12.00	0.028	42.49	150
0	2.0	24.60	0.028	61.46	150
0	2.5	42.60	0.028	79.14	150
0	3.0	67.20	0.028	100.04	150
0	3.5	100.80	0.028	122.17	150
0	4.0	144.00	0.028	146.84	150
Tc	**Th**	**Pout**	**Iout**	**Vout**	**Rload**
0	0.5	0.60	0.028	5.22	200
0	1.0	5.60	0.028	33.91	200
0	1.5	16.0	0.028	56.52	200
0	2.0	32.80	0.028	80.87	200
0	2.5	56.80	0.028	107.83	200
0	3.0	88.80	0.028	133.91	200
0	3.5	133.60	0.028	164.35	200
0	4.0	191.20	0.028	195.65	200
Tc	**Th**	**Pout**	**Iout**	**Vout**	**Rload**
0	0.5	0.80	0.028	7.83	350
0	1.0	9.60	0.028	48.26	350
0	1.5	22.80	0.028	84.78	350
0	2.0	47.88	0.028	120.00	350
0	2.5	86.16	0.028	161.74	350
0	3.0	133.68	0.028	200.87	350
0	3.5	199.68	0.028	245.22	350
0	4.0	286.80	0.028	293.48	350

Tc	Th	Pout	Iout	Vout	Rload
0	0.5	0.019	0.11mA	0.026	1000
0	1.0	0.043	0.161	0.174	1000
0	1.5	0.125	0.284	0.278	1000
0	2.0	0.162	0.398	0.401	1000
0	2.5	0.266	0.530	0.530	1000
0	3.0	0.439	0.674	0.661	1000
0	3.5	0.688	0.821	0.801	1000
0	4.0	0.941	0.962	0.957	1000
0	4.5	1.286	1.129	1.122	1000
0	5.0	1.680	1.278	1.287	1000
0	5.5	2.096	1.466	1.461	1000
0	6.0	2.644	1.630	1.635	1000
0	6.5	3.258	1.806	1.800	1000
0	7.0	3.902	1.974	2.00	1000
Tc	**Th**	**Pout**	**Iout**	**Vout**	**Rload**
0	0.5	0.012	0.020	0.036	2000
0	1.0	0.048	0.144	0.293	2000
0	1.5	0.120	0.248	0.499	2000
0	2.0	0.252	0.363	0.725	2000
0	2.5	0.444	0.477	0.951	2000
0	3.0	0.708	0.592	1.198	2000
0	3.5	1.056	0.732	1.465	2000
0	4.0	1.512	0.867	1.753	2000
0	4.5	2.064	1.013	2.030	2000
0	5.0	2.748	1.158	2.353	2000
Tc	**Th**	**Pout**	**Iout**	**Vout**	**Rload**
0	0.5	0.008mW	16.41uW	0.049v	3000
0	1.0	0.048	0.125	0.378	3000
0	1.5	0.128	0.213	0.646	3000
0	2.0	0.280	0.309	0.926	3000
0	2.5	0.512	0.408	1.230	3000
0	3.0	0.808	0.518	1.541	3000
0	3.5	1.200	0.633	1.907	3000
0	4.0	1.720	756.92	2.236	3000
0	4.5	1.848	781.34	2.353	3000
Tc	**Th**	**Pout**	**Iout**	**Vout**	**Rload**
0	0.5	0.002mW	16.56uA	0.057	4000
0	1.0	0.056	0.106	0.447	4000
0	1.5	0.140	0.190	0.745	4000
0	2.0	0.284	0.267	1.085	4000
0	2.5	0.500	0.354	1.444	4000
0	3.0	0.806	0.452	1.804	4000
0	3.5	1.226	0.552	2.215	4000
0	4.0	1.376	589.44	2.235	4000
Tc	**Th**	**Pout**	**Iout**	**Vout**	**Rload**
0	0.5	0.004mW	11.60uA	0.067v	5000
0	1.0	0.051	0.095	0.468	5000
0	1.5	0.134	0.163	0.807	5000
0	2.0	0.285	0.238	1.187	5000

0	2.5	0.493	0.313	1.568	5000
0	3.0	0.784	0.394	1.986	5000
0	3.5	1.096	0.467	2.353	5000
Tc	**Th**	**Pout**	**Iout**	**Vout**	**Rload**
0	0.5	0.016mW	10.00Ua	0.058	6000
0	1.0	0.047	0.084	0.517	6000
0	1.5	0.141	0.146	0.865	6000
0	2.0	0.276	0.214	1.244	6000
0	2.5	0.463	0.281	1.687	6000
0	3.0	0.734	0.352	2.098	6000
0	3.5	0.921	0.390	2.353	6000
Tc	**Th**	**Pout**	**Iout**	**Vout**	**Rload**
0	0.5	6.40uW	9.60uA	0.063	7000
0	1.0	0.041	0.078	0.522	7000
0	1.5	0.118	0.131	0.917	7000
0	2.0	0.249	0.188	1.333	7000
0	2.5	0.441	0.251	1.770	7000
0	3.0	0.707	0.316	2.219	7000
0	3.5	0.793	0.337	2.239	7000
Tc	**Th**	**Pout**	**Iout**	**Vout**	**Rload**
0	0.5	2.80uW	8.28uA	0.065	8000
0	1.0	0.039	0.071	0.541	8000
0	1.5	0.114	0.117	0.961	8000
0	2.0	0.238	0.171	1.371	8000
0	2.5	0.417	0.227	1.825	8000
0	3.0	0.663	0.286	2.289	8000
0	3.5	0.694	0.293	2.354	8000
Tc	**Th**	**Pout**	**Iout**	**Vout**	**Rload**
0	0.5	0.002	0.007	0.067	9000
0	1.0	39.60	62.40	0.581	9000
0	1.5	0.102	0.108	0.972	9000
0	2.0	0.224	0.156	1.431	9000
0	2.5	0.391	0.207	1.876	9000
0	3.0	609.84	260.40	2.358	9000

Larger loads

Tc	**Th**	**Pout**	**Iout**	**Vout**	**Rload**
0	0.5	0.35Uw	0.97Ua	0.076	100k
0	1.0	4.53	6.94	0.711	100k
0	1.5	0.015	0.012	1.224	100k
0	2.0	31.05	17.48	1.783	100k
0	2.5	54.77	23.45	2.353	100k
Tc	**Th**	**Pout**	**Iout**	**Vout**	**Rload**
0	0.5	0.12uW	0.38uA	0.076	200k
0	1.0	2.40	3.55	0.711	200k
0	1.5	7.44	6.10	1.224	200k
0	2.0	15.84	8.88	1.783	200k
0	2.5	27.60	11.66	2.353	200k
Tc	**Th**	**Pout**	**Iout**	**Vout**	**Rload**
0	0.5	0.08uW	0.21uA	0.076	300k

0	1.0	1.68	2.368	0.711	300k
0	1.5	4.968	4.128	1.224	300k
0	2.0	10.56	5.994	1.783	300k
0	2.5	18.24	7.324	2.353	300k
Tc	**Th**	**Pout**	**Iout**	**Vout**	**Rload**
0	0.5	0.06uW	0.261uA	0.076	400k
0	1.0	1.29	1.766	0.711	400k
0	1.5	3.81	3.072	1.224	400k
0	2.0	7.95	4.464	1.783	400k
0	2.5	13.89	5.880	2.353	400k
Tc	**Th**	**Pout**	**Iout**	**Vout**	**Rload**
0	0.5	0.05uW	0.160Ua	0.076	500k
0	1.0	1.01	1.414	0.711	500k
0	1.5	3.02	2.470	1.224	500k
0	2.0	6.43	3.592	1.783	500k
0	2.5	10.99	4.692	2.353	500k

A Sample for Parameter extraction on MATLAB:

A=1.0

Rp =

192.5105

Method 1 - complete model

Rp_min = 187.976190

Rp = 192.510500

Rs_max = 4.523810

Rs = 0.002000

a = -140.559967

T = 25.000000

G = 1000.000000

Pmax,m = 1.094266 (model)

Pmax,e = 0.808500 (experimental)

tol = 0.000100

P_error = 0.285766

Ipv = 0.230001

Isc = 0.230000

Ion = -0.278889

A=1.1

Rp =

192.5105

Method 1 - complete model

Rp_min = 187.976190

Rp = 192.510500

Rs_max = 4.523810

Rs = 0.002000

a = -140.559967

T = 25.000000

G = 1000.000000

Pmax,m = 1.094266 (model)

Pmax,e = 0.808500 (experimental)

tol = 0.000100

P_error = 0.285766

Ipv = 0.230001

Isc = 0.230000

Ion = -0.278889

A=1.2

Rp =

192.5105

Method 1 - complete model

Rp_min = 187.976190
Rp = 192.510500
Rs_max = 4.523810
Rs = 0.002000
a = -140.559967
T = 25.000000
G = 1000.000000
Pmax,m = 1.094266 (model)
Pmax,e = 0.808500 (experimental)
tol = 0.000100
P_error = 0.285766
Ipv = 0.230001
Isc = 0.230000
Ion = -0.278889

A=1.3

Rp =

192.5105

Method 1 - complete model

Rp_min = 187.976190
Rp = 192.510500
Rs_max = 4.523810
Rs = 0.002000
a = -140.559967
T = 25.000000

G = 1000.000000

Pmax,m = 1.094266 (model)

Pmax,e = 0.808500 (experimental)

tol = 0.000100

P_error = 0.285766

Ipv = 0.230001

Isc = 0.230000

Ion = -0.278889

Rp_min = 187.976190

Rp = 405.386687

Rs_max = 4.523810

Rs = 1.536000

a = 8.059040

T = 25.000000

G = 1000.000000

Pmax,m = 0.808597 (model)

Pmax,e = 0.808500 (experimental)

tol = 0.000100

P_error = 0.000097

Ipv = 0.230872

Isc = 0.230000

Ion = 1.87366e-11